SEISMIC RETROFIT OF CISS PILE BENT CAP CONNECTIONS

by

MICHAEL LUBIEWSKI

PEDRO SILVA

GENDA CHEN

UTC

R86/R108

Technical Report Documentation Page

1. Report No. UTC R86/R108	2. Government Accession No.	3. Recipient's Catalog No.
4. Title and Subtitle Seismic Retrofit of CISS Pile Bent Cap Connections		5. Report Date June 2006
		6. Performing Organization Code
7. Author/s Michael Lubiewski, Pedro Silva, Genda Chen		8. Performing Organization Report No. 00001406/0008404
9. Performing Organization Name and Address Center for Infrastructure Engineering Studies/UTC program University of Missouri - Rolla 223 Engineering Research Lab Rolla, MO 65409		10. Work Unit No. (TRAIS)
		11. Contract or Grant No. DTRS98-G-0021
12. Sponsoring Organization Name and Address U.S. Department of Transportation Research and Special Programs Administration 400 7th Street, SW Washington, DC 20590-0001		13. Type of Report and Period Covered Final
		14. Sponsoring Agency Code

15. Supplementary Notes

16. Abstract

This report presents results from a research investigation of a total of three 4/5 scale units that were cast, retrofitted, and tested under simulated fully-reversed cyclic lateral loading for the State of Alaska Department of Transportation and Public Facilities. These three units consisted of a cast in place steel shell (CISS) column foundation shaft and a bent cap configured to form a tee connection. In addition, these units were built to model a bridge bent and tested under simulated seismic loads at the University of Missouri Rolla experimental facilities. Based on the experimental study, this report presents an upgrade method that can be implemented in field conditions for improving the seismic performance of bridges built in the state of Alaska. Specific seismic improvements made to the column and the bent cap system were: (1) the moment capacity of the column was reduced by cutting a portion of the column longitudinal reinforcement at the connection to the bent cap to levels that can ensure a proper ductile seismic response, (2) a section of the steel shell was cut and removed leaving a gap between the steel shell and the bent cap, and (3) the bent cap dimensions were increased to ensure proper reinforcement spacing and to install the additional flexure and joint shear reinforcement, which was designed according to well established joint shear force transfer mechanism models. Each unit was retrofitted in the column, bent cap, and their connection according to current seismic design standards in order to ensure a ductile performance under the applied lateral loads. In all the test units, the main failure mode was characterized by strength degradation of the columns due to joint shear failure beyond a displacement ductility capacity of 6. Based on this information, the research team suggests that a limiting force reduction factor of 4 be employed in retrofit design using any of the upgrade details discussed in this report. Furthermore, this research program studied the feasibility of the upgrade method for direct implementation in the field. This report presents the test results, design philosophy, and recommendations for further research in order to improve the proposed retrofit scheme.

17. Key Words Retrofitting, Cyclic lateral loading, CISS, Seismic loading, Moment capacity, Bent cap, Shear failure, Force reduction factor	18. Distribution Statement No restrictions. This document is available to the public through the National Technical Information Service, Springfield, Virginia 22161.		
19. Security Classification (of this report) unclassified	20. Security Classification (of this page) unclassified	21. No. Of Pages 147	22. Price

Form DOT F 1700.7 (8-72)

CIES MISSION

The mission of CIES is to provide leadership in research and education for solving society's problems affecting the nation's infrastructure systems. CIES is the primary conduit for communication among those on the UMR campus interested in infrastructure studies and provides coordination for collaborative efforts. CIES activities include interdisciplinary research and development with projects tailored to address needs of federal agencies, state agencies, and private industry as well as technology transfer and continuing/distance education to the engineering community and industry.

Center for Infrastructure Engineering Studies (CIES)
University of Missouri-Rolla
223 Engineering Research Lab
1870 Miner Circle
Rolla, MO 65409-0710
Tel: (573) 341-6223; fax -6215
E-mail: cies@umr.edu
Web Page: www.cies.umr.edu

Seismic Retrofit of CISS Pile Bent Cap Connections

by

Michael Lubiewski
Graduate Research Assistant

Pedro Silva
Assistant Professor of Civil Engineering

Genda Chen
Associate Professor of Civil Engineering

Final Report

Report No. CIES 06-64

Department of Civil, Architectural and Environmental Engineering
Center for Infrastructure Engineering Studies
University of Missouri – Rolla

April 2006

TABLE OF CONTENTS

LIST OF SYMBOLS

A_{jh} = Area of horizontal joint shear reinforcement

A_{jv} = Area of vertical joint shear reinforcement

A_{jv}^{ext} = Area of external vertical joint shear reinforcement, outside the joint region

A_{jv}^{int} = Area of internal vertical joint shear reinforcement, within the joint region

A_{sc} = Area of the column longitudinal reinforcement

b_{je} = Width of the joint over which the shear force is applied

d_b = Bar diameter

D_c = Inside diameter of CISS steel shell

D_c' = Diameter of column concrete core

E_s = Modulus of elasticity of reinforcement steel

f_a = Axial stress

f_c' = Concrete compressive strength

f_l = Joint confining pressure

f_{sh} = Stress in the horizontal confining steel

f_y = Reinforcement yield stress

$f_{y,b}$ = Bent cap longitudinal reinforcement yield stress

$f_{y,c}$ = Column reinforcing specified yield strength

f_{yc}° = Overstrength stress in the column longitudinal reinforcement, $f_{yc}^{\circ} = \lambda_0 f_y$

$f_{c,b}'$ = Bent cap specified design compressive concrete strength

f_p = Transverse presstressing stress

H = Distance from the centerline of the retrofitted bent cap to the centerline of the applied lateral load

H_b = Height of the retrofitted bent cap

L = Distance between the end supports

l_a = Anchorage length of column longitudinal reinforcement, $l_a = 0.7 h_b$

l_d = Development length

L_1 = Distance between the bridge girders

M_b^D = Bent cap centerline moment at node D

M_c^F = Column centerline moment at node F

P	=	Axial force in the column
p_c	=	Principle compressive stress
p_t	=	Principle tensile stress
$p_{t,m}$	=	Principle tensile stress limit requiring full joint shear reinforcement
v_h	=	Joint shear stress
V_h	=	Shear force in joint due to applied moment
α	=	Factor to calculate moment at column face
β	=	Factor to calculate moment at column face
ΔA_{bb}	=	Additional bottom beam longitudinal reinforcement
ΔA_{tb}	=	Additional top beam longitudinal reinforcement
λ	=	Principle stress determined from Eigenvector
λ_0	=	material over strength factor, equal to 1.4 for when design yield strength is used
σ_{xx}	=	Stress in the x-x direction
σ_{yy}	=	Stress in the y-y direction, $\sigma_{yy} = f_a$
σ_{zz}	=	Stress in the z-z direction, $\sigma_{zz} = f_p$
ρ_l	=	Column longitudinal reinforcement ratio
ρ_s	=	Column volumetric transverse reinforcement ratio
τ_{xy}	=	Shear stress in x-y direction, $\tau_{xy} = v_h$
τ_{zx}	=	Shear stress in the z-x direction
τ_{zy}	=	Shear stress in the z-y direction
μ	=	Displacement ductility level

LIST OF FIGURES

LIST OF TABLES

ABSTRACT

This report presents results from a research investigation of a total of three 4/5 scale units that were cast, retrofitted, and tested under simulated fully-reversed cyclic lateral loading for the State of Alaska Department of Transportation and Public Facilities. These three units consisted of a cast in place steel shell (CISS) column foundation shaft and a bent cap configured to form a tee connection. In addition, these units were built to model a bridge bent and tested under simulated seismic loads at the University of Missouri Rolla experimental facilities. Based on the experimental study, this report presents an upgrade method that can be implemented in field conditions for improving the seismic performance of bridges built in the state of Alaska.

Specific seismic improvements made to the column and the bent cap system were: (1) the moment capacity of the column was reduced by cutting a portion of the column longitudinal reinforcement at the connection to the bent cap to levels that can ensure a proper ductile seismic response, (2) a section of the steel shell was cut and removed leaving a gap between the steel shell and the bent cap, and (3) the bent cap dimensions were increased to ensure proper reinforcement spacing and to install the additional flexure and joint shear reinforcement, which was designed according to well established joint shear force transfer mechanism models.

Each unit was retrofitted in the column, bent cap, and their connection according to current seismic design standards in order to ensure a ductile performance under the applied lateral loads. In all the test units, the main failure mode was characterized by strength degradation of the columns due to joint shear failure beyond a displacement ductility capacity of 6. Based on this information, the research team suggests that a limiting force reduction factor of 4 be employed in retrofit design using any of the upgrade details discussed in this report. Furthermore, this research program studied the feasibility of the upgrade method for direct implementation in the field. This report presents the test results, design philosophy, and recommendations for further research in order to improve the proposed retrofit scheme.

1.1. OVERVIEW

Seismic design in the United States has evolved significantly since the 1971 San Fernando Earthquake in California (Buckle, 2000; Krawinkler, 1995; 1999). During the aftermath of this earthquake a large number of bridges in this region failed catastrophically due to insufficient span seating. In response to these failures, the California Department of Transportation (Caltrans, 2001, 2004) initiated a bridge retrofit program to retrofit all bridges against unseating with cable restrainers during strong-motion earthquakes, thus preventing the supported end of the bridge from collapsing (DesRoches and Fenves, 2001; Priestley et al., 1995). Then, following the 1989 Loma Prieta Earthquake in California, major advances were implemented in seismic design leading to the current capacity philosophy for the seismic design of bridges. According to the capacity design philosophy the main performance goal is to allow the development of plastic hinges at the end(s) of columns for optimum energy dissipation. This can be realized by carefully selecting and detailing the plastic hinge areas, while the remaining regions are designed to remain elastic throughout the design seismic event (Priestley *et al.,* 1996; Mazzoni and Moehle, 2001; ATC-32, 1996).

It is well documented in current seismic design codes that the purpose of limiting the plastic hinges in the columns is because post-earthquake repair of columns may be completed without disruption to the daily traffic flow (Caltrans, 2004). Another benefit of this practice is that post-earthquake inspection consisting of nondestructive measures can be easily undertaken. Previous research has shown that existing bridges built in the state of Alaska do not comply with the current seismic design philosophy leaving them prone to significant damage and undesirable failure modes when subjected to seismic events. A common practice in the construction of bridge bents in Alaska and other regions that experience long winter and deicing seasons is the use of a thick steel shell to form a cast-in-drilled-hole (CIDH) foundation shaft system and to act as the external longitudinal and transverse reinforcement for the system. The shell, which improves constructability of the bent by serving as a casing for the CIDH shaft and formwork for the column, have been typically embedded into the bent cap and the connection to the bent cap is effected by providing mild steel longitudinal reinforcement in the top portion of the column. Based on a preliminary evaluation of bridges built in Alaska, (Silva *et al.*, 1999), some of the design deficiencies common to these typical as-built bridges are:

1) The CISS column foundation shafts have excessive longitudinal reinforcement ratios, which impose high demands in the joints and the bent caps.

2) The yield moment capacity of the bent cap is below the maximum feasible moment that develops at the column faces, which leads to the formation of plastic hinges in the bent cap.

3) The steel shells are partially embedded in the joint region, which under low levels of rotation impose extensive damage on the bent cap, and

4) The joints have inadequate amounts of joint shear reinforcement to sustain the levels of principal tensile stresses that develop within the joint region, which leads to anchorage failure of the column longitudinal reinforcement and significant strength degradation below yielding of the column longitudinal reinforcement.

Under seismic loading, these design deficiencies lead to damage of the bent cap and joint, which do not meet current capacity design standards for a proper seismic response of bent cap systems (AASHTO 1996, Caltrans 2001, Priestley 1996). Because of the design deficiencies outlined above, there is a need to develop procedures for the seismic upgrade of these systems. As such, the main objective of this research program was to provide upgrade design guidelines and evaluations methodologies for bridge system consisting of CIDH foundation shafts.

1.2.   RESEARCH SIGNIFICANCE

This research program investigated an upgrade method for improving the seismic performance of bridge bents built in the state of Alaska. Research results were then used to establish reliable displacement ductility levels for design of bridge bents using the proposed upgrade method. As such, a laboratory model was designed, constructed, and tested under simulated seismic loads with the main goal of investigating the feasibility for field implementation of the proposed upgrade scheme.

1.3.   LITERATURE REVIEW

Most of reinforced concrete columns built prior to the 1970's were deficient in shear strength and flexural ductility (Sanders et al., 1992; Priestley *et al.*, 1995). Each of these design deficiencies corresponds to a potential failure mode that is associated with insufficient amounts of transverse reinforcement and/or seismic detailing. However, the associated failure modes are mostly eliminated when using steel shells encasing reinforced or unreinforced concrete sections, especially in seismic regions, because of the satisfactory performance of steel casings to enhance the ductility capacity of reinforced concrete sections through confinement of the concrete core (Chai *et al.*, 1991; Priestley *et al.*, 1995; Silva *et al.*, 1997).

With the presence of the steel shells in the construction of the columns and/or foundation shafts in many of the bridges built in the state of Alaska none of these undesirable failure modes are likely to develop under reversed cyclic loading and, as such, no retrofit is required in these

members. However; up until recently, the steel shells in these CIDH shafts have been embedded into the bent cap in the design of bridge bents. This detail has been experimentally investigated to cause extensive damage to the joint region due to the prying action expected under lateral cyclic loads (Silva and Seible, 2001). As demonstrated by Silva *et al.* (1997), such damage can be easily prevented by terminating the steel shells below the bent cap. This detail was also adopted in this research program and the corresponding construction/upgrade details are clearly described in Section 1.10.

Recent earthquakes worldwide have illustrated the vulnerability of existing reinforced concrete (RC) beam-column joints to seismic loading (Sritharan, 1998). Poorly detailed joints, especially exterior ones, have been identified as critical structural elements, which appear to fail prematurely (Mazzoni and Moehle, 2001). Strengthening of RC joints is a challenging task that poses major practical difficulties. A variety of techniques applicable to concrete elements have also been applied to joints with the most common ones being the construction of concrete jackets with or without the use of prestressing (Mazzoni and Moehle, 2001; Ingham, 1995). However, one of the main disadvantages of providing concrete jackets is the increase in the dimensions and weight of the bent caps.

Longitudinal prestressing of a beam-column joint reduces the tendency for joint cracking due to increase in horizontal stresses, and increases the shear and flexural strength of the bent cap. Prestressing is designed to increase the bent cap flexural strength sufficiently to ensure that column plastic hinges are developed for both positive and negative moments. However, prestressing the joint increases the principal compression stress within the joint, and design of the prestressing force should ensure that the principle compressive stress limit of $0.3f'c$ is not exceeded. In this research program post tensioning was also evaluated; but in this case, only prestressing in the transverse direction of the bent cap was implemented. Although not as effective as prestressing in the longitudinal direction, this is a detail solution that has not been previously investigated.

Prestressing is likely to be the most effective retrofit technique when the principal tensile stresses within the joint are reduced below $0.29\sqrt{f'_c}$ (MPa). For higher levels of principal tensile stresses it may be unfeasible or even impractical to solely use prestressing. In this case, jacketing the joint by concrete, steel, or composite-materials may be also required to ensure that the performance of the joint is not likely to degrade, which results in increased drift levels due to joint degradation. Typically, the jacket will extend beyond the original joint dimensions into the bent cap and column in the form of a haunch section. Dimensioning of this haunch section is also

critical in ensuring that the joint stresses are properly dissipated over a wider region (Sritharan, 1998).

Jacketing can also be used to increase the joint dimensions, thus reducing principle joint stress levels. Extending the size of the joint into the existing column and bent cap also increases the development length of the column and longitudinal reinforcement and it creates new critical sections for moment capacity at the edge of the jacket. These details were further evaluated and implemented in this research program to enhance the seismic performance of the bent cap and joint region and construction and design details are clearly described in Sections 1.11 and 1.12.

1.4.   SCOPE OF RESEARCH

A prototype unit consisting of an interior column and corresponding bent cap was designed and constructed in a T-configuration by including the aforementioned deficiencies discussed in Section 1.1. After construction, the as-built portion of the test units was modified in order to investigate seismic improvements and propose procedures for field implementation. To accomplish the research objectives, a total of three 4/5 scale units were cast, retrofitted, and tested under simulated fully-reversed cyclic lateral loading. The proposed seismic upgrade procedures were experimentally investigated in this research program and are presented in this report. Briefly, the seismic improvements made to the column and the bent cap system were:

1) The moment capacity of the column was reduced by cutting a portion of the column longitudinal reinforcement at the connection to the bent cap to levels that can ensure a proper ductile seismic response. Previous research has shown that the column reinforcement ratios should be limited to 4.0% if joint shear stresses are to be limited and congestion of reinforcement is avoided within the joint region (Priestley *et. al,* 1995, Silva *et. al,* 1999). As such, this limit was also used as a benchmark for this research program.

2) A section of the steel shell was cut and removed leaving a gap between the steel shell and the bent cap. As before, previous research has shown that leaving this gap avoids significant damage to the bent cap under small rotations because the prying action of the steel shell against the surrounding concrete is avoided (Silva *et. al,* 1999). In addition, the steel shell was removed to provide access to cut the column longitudinal reinforcement thereby reducing the reinforcement ratio as designated above.

3) The bent cap dimensions were increased to ensure proper reinforcement spacing and to install the additional flexure and joint shear reinforcement, which was designed according to well established joint shear force transfer mechanism models (Sritharan and Ingham, 2003). Increasing the bent cap sizes also reduced the principle tensile stresses and provides for a better transfer of stresses within the joint region. In addition, enlarging the bent cap also provides for a

greater development length of the column longitudinal reinforcement, thereby increasing the anchorage capacity of this reinforcement. Lastly, the bent cap was enlarged to levels that can prevent reinforcement congestion within the joint region.

Construction and design implementation of these details are discussed and presented in greater detail within this report. Results from a cyclic testing of the upgraded units showed a ductile response up to the displacement ductility of 4 for the three units without significant decreases in the strength of the test units. Beyond this ductility level, the main failure mode of Unit 1 was attributed to joint shear failure due to excessive transverse dilations in the joint region. An improved joint detail was implemented for Unit 2, and the main failure mode was attributed to low cyclic fatigue of the column longitudinal reinforcement. However, joint degradation was recorded beyond the displacement ductility of 6. In Unit 3 the joint was post-tensioned in the transverse direction while also decreasing the gap length between the steel shell and the bent cap. Beyond ductility level 6 degradation of the lateral load capacity of the column occurred due to joint shear failure. Detailed description for the design of these units and experimental results are discussed within this report.

Based on the experimental results the research team proposes that a displacement ductility of 4 be implemented in the retrofit design for the maximum credible earthquake. At this level it is expected that some level of strength degradation will be observed in the column, but this will not either cause significant decrease in the column axial capacity nor significant wide open cracks in the joint region. Furthermore, any cracks at this level will close under the gravity loads. In addition, for columns with lower reinforcement ratios the full dependable moment capacity and displacement ductility of the column can be expected to develop. As such, for these columns higher displacement ductilities levels may be accepted for assessment investigation.

1.5. REPORT LAYOUT

Following an introduction to the seismic design of reinforced concrete bridge bents, and scope of the current study in this section, Section 0 describes the test matrix, the geometry of the test setup and loading protocol, the reinforcement layout for the test as-built section and the material properties. Following description of the as-built section in Section 0, Section 0 describes in detail the design considerations for the column, bent cap and joint region for Unit 1, along with the analytical predictions and evaluation for this test unit. Section 0 describes the design procedure for Unit 2, while Section 0 covers the design of Unit 3, and Section 0 describes the instrumentation layout for the three test units. Then in Section 0 the predicted response of the test units is presented, and in Sections 0, 0, and 0 experimental results are described in great detail for Units 1, 2, and 3, respectively. Finally, this report concludes with specific recommendations

for the seismic upgrade of reinforced concrete bridge bents with cast-in-place steel shell pile-shaft/columns, as presented in Section 0 and 0.

1.6.   TEST MATRIX

In this research program three test units, designated as Units 1, 2, and 3, were tested under reversed seismic loads to investigate different retrofit/upgrade schemes with the main objective of increasing the performance of bridge bents under seismic loads. In these three units the retrofit scheme for the bent cap was identical, to the exception that within the column and joint region a few minor modifications were implemented as discussed in Sections 0, and 0. Design of Unit 2 was accomplished after testing of Unit 1; meanwhile, design of Unit 3 was accomplished after testing of Unit 2.

1.7.   TEST SETUP

Laboratory conditions placed a limit on the size and setup for the test units. For safety precautions the test units were built and tested in an inverted position, as shown in Figure 0-1. The test units consisted of a column and respective bent cap arranged in a tee configuration. In the as-built conditions, the columns were 610 mm in diameter with a height from the bent cap interface to the height of load application of 2.87 m. The bent caps were 737 mm (wide) x 743 mm (depth) x 5.18m (length) with a clear span between supports of 4.57 mm.

After retrofitting, the bent cap size dimensions were increased to 1,054 mm (wide) x 895 mm (depth), resulting in a reduced column height of 2.72 m or an aspect ratio of 4.5. Design considerations for the retrofit and upgrade of the test units are presented in detail in Sections 0, 0, and 0 of this report.

As shown in Figure 0-1 for application of the simulated gravity and lateral loads, the top of the columns was terminated in the form of a cubic load stub. On the top surface of the load stub a hydraulic jack was used to apply the simulated gravity load. This axial load was then transferred to the bent cap through I-sections to simulate as closely as possible the position of the prototype bridge girders. These I-sections were positioned on the underside of the bent cap at a distance of 1.83 m, and the total axial load applied on the column was 710 kN, which corresponds to an estimated axial load ratio of 8%.

On the side surface, a servo-controlled hydraulic actuator was connected to apply the simulated reversed cyclic lateral loads. The lateral loading protocol is described in further detail in Section 1.25.
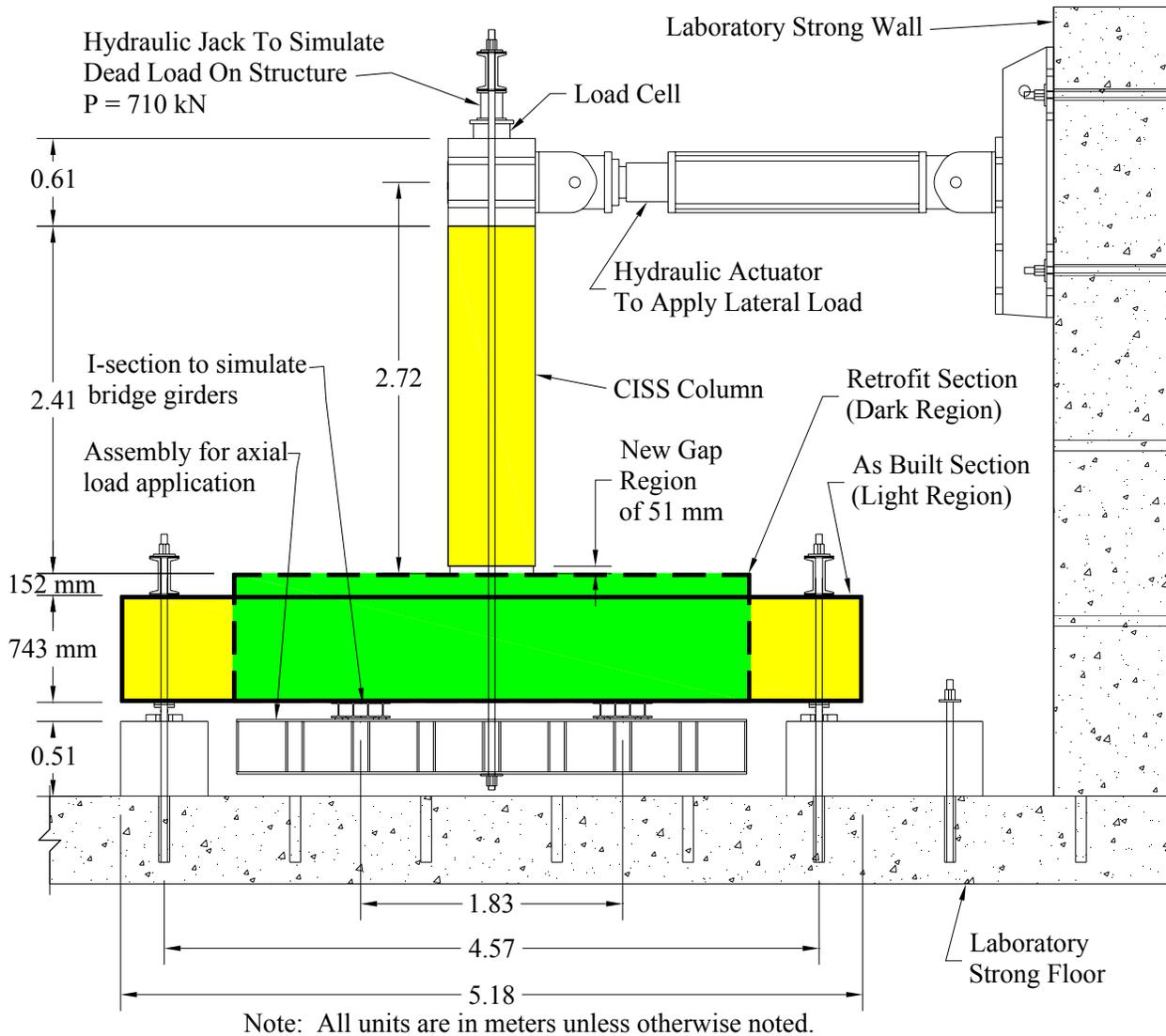
Figure 0-1. Test Setup

1.8. AS-BUILT SECTIONS

The three test units were constructed in a similar manner as in field conditions. However, in order to ensure proper safety precautions during and after construction and testing, each unit was built in an inverted position. Construction of the three test units was performed in two phases. In the first phase the corresponding as-built sections were built. In the second phase, the as-built portion was modified as needed and the new retrofit section was added. The as-built section was identical in all the three test units; however, the retrofit section in all three test units was constructed with minor deviations for investigation of different retrofit details, which will be discussed in detail in Sections 0, 0, and 0. The as-built column and bent cap cross sections and reinforcement layout are shown in Figure 0-2.

As previously discussed and based on current seismic evaluation methodologies, in its as-built condition the main failure mode of these units was by flexural yielding of the bent cap longitudinal reinforcement with significant shear deformations within the joint regions. Each of these failure modes do not comply with current seismic design criteria for the response of bridge bents under seismic loads. According to these failure modes, plastic hinges form in the bent cap and joint shear failure, leading to anchorage failure of the column longitudinal reinforcement at displacement levels below yielding of the column which are insufficient to sustain the design seismic event. In Section 0 of this report a detailed analytical investigation of the as-built system is presented in further detail along with the recommended design improvements and the proposed methodology.

(a) Longitudinal Cross-Section   **(b)** Cross-Section
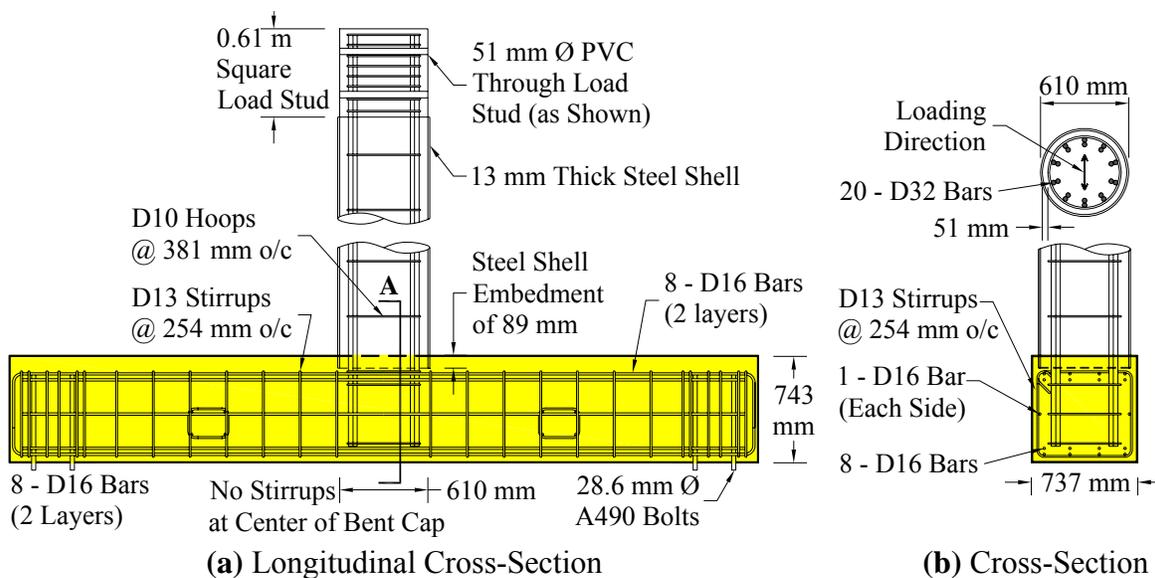
Figure 0-2. As-Built Reinforcement Layout

1.8.1. Column Reinforcement

The as-built column section consisted of 20 – D32 bars for the longitudinal reinforcement that were encased in a 13 mm thick steel shell with a cover concrete of 51 mm leading to a longitudinal reinforcement ratio of 6.1%. Furthermore, the steel shell was embedded 89 mm into the bent cap and the anchorage length of the column longitudinal reinforcement was 690 mm. The transverse reinforcement in the column was only provided for construction purposes, which under typical field conditions consists of D10 hoops at 381 mm on center. By providing this large level of column longitudinal reinforcement ratio poses severe difficulties in providing for a reliable joint shear force transfer mechanism model and subsequently design of the joint shear reinforcement.

On the other hand, research has clearly shown that by embedding the steel shell imposes significant damage within the seating region due to the prying action of the steel shell (Silva *et al.*, 1999). Meanwhile, one of the main advantages in using steel shells encasing reinforced concrete sections, especially in seismic regions, is the satisfactory performance of steel casings to enhance the ductility capacity of reinforced concrete sections through confinement of the concrete core.

1.8.2. Bent Cap Reinforcement

The main longitudinal reinforcement for the bent cap was the same for both the top and bottom layers and consisted of 8 – D16 bars that were placed in two layers. The clear distance between the two layers was 25.4 mm and the distance between the centroid of the top and bottom layer was nearly 198 mm, leading approximately to a reinforcement ratio of 0.40%. As discussed in Sections 0 and 0, this level of longitudinal reinforcement ratio is not appropriate to develop the yielding moment capacity necessary to ensure that the bent cap will remain essentially elastic under the input column plastic moment. Matching the as-built bent cap, no transverse reinforcement was provided within the joint region. The transverse reinforcement consisted of closed D13 stirrups spaced at 254 mm to either side of the columns (see Figure 0-2). However, it is important to emphasize that this construction detail does not comply with existing seismic design standards, and large inelastic actions are expected under reversed cyclic loading. As such, the retrofit and/or upgrade details discussed in Sections 0, 0, and 0 of this report investigate the feasibility of mediating the response of bridge bents under seismic loadings.

1.9.   MATERIAL PROPERTIES

In Sections 0 and 0, analytical investigations of the as-built and new retrofit sections are presented in detail. In this section a detailed list of all the material properties used in these analyses are presented. Concrete and steel properties used in the analysis are presented in Table 0-1 through Table 0-3, respectively. Concrete cylinders (102 x 203 mm) were cast for each lift of concrete and stored next to the Unit. Rebar samples were taken from each lot of steel and tested. Reinforcing steel material properties for the as-built and retrofit sections are shown, respectively in Table 0-2 and Table 0-3. All material tests for either the concrete or reinforcing steel were done in sets of three and averaged.

Table 0-1. Concrete Material Properties

Unit No.	Test *	Column	Bent Cap	
			As-Built	Retrofit
1	28 Day (MPa)	27.1	29.0	33.8
	Day of Test (MPa)	29.3	33.8	36.9
2	28 Day (MPa)	28.0	33.5	36.6
	Day of Test (MPa)	30.8	38.3	38.9
3	28 Day (MPa)	39.3	26.2	36.6
	Day of Test (MPa)	43.7	27.1	38.8

* Specified nominal strength was 34.5 MPa

Table 0-2. Reinforcing Steel Material Properties – As Built Section

Unit No.	Bar Size	Bar Location	f_y (MPa)	f_u (MPa)	E (GPa)
1 and 2	D10	Column Hoops	310	474	215
	D13	Bent Shear	425	638	195
	D16	Bent Longitudinal	554	689	196
	D32	Column Longitudinal*	519	671	189
3	D10	Column Hoops	435	632	174
	D13	Bent Shear	503	669	192
	D16	Bent Longitudinal	476	702	195
	D32	Column Longitudinal	497	746	209

* Calculated yield strain of 2,740 $\mu\varepsilon$

Table 0-3. Reinforcing Steel Material Properties – Retrofit Section

Unit No.	Bar Size	Bar Location	f_y (MPa)	f_u (MPa)	E (GPa)
1	D13	Bent Shear	506	674	215
	D16	Bent Transverse	486	652	200
	D19	Bent Longitudinal	493	775	195
2	D13	Bent Shear	503	669	192
	D16	Bent Transverse	476	645	193
	D19	Bent Longitudinal	472	696	182
3	D13	Bent Shear	506	674	215
	D16	Bent Transverse	486	652	200
	D19	Bent Longitudinal	493	775	195
	D19*	Pre-Stress Rods	517	689	200

* Threaded Rod, Manufacturer's Specifications

As previously discussed, after the as-built section was constructed, modifications were implemented according to well established seismic design principles. The overall section dimensions and reinforcement layout of the modified cross section for Unit 1 are shown in Figure 0-1. In this figure the shaded region represents the as-built bent cap section. Further modifications were implemented in the design of Units 2 and 3, which are discussed in further detail in Sections 0 and 0. In this section, design of the upgrade scheme for Unit 1 is explained in further detail.
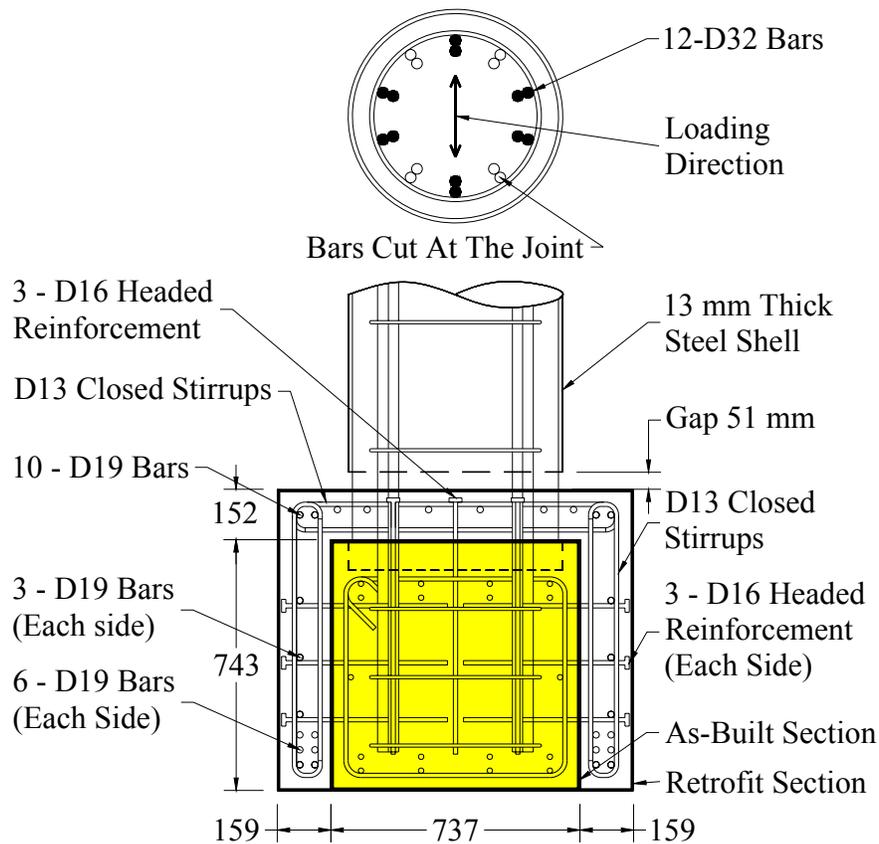
Note: All units are in mm unless otherwise noted

Figure 0-1. Unit 1 Retrofitted Cross-Section

1.10. COLUMN DESIGN CONSIDERATIONS

In the joint region the column longitudinal reinforcement was reduced to a reinforcement ratio below 4.0%, as suggested by Priestley *et al.* (1996). This reinforcement ratio was suggested in order to avoid excessive amounts of joint shear reinforcement that can lead to reinforcement

congestion within the joint region. As such, eight of the twenty column longitudinal bars were cut, thereby reducing the reinforcement ratio from 6.1 % to 3.7%.

In order to access the column longitudinal reinforcement, the steel shell was also cut and a portion removed. After the steel shell was cut and the column reinforcement was exposed by removing the cover concrete, the designated column bars were cut immediately above the as-built bent cap section, as shown in Figure 0-2.   As such, the new column section consisted of 12 – D32 longitudinal reinforcement and a gap region of 51 mm was left between the steel shell and the new bent cap section as shown in Figure 0-1.
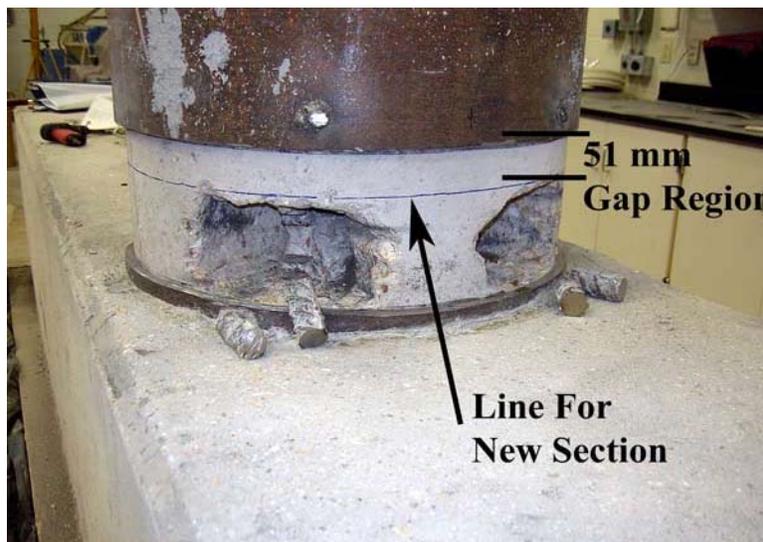
Figure 0-2. Cut Longitudinal Reinforcement

1.10.1. Moment-Curvature Analysis

A moment-curvature analysis was performed for both of these reinforcement ratios (i.e. 6.1% and 3.7%) corresponding to the as-built and the retrofitted sections. Results of this analysis are shown in Figure 0-3. For the as-built section, the moment curvature analysis was implemented considering that in the compression block the concrete, longitudinal reinforcement and steel shell are effective in transferring forces (Silva, 1997). Meanwhile within the tension block, only the longitudinal reinforcement was considered effective in transferring forces. Furthermore, the entire concrete compression block was assumed confined by the action provided by the steel shell based on expressions developed by Chai *et al.* (1991). Based on this analysis the ultimate moment capacity for the as-built column section was computed at 2,736 kN-m with an ultimate curvature ductility capacity of approximately 17.

Since the steel shell was cut at the bent cap interface to provide for a gap between the steel shell and the increased bent cap, for the retrofitted section, the moment curvature analyses was

implemented considering that in the compression block only the concrete and longitudinal reinforcement are effective in transferring forces (Silva, 1997). In this case the concrete compression block was assumed confined by an equivalent spiral confined section with a spiral size and pitch of 13x13 mm and 51 mm, respectively. These numbers correspond to the steel shell thickness and the gap at the interface with the bent cap (see Figure 0-1). Based on this analysis the ultimate moment demand for the modified column section was computed at 1,414 kN-m with an ultimate curvature ductility capacity of approximately 18.
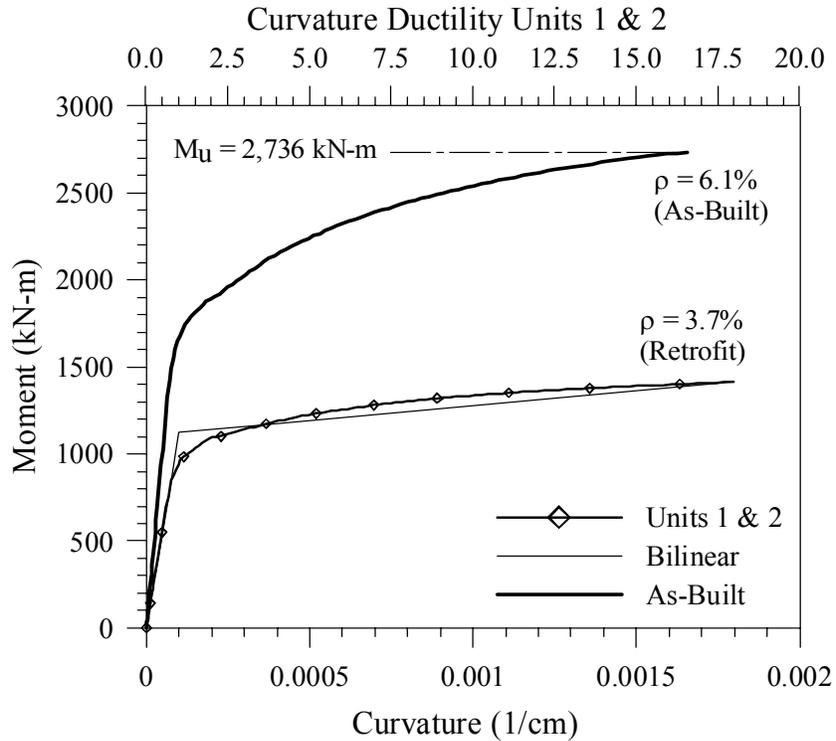
Figure 0-3. Column Moment Curvature

Referring to this figure, it is clear that the moment capacity of the retrofitted section (i.e. 3.7%) was reduced by nearly a factor of 2. Proportionally, this decrease is much less than the decrease in the reinforcement ratio or by a factor of 1.66. This can be explained because in addition to the decrease in the reinforcement ratio, the gap between the steel shell and the new bent cap section also decreased the confinement action of the steel shell and the effects of the steel shell on the bending moment capacity of the column section. In addition, analysis for the reduced reinforcement ratio without the compression action of the steel shell shows a pronounced elasto-plastic response when compared against the original section. This is also a desirable characteristic in the seismic design of structures because it sets the limiting actions in the system at low displacement ductility levels as compared to the as-built section where the capacity of the

section increases up to ultimate. This new reinforcement ratio of 3.7%, was then used as the parameter to design the additional flexural, shear, and joint shear reinforcement for the bent cap.

1.11. BENT CAP DESIGN CONSIDERATIONS

The moment demand placed on the bent cap was determined based on the ultimate moment capacity of the column, the applied axial load, and the structural layout of the test unit. Then an analysis was performed along the centerline of the bent cap at the critical locations, as shown in Figure 0-4(a). Based on the bending moment diagram depicted in Figure 0-4(b), the critical location used for design of the bent cap was established at node F.

(a) Model Structure

(b) Moment Diagram

Figure 0-4. Bent Cap Moment Demand Design Considerations

The maximum moment demand placed on the bent cap was determined according to the bending moment diagram presented in Figure 0-4(b) and computed at node F based on the expression

$$M_B^F = \frac{M_C^G}{2}\left(\frac{L_C + {}^{H_b}\!/_2}{L_C}\right)\left(\frac{L_B - D_c}{L_B}\right) + P\left(\frac{L_B' - D_c}{4}\right) \tag{0-1}$$

Referring to Figure 0-4, M_B^F is the bent cap centerline moment at the critical node F, M_C^G is the retrofitted column bending moment capacity estimated according to the moment curvature analysis presented in Figure 0-3 for the column with the reduced reinforcement ratio, ρ_l, of 3.7%, L_B' is the distance between the bridge girders, which for these test units was modeled at 1.83 m, as shown in Figure 0-1, D_c for CISS sections is the inside diameter of the steel shell or 584 mm for these test units, and P is the axial load applied to the column. Furthermore, $\underline{H_b}$ is the height of

the retrofitted bent cap, L_C is the distance from the top surface of the bent cap to the centerline of the applied lateral load or the distance between nodes C and G, and L_B is the distance between the end supports or the distance between nodes A and B or 4.57 m, as shown in Figure 0-1 and Figure 0-4(a).

1.11.1. Moment-Curvature Analysis

From the moment-curvature analysis depicted in Figure 0-5, it can be shown that the as-built bent cap moment capacity was deficient compared to the moment demand obtained by using Eq. (0-1). In this analysis the column capacity was evaluated based on the section with the reduced reinforcement ratio of 3.7%. As such, additional longitudinal reinforcement was added to the bent cap to increase its yield moment capacity above the moment demand imposed on the bent cap from the column, M_c^G.
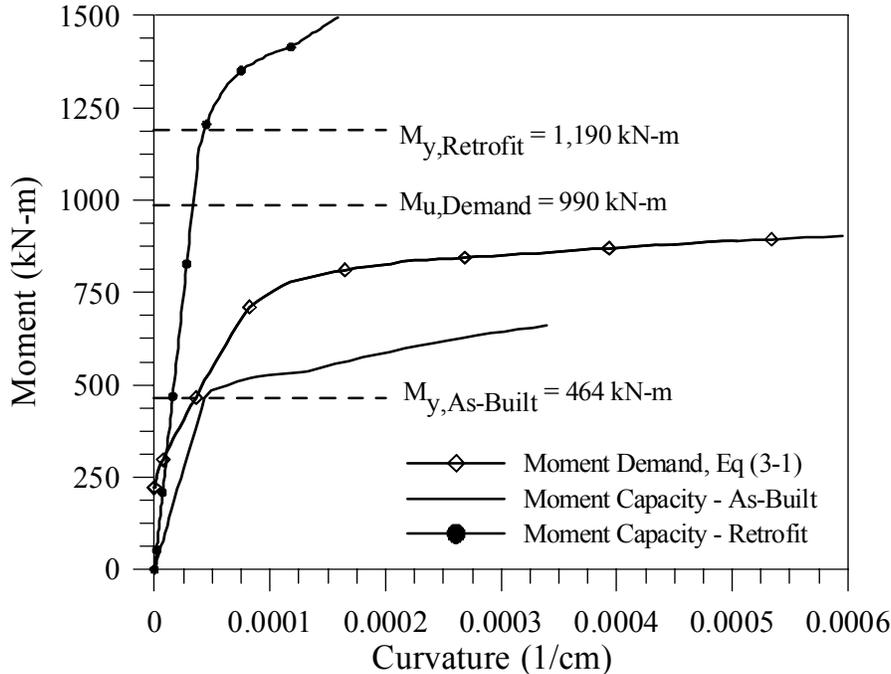
Figure 0-5. Bent Cap Moment Curvature

Referring to Figure 0-5, the maximum moment demand that can be imposed on the bent cap was nearly 990 kN-m and the computed yield moment capacity of the as-built bent cap was nearly 464 kN-m. Previous research by Silva *et al.* (1999) has suggested that the first yield moment capacity of the bent cap, $M_{y,b}$, should be at least 1,110 kN-m as given by

$$M_{y,b} = \frac{\lambda_o}{\phi_f} M_b^D = \frac{1.0}{0.9} \times 990 = 1,100 \, kN - m \tag{0-2}$$

Where λ_0 is the material over-strength factor equal to 1.4 when the reinforcement design yield stress is used, otherwise λ_0 is 1.0, M_B^F is the bent cap centerline moment at location F given by Eq. (0-1), and ϕ_f is the flexural strength reduction factor equal to 0.9. In order to increase the yield moment capacity of the bent cap to 1,100 kN-m, additional longitudinal reinforcement in the amount of approximately 800 mm^2 top and bottom were required along with increasing the bent cap dimensions. This limit required a total of 3-D19 bars; however, as shown in Figure 0-1, the total amount of additional reinforcement provided in the bent cap was 10-D19 on the top and 12-D19 on the bottom. These values exceed the required limit because of joint shear design considerations, which will be discussed in a later section.

1.11.2. Retrofitted Bent Cap Sizing
In order to install the longitudinal reinforcement in the bent cap and to meet current seismic design standards, the minimum width of the bent cap, W_b, required was
$$W_b = 1.5D_c = 1.5 \times 584mm = 876\,mm \tag{0-3}$$

However, the required width of the bent cap necessary to meet current ACI (ACI 2002) bar spacing and cover concrete specifications (see Figure 0-1) was 1,054 mm. Completing the bent cap resizing design, the height of the bent cap was determined based on limits to provide adequate anchorage length for the column longitudinal reinforcement. Using Priestley's (1996) recommendations, the development length, l_d, was computed based on the expression

$$l_d = 0.3d_b \frac{f_{yc}}{\sqrt{f'_{cb}}} = 0.3 \times 32mm \times \frac{414MPa}{\sqrt{34.5MPa}} \approx 677\,mm \tag{0-4}$$

Where d_b and f_{yc} are the column longitudinal reinforcement diameter and specified design yield strength, respectively, and f'_{cb} is the bent cap specified design concrete compressive strength. Since the as-built bent cap section provided only for a development length of 629 mm, there was the need to increase the height of the bent cap. The bent cap height was increased by a length of 152 mm for a total depth of 895 mm. This new height led to a total development length for the column longitudinal reinforcement of 790 mm, which exceeds the required anchorage length of 677 mm.

1.12. JOINT DESIGN CONSIDERATIONS
1.12.1. Joint Principle Stress Evaluation
Recent earthquakes have demonstrated the high risks associated with joint shear failure that can lead to collapse of entire bridge systems. Joint shear failure has been attributed largely to poorly detailed joints, performing as weak links in RC frames (Mazzoni and Moehle 2001). According to the National Cooperative Highway Research Program seismic design guidelines (NCHRP,

2003) and further corroborated by experimental investigation many existing bridges are vulnerable in the connection of the columns to the bent cap under seismic loads (Priestley et al., 1995; Yashinsky and Karshenas, 2003). Although flexibility in these connections is likely under seismic actions, these connections should retain reserved strength capacity under reversal cyclic loading in order to prevent large strength decreases in the system caused by shear failure of the joint core, or, as importantly, to prevent pull-out of the column longitudinal reinforcement.

Forces acting upon a typical bridge bent tee joint are depicted in Figure 0-6. Since large shear forces develop in bridge joints, as illustrated in Figure 0-6(c), conventional design methods that are based on joint shear forces typically demand considerable amounts of joint shear reinforcement. This design approach results in steel congestion within the joint regions creating difficulties in the construction of concrete bridge joints. A procedure that is nowadays used for the design of the joints is based on strut and tie models, which will be discussed in the next section.

(a) Tee joint Forces   (b) Joint Moments   (c) Joint Shear Forces
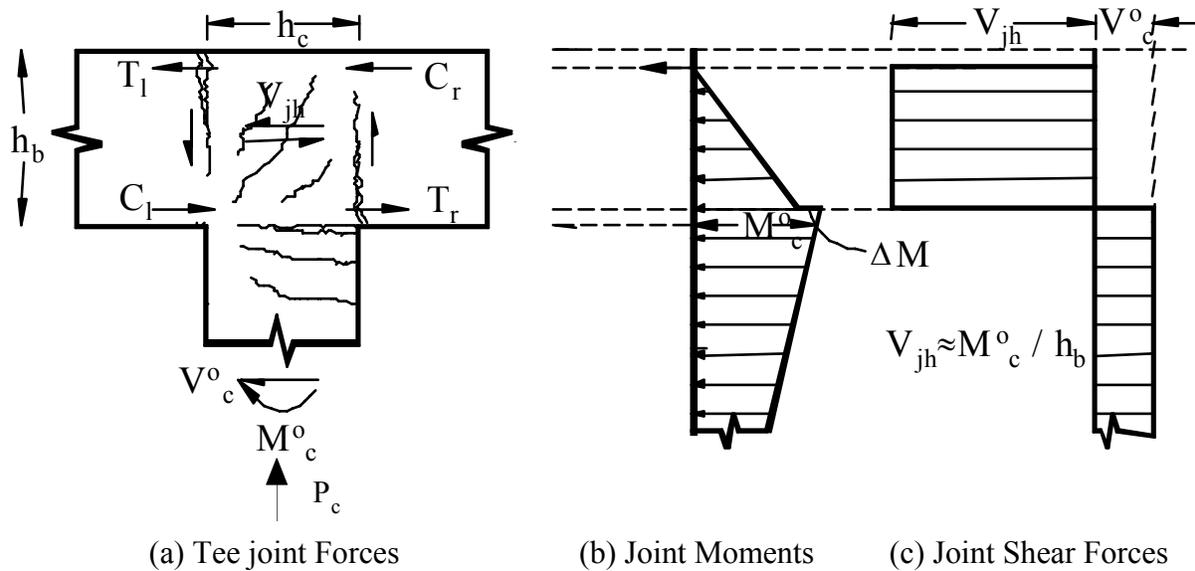
Figure 0-6. Joint Shear Forces in Bridge Tee Joints

In this research program, design of the joint was preceded by an evaluation of the principle compressive and tensile stresses computed from a Mohr's circle of analysis in order to anticipate its seismic performance (Priestley 1996, Silva 1999, Sritharan 2003). For the design of joints Priestley *et al*. (1996) recommends the following values as limits to establish a criterion for the design of the joint shear reinforcement:

$$p_c \leq 0.3 f_c^{'} \tag{0-5}$$

$$p_t \leq 0.29\sqrt{f_c^{'}} \; MPa \tag{0-6}$$

$$p_{t,m} \geq 0.42\sqrt{f_c'} \; MPa \tag{0-7}$$

The principle compressive stress limit, p_c, stipulated by Eq. (0-5), corresponds to the value at which crushing of the diagonal compression strut through the joint region initiates. In this research program, the bent cap sizing was inspected to ensure that the computed principle compressive stresses were below this value. Based on the column moment demand and bent cap sizes the principle compressive stresses were evaluated at $0.13f_c'$, which are significantly lower than the limit value of $0.30f_c'$.

The principle tensile stress limit, p_t, stipulated by Eq. (0-6) indicates the limit at which diagonal cracking in the joint is initiated and nominal joint shear reinforcement is required. Eq. (0-7) stipulates the principle tensile stress limit, $p_{t,m}$, at which full joint shear reinforcement is required. Interpolation between nominal and full joint shear reinforcement is typically required between these two limits. Given the applied axial load in the column of 710 kN and using the retrofitted column's predicted ultimate moment capacity of 1,440 kN-m (see Figure 0-3), the joint shearing stress, v_j, and the axial stress, f_a, are

$$v_j = \frac{V_h}{b_{je}D_c} = \frac{21974kN}{0.826\,m \times 0.584\,m} = 4.09\,MPa \tag{0-8}$$

$$f_a = \frac{P}{\sqrt{2}D_c b_w} = \frac{710kN}{\sqrt{2} \times 0.584\,m \times 1.055\,m} = 0.82\,MPa \tag{0-9}$$

Where V_h is the shear force in the joint due to the applied moment, b_{je} is the width of the joint over which the shear force is applied, D_c is the inside diameter of the steel shell, and P is the axial force in the column, and V_h and b_{je} are given by

$$V_h = \frac{M_c^F}{d} \approx \frac{M_c^F}{0.8h_b} = \frac{1414\,kN-m}{0.8 \times 0.895\,m} = 1{,}974\,kN \tag{0-10}$$

$$b_{je} = \sqrt{2}D_c \leq b_w$$
$$b_{je} = \sqrt{2} \times 0.584\,m = 0.826\,m \leq 1.055\ m \tag{0-11}$$

In Eq. (0-10), M_c^G is the ultimate moment capacity of the column derived from the moment curvature analysis. Using the Mohr's circle of analysis and the results from Eqs. (0-8) and (0-9), the principle stresses are then given by

$$p_c, p_t = \frac{f_a}{2} \pm \sqrt{\frac{f_a^2}{4} + v_j^2} = \frac{0.82}{2} \pm \sqrt{\frac{0.82^2}{4} + 4.09^2} = 4.5, -3.7\,(MPa) \tag{0-12}$$

Normalizing the results derived from Eq. (0-12) in terms of the nominal design concrete compressive strength of 34.5 MPa for f_c', yields the normalized principle compressive, p_c, and

tensile stresses, p_t, of $0.13f'_c$ and $0.63\sqrt{f'_c}$ respectively. Joint principle tensile stresses, p_t, were then computed using the entire moment curvature envelope based on the retrofitted column section shown in Figure 0-3. As shown in Figure 0-7 results indicate that the principle tensile stresses, p_t, exceed the limits stipulated by Eq. (0-7) and, as such, full joint shear reinforcement was required for the joint. In the next section, the joint shear design is presented in further detail.
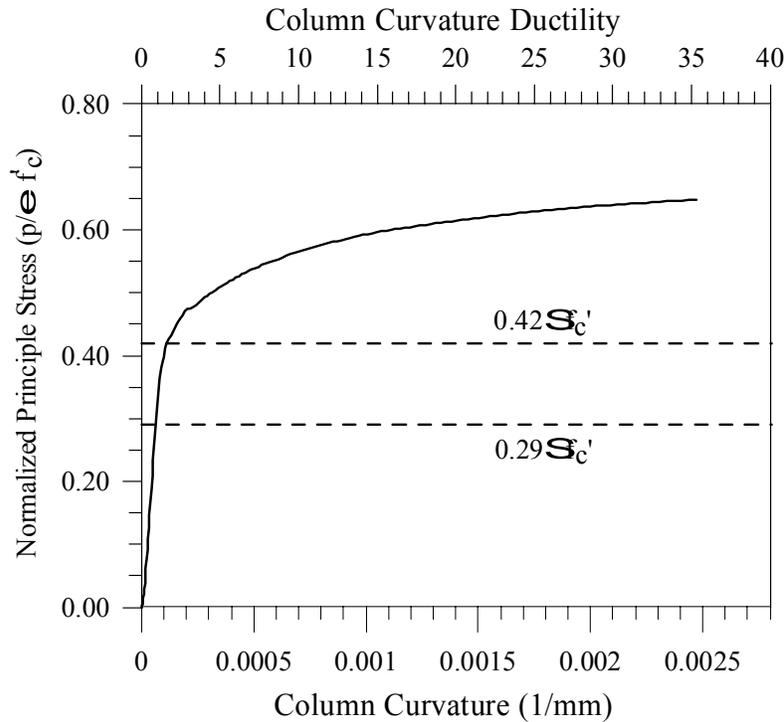
Figure 0-7. Joint Principle Tensile Stresses - Retrofitted Column

1.12.2. Joint Shear Reinforcement

Extensive information exists in the literature that clearly delineates the procedure of establishing strut and tie models for the design of joints and its benefits of transferring forces across the joint (Sritharan, 1999; Mazzoni, 2001). Sritharan (1999) has proposed a strut and tie model that has been successfully used to design the reinforcement in the joint region and was used in this research program for the design of the joint shear reinforcement. Referring to Figure 0-8, design of the test unit upgrade scheme was based on the modified external strut force transfer model (Sritharan,1999). This model typically requires the least amount of reinforcement when compared to other possible models. Design of joints using this approach has also been successfully used previously in the design of a three multiple column bridge bent (Silva *et al.*, 1999). Based on the strut and tie model of Figure 0-8, joint design includes (see Figure 0-9)

1. Top, ΔA_{tb}, and bottom, ΔA_{bb}, additional bent cap longitudinal reinforcement.

2. Vertical reinforcement outside and inside the joint region, A_{jv}, and

3. Horizontal joint reinforcement, A_{jh}.

Typically, the top, ΔA_{tb}, and bottom, ΔA_{bb}, longitudinal reinforcement is provided by additional reinforcement in the bent cap. Reference to top and bottom reinforcement are for a bent cap in its upright position; which in the test units these are inverted. The vertical reinforcement outside and inside the joint region, A_{jv}, is provided by closed stirrups or properly anchored headed reinforcement, and finally, the horizontal reinforcement, A_{jh}, is provided also by closed stirrups or headed reinforcement. Each of these along with the design requirements are described next.
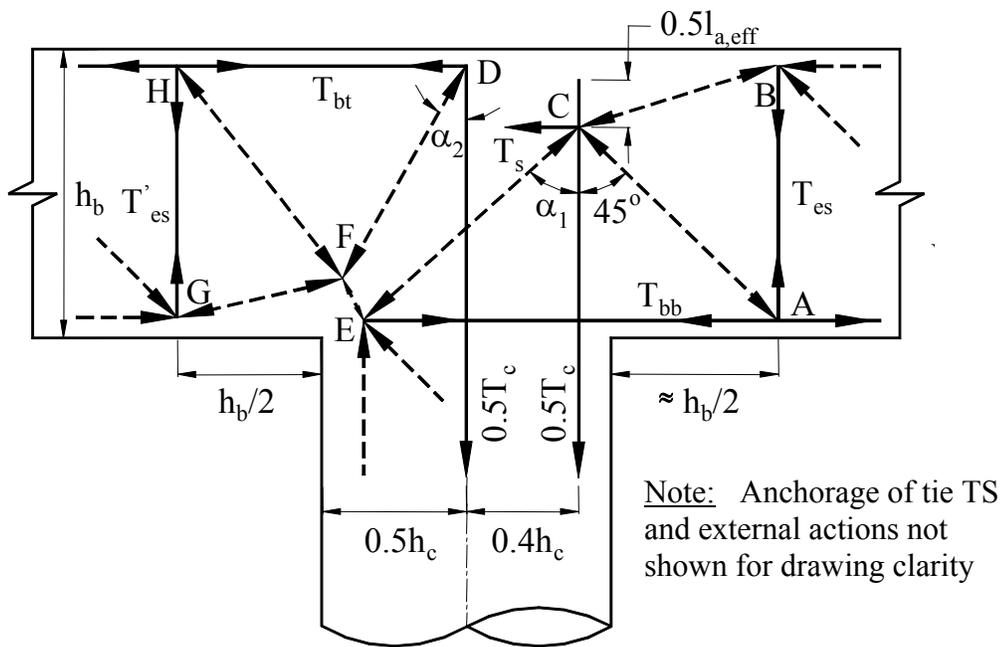
Figure 0-8. Joint Force Transfer Model (Sritharan, 1999)
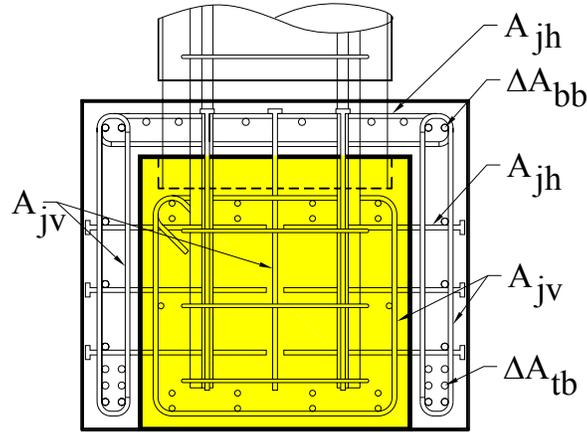
Figure 0-9. Joint Shear Reinforcements

1.12.3. Additional Longitudinal Reinforcement

Based on the strut and tie model presented in Figure 0-8 (Sritharan, 1999), additional longitudinal reinforcement is required to resist the joint shear forces and must be placed in the bent cap. As such, in addition to the required longitudinal reinforcement to satisfy flexural requirements, the area of additional top, ΔA_{tb}, and bottom, ΔA_{tb}, longitudinal reinforcement required was:

$$\Delta A_{tb} = 0.17\lambda_0 A_{sc} \frac{f_{yc}}{f_{yb}} = 0.17 \times 1.0 \times 12 \times 819.4 \times \frac{519}{493} = 1,759\, mm^2 \tag{0-13}$$

$$\Delta A_{bb} = 0.15\lambda_0 A_{sc} \frac{f_{yc}}{f_{yb}} = 0.15 \times 1.0 \times 9832.8 \times \frac{519}{493} = 1,552\, mm^2 \tag{0-14}$$

Where λ_0 is the material over-strength factor equal to 1.4 when the reinforcement design yield stress is used, otherwise $\lambda_0 = 1.0$, A_{sc} is the area of the column longitudinal reinforcement, f_{yc} is the column longitudinal reinforcement yield stress, and f_{yb} is the bent cap longitudinal reinforcement yield stress. It is required that this reinforcement be provided in addition to the reinforcement required to increase the yield moment capacity of the bent cap given by Eq. (0-2). Using a column longitudinal reinforcement of 12-D32 with a tested grade, f_{yc}, of 519 MPa, a tested grade for the additional bent cap longitudinal reinforcement (D19) of 493 MPa, along with using $\lambda_0 = 1.0$, the required limits for ΔA_{tb} and ΔA_{bb} were 1,759 mm^2 (7-D19) and 1,552 mm^2 (6-D19), respectively. From the bent cap longitudinal reinforcement provided, and subtracting the reinforcement required for the flexural capacity of the bent cap, 9-D19 and 7-D19 were available for ΔA_{tb} and ΔA_{bb}, respectively, which exceeds the required limits of 7 and 6, respectively.

1.12.4. Additional Internal and External Vertical Reinforcement

Based on the selected strut and tie model, the area of internal vertical joint shear reinforcement, A_{jv}^{int}, required within the joint region was (Silva 1999)

$$A_{jv}^{\text{int}} = 0.095\lambda_0 A_{sc} \frac{f_{yc}}{f_{yv}} = 0.095 \times 1.0 \times 9832.8 \times \frac{519}{506} = 958\,mm^2 \text{ (Internal)} \qquad (0\text{-}15)$$

Where f_{yv} is the yield stress of the vertical stirrups. In addition, an area of external vertical joint shear reinforcement, A_{jv}^{ext}, was placed at a distance of H_b away from the column face (Silva 1999) given by

$$A_{jv}^{ext} = 0.125\lambda_0 A_{sc} \frac{f_{yc}}{f_{yv}} = 0.125 \times 1.0 \times 9832.8 \times \frac{519}{506} = 1,261\,mm^2 \text{ (External)} \qquad (0\text{-}16)$$

For the design of the internal and external joint shear reinforcement D13 closed stirrups were used. With a tested grade for the closed stirrups of 506 MPa the required A_{jv}^{int} was 958 mm^2 or 8 legs of D13, and A_{jv}^{ext} was 1261mm^2 or 10 legs of D13, respectively. Referring to Figure 0-1 and Figure 0-10, outside the joint region and within a distance of H_b, four D13 closed stirrups were provided on either side of the existing bent cap and within the joint three D13 stirrups were provided on either side of the existing bent cap, which exceeds the required reinforcement to satisfy A_{jv}^{int} and A_{jv}^{ext}, respectively.

1.12.5. Additional Horizontal Reinforcement

As in the previous two sections and based on the selected strut and tie model, an area of horizontal joint shear reinforcement, A_{jh}, was required within the joint region (Silva, 1999). In the design of new joints this reinforcement is typically provided in the form of spirals or hoops around the column longitudinal reinforcement and installed along the anchorage length of the column longitudinal reinforcement.

In other retrofit projects this reinforcement is typically provided in the form of U-shaped hoops, but in this case the entire concrete within the joints must be removed in order to install the reinforcement. In this research program a different detail was implemented in which the horizontal reinforcement was provided in the form of horizontal headed reinforcement that was embedded in pre-drilled holes; thus, avoiding the need to remove any concrete from the joints and speeding up the construction process. Design of this headed reinforcement is discussed next.

Headed reinforcement was placed on all surfaces between the as-built and the retrofit sections. As such, the headed reinforcement extended halfway into the bent cap to form a mechanism to confine the concrete in the joint region due to insufficient detailing of the as-built section. This headed reinforcement was also effective in providing shear flow between the as-built section and the retrofit section ensuring composite action between these two sections. In addition, as shown

in Figure 0-1, horizontal D13 closed stirrups were also placed across the top of the bent cap and outside of the joint region to confine this portion of the retrofit bent cap.

Vertical headed reinforcement was also added on the top surface of the bent cap. According to this detailing the headed reinforcement extended to a depth equal to the depth of the anchorage length of the column longitudinal reinforcement. This vertical reinforcement was placed near the middle of the bent cap to ensure that the compression struts formed from the column longitudinal reinforcement, as shown in Figure 0-11, are balanced by the ties that develop from this vertical headed reinforcement.

Priestley (1996) recommends a clamping confining pressure required to prevent excessive transverse strains in the concrete be no less than

$$f_l = 0.5\rho_s f_{sh} = \frac{0.23\lambda_0 A_{sc} f_{yc}}{D_c' l_a} \tag{0-17}$$

Where f_l is the confining pressure, ρ_s is the volumetric transverse reinforcement ratio, f_{sh} is the stress in the confining steel, l_a is the anchorage length of the column longitudinal reinforcement in the joint region ($l_a = 0.7 \, h_b$), and D_c' is the diameter of the column concrete core. To prevent pullout of the column reinforcement, Priestley recommends limiting the strain in the concrete to 1.5 mm/m, which also leads to limiting the strain in the reinforcing hoops to 1.5 mm/m. For Grade 60 steel, this strain value is below the yield strain which due to force equilibrium leads to

$$A_{st} 0.0015E_s = 0.23\lambda_0 A_{sc} f_{yc} \Rightarrow A_{st} = \frac{0.23 \times 1.0 \times 9832.8 \times 519}{0.0015 \times 188,900} = 4,142 \, mm^2 \tag{0-18}$$
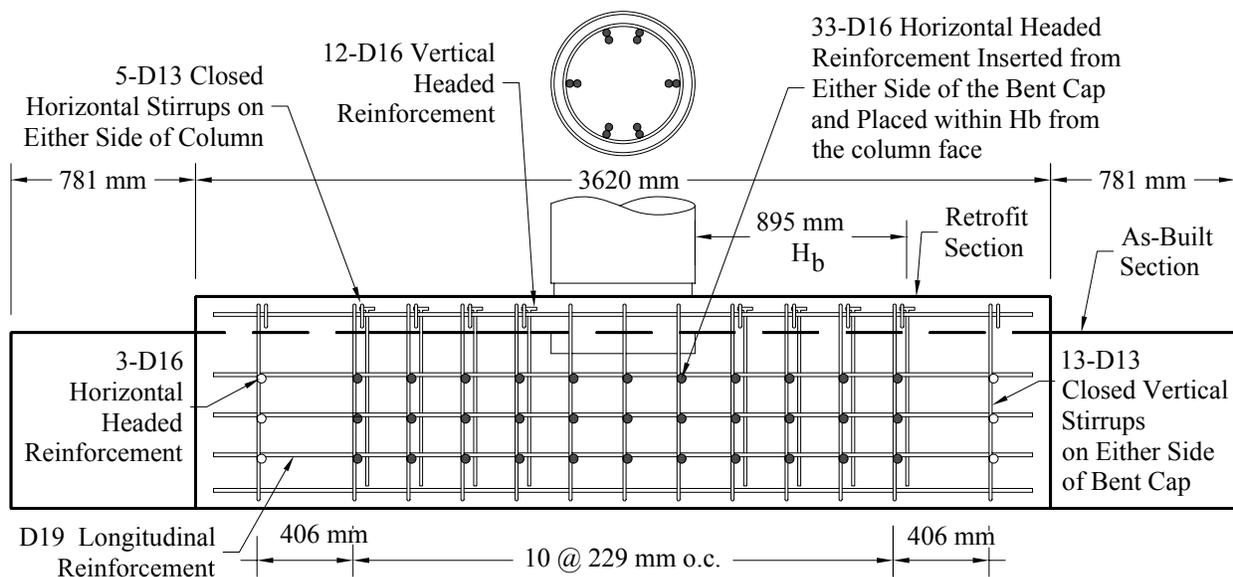
Note: As-built reinforcement not shown for drawing clarity

- 24 -

(a) Side View
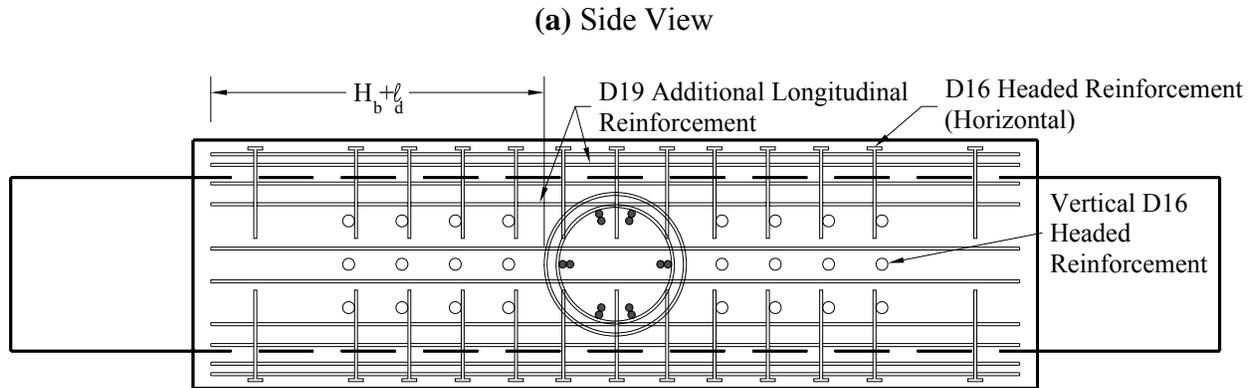
Note: Only headed and longitudinal reinforcement are shown for drawing clarity

(b) Top view

Figure 0-10. Unit 1 Bent Cap Reinforcement Layout
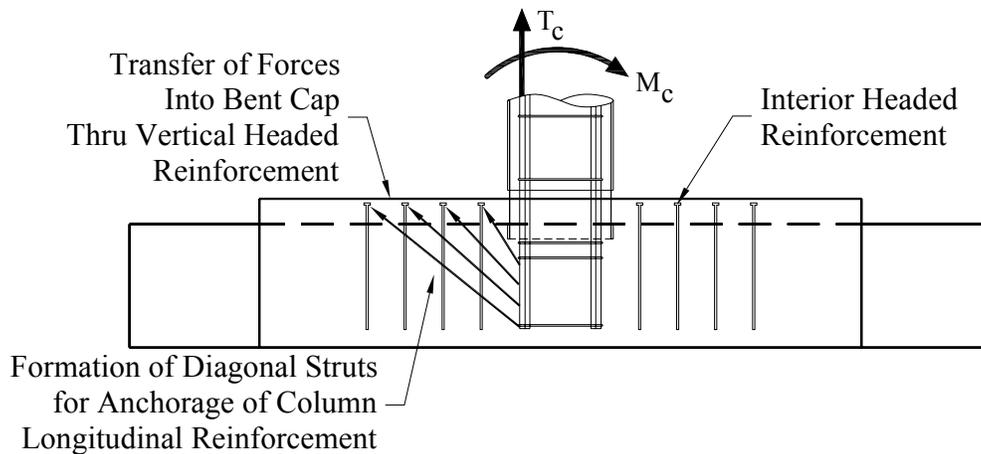
Figure 0-11. Column Strut Forces

For this retrofit, using the tested ultimate strength of the column longitudinal reinforcement of 671 MPa and the tested modulus of elasticity of 189 GPa, leads to a required transverse reinforcement area, A_{st}, of 4,142 mm², which was provided by at least 20-D16. Figure 0-1 shows the final retrofit cross-section with the longitudinal reinforcement provided to increase the elastic moment capacity and additional vertical and horizontal joint shear reinforcement, where the spacing of the stirrups and headed reinforcement are shown in Figure 0-10.

1.13. CONSTRUCTION OF THE AS-BUILT SECTION

As previously discussed, the as-built section was identical in all the three test units. A brief description of the steps used in the construction of the as-built section is described next.

Initially, the bent cap and column reinforcement cages were assembled (see Figure 0-12 and Figure 0-13). This was followed by placing bent cap reinforcing cage inside the form work and

installation of the column reinforcement cage and steel shell casing, as shown in Figure 0-14 thru Figure 0-16, respectively. With the column reinforcement cage and steel shell casing in place, the next step consisted of casting first the bent cap, as shown in Figure 0-17. As a final step in the construction of the as-built sections, the load stub was assembled, followed by casting of the column and load stub simultaneously (see Figure 0-18). The completed as-built section before any modifications is shown in Figure 0-19.

Figure 0-12. Column & Cap Reinforcing Cage

Figure 0-13. Bent Cap Reinforcing Cage

Figure 0-14. Bent Cap Inside Form Work

Figure 0-15. Colum Reinforcing Cage

Figure 0-16. Installation of Column Cage

Figure 0-17. Casting of the Bent Cap

Figure 0-18. Construction of the Load Stub

Figure 0-19. Completed As-Built Section

1.14. CONSTRUCTION OF UNIT 1 UPGRADE SECTION

As previously discussed, after the as-built section was constructed, modifications were
implemented in order to install the retrofit section reinforcement. As such, after the form work
for the as-built section was removed (see Figure 0-19), the first step in the retrofit operation
consisted of cutting the steel shell followed by cutting the column longitudinal reinforcement.
This procedure is shown in Figure 0-2 and Figure 0-20. Next, the headed reinforcement was
embedded in predrilled holes thru the as-built section (see Figure 0-21) by using U.S Anchor
Corp.'s HS-200 epoxy, which is a rapid setting high strength structural epoxy.

From an installation procedure, before embedding the headed reinforcement in the predrilled holes, these holes were first cleaned with compressed air in order to remove any loose particles or dust. Then the epoxy was injected into each hole until it was approximately half full. The rebar was inserted with a twisting motion to avoid any air voids. The installed headed reinforcement for the retrofit section is shown in Figure 0-21. As a procedural recommendation, the headed reinforcement should be installed before any other reinforcement is placed around the existing bent cap.

After the epoxy had cured, the retrofit longitudinal and vertical steel was tied in place as shown in Figure 0-22 to Figure 0-24. The retrofit bent cap was then formed and the concrete was poured (see Figure 0-25). Finally, the retrofitted Unit 1 before testing is shown completed in Figure 0-26.

Figure 0-20. Cutting Steel Shell Casing

Figure 0-21. Installing Headed Reinforcing

Figure 0-22. Retrofit Section Reinforcing Cage

Figure 0-23. Joint Region Detail

Figure 0-24. Retrofit Section Reinforcing Cage

Figure 0-25. Forming Retrofit Section
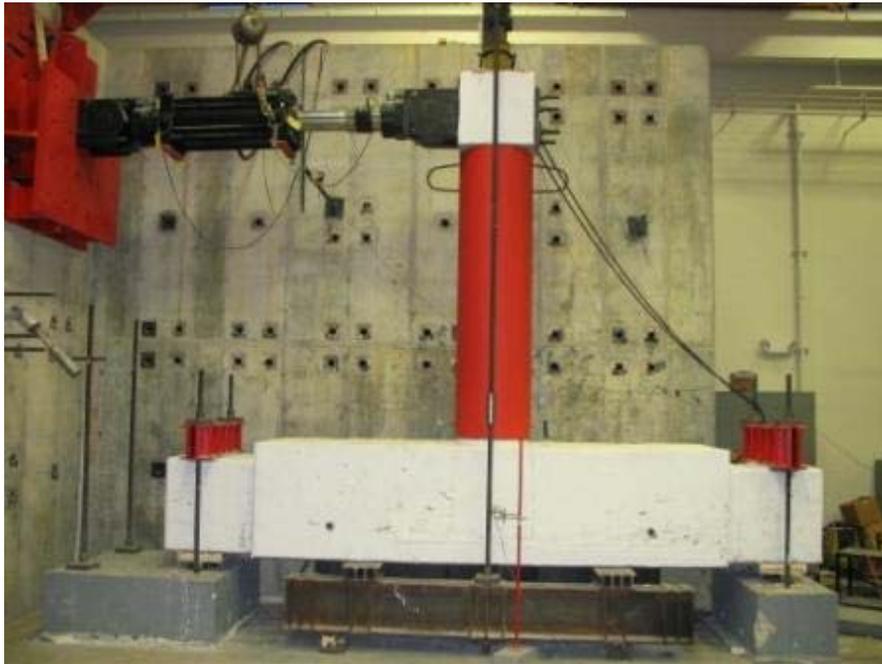
Figure 0-26. Completed Unit 1 Before Testing

Following testing of Unit 1 a few modifications were implemented for the construction of Unit 2. The main objective for these modifications was to increase the shear force transfer capacity through the joint and to improve the response of the test unit under cyclic loading. Listing of these modifications are described next.

First in Unit 2, the horizontal headed reinforcement through the joint region was installed as a single piece instead of two separate pieces. In Unit 1 the headed reinforcement was installed from either side of the bent cap leaving a gap between the headed reinforcement inside the joint region, as shown in Figure 0-1. Although this detailing provided for an easier construction practice as discussed in Section 1.26, this detail was not suitable for preventing excessive dilations in the transverse direction of the bent cap. In order to accomplish this construction layout in one of the sides of this reinforcement the head was welded to the rebar and at the other end threads were used for the installation of the closing head. This type of headed reinforcement is commonly produced by companies specializing in the production of headed reinforcement. Figure 0-1 shows the continuous headed reinforcement running through the transverse direction of the bent cap.
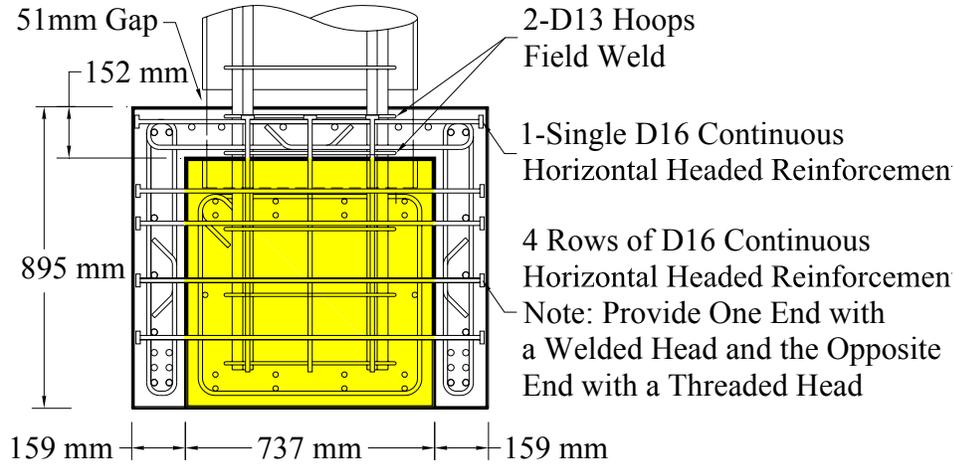
Figure 0-1. Unit 2 Retrofit Cross-Section

Second, during testing of Unit 1, it was observed that the column longitudinal reinforcement began to buckle immediately after crushing of the cover concrete as a result of insufficient transverse reinforcement within the gap region. In order to improve the anti-buckling resistance for the longitudinal reinforcement two additional D-13 field welded hoops were provided within the steel shell gap region. This detail will be further discussed in the next section or Section 1.15.

Finally, during the final stages of testing of Unit 1 wide open cracks were observed in the bent cap near the column interface. As such, the following modifications were implemented as shown in Figure 0-2: (1) the D16 horizontal headed reinforcement within the joint region were placed at a much closer pattern near the joint, (2) an additional headed rebar was installed through the gap region and within the column longitudinal reinforcement, and (3) an additional D13 closed stirrup was provided on either side of the bent cap. The retrofit cross-section and reinforcing layout for the second unit are shown in Figure 0-1 and Figure 0-2.
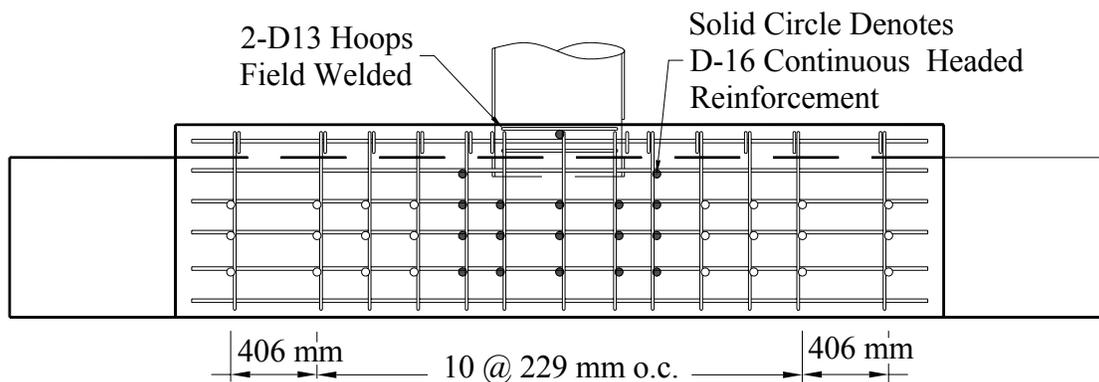
Figure 0-2. Unit 2 Retrofit Reinforcement Layout

1.15. CONSTRUCTION OF UNIT 2 UPGRADE SECTION

As in Unit 1, after the as-built section was constructed, modifications were implemented in order to install the retrofit section reinforcement. As before, the first step in the retrofit operation consisted of cutting the steel shell followed by cutting the column longitudinal reinforcement (see Figure 0-3). Unlike Unit 1, in Unit 2, the next step consisted of removing first all of the concrete cover surrounding the column longitudinal reinforcement, as shown in Figure 0-3 and Figure 0-4.

Next, the continuous horizontal and vertical headed reinforcement was embedded in predrilled holes but in this unit the holes were predrilled through the entire width of the bent cap as-built section. After installation of the headed reinforcement the closing head was threaded followed by installation of the remaining reinforcement, as shown in Figure 0-5 and Figure 0-6. Installation of the headed reinforcement and completion of the construction of the upgrade section followed the same procedures outlined in Section 1.14.

Figure 0-3. Detail at Bent Cap Interface

Figure 0-4. Detail at Bent Cap Interface

Figure 0-5. Bent Cap Retrofit Section

Figure 0-6. Bent Cap Retrofit Section

1.16. INTRODUCTION

A modified version for the upgrade section was implemented for the third unit, and these modifications are described in this section. As discussed in Section 1.33, the continuous reinforcement though the joint region was adequate in preventing dilation of the bent cap in the transverse dilation; however, strength degradation in Unit 2 was still recorded as a result of inelastic actions within the joint region and buckling of the column longitudinal reinforcement at a displacement ductility level close to 6. As such in the third test unit the steel shell gap was reduced from 52mm to 13mm, and the horizontal headed reinforcement was replaced by post-tensioned rods to further enhance the joint performance. The retrofitted cross-section and the reinforcing layout for Unit 3 are shown in Figure 0-1 and Figure 0-2.
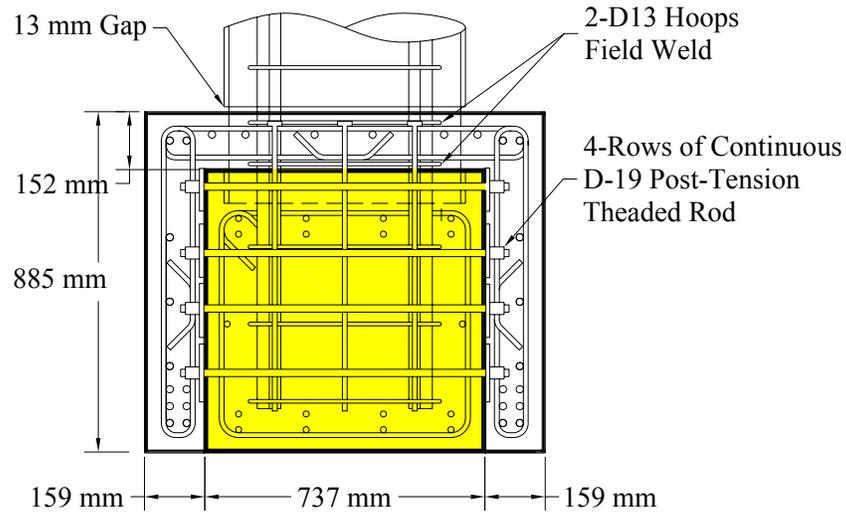
Figure 0-1. Unit 3 Retrofit Cross-Section
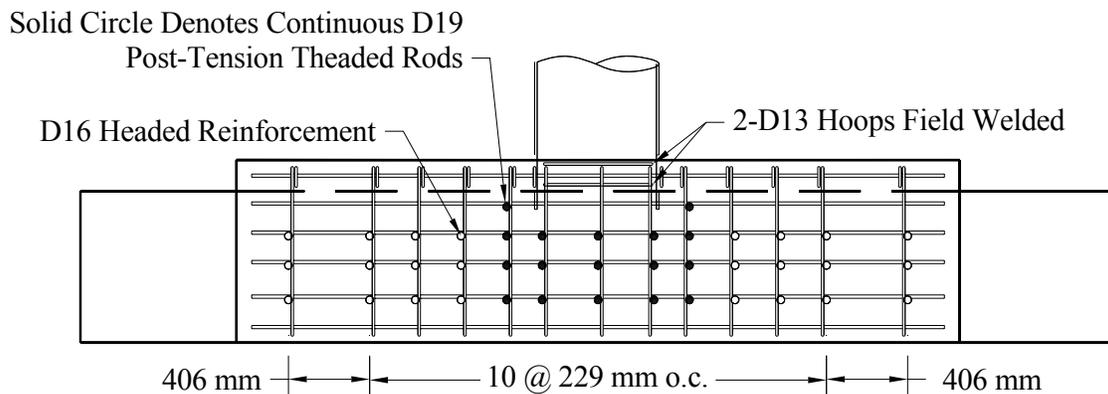
Figure 0-2. Unit 3 Retrofit Reinforcement Layout

Since transverse stresses are only effective in improving the joint shear capacity and the bond strength of the column longitudinal reinforcement, the post-tensioned rods were only used within the joint region, as shown in Figure 0-3. Also by placing the pre-stressing rods throughout the length of the bent cap would not provide for further enhancement to the joint region. Each pre-stressing rod was 19 mm in diameter, with a yield strength of 517 MPa according to the manufacturer. The pre-stressing rods were stressed to 60% of f_y by tightening a nut at each end of the rod. The stress on the rods was measured by a calibrated torque wrench. The stressed joint for Unit 3 is shown in Figure 0-3.
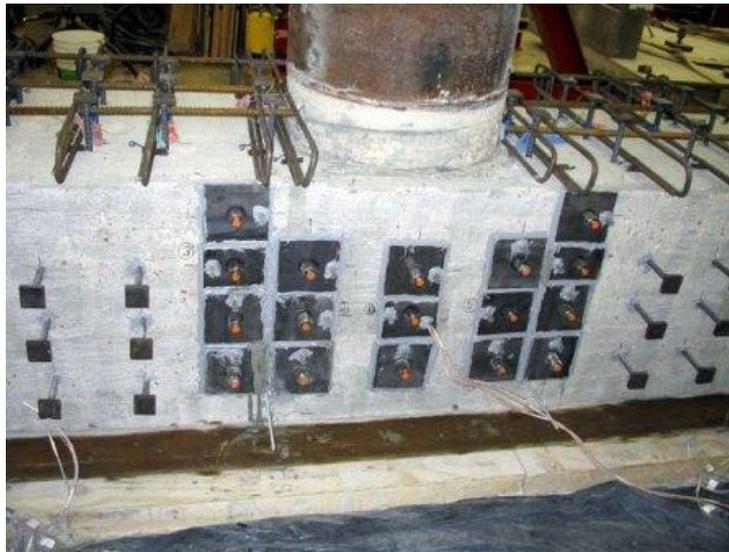
Figure 0-3. Unit 3 Pre-stressed Joint

1.17. MOMENT-CURVATURE ANALYSIS

Since the steel shell gap in the column of Unit 2 was identical to Unit 1 the moment curvature analysis for these two units' column was identical. In Unit 3 the steel shell gap was reduced from 51mm to 13mm and, as a result, a new moment-curvature analysis was performed for this unit's column. Results of this analysis are shown in Figure 0-4. In this unit, the column moment curvature analysis was nearly the same as in the previous two units to the exception that the concrete compression block was assumed confined by an equivalent spiral size and pitch of 13x13 mm and 13 mm, respectively.

The moment curvature analysis for the test units are shown in Figure 0-4 and relevant data is outlined in Table 0-1. In Unit 3 the ultimate moment demand for the modified column section was computed at 1,588 kN-m with an ultimate curvature ductility capacity of approximately 18, which was the same for the previous two units.
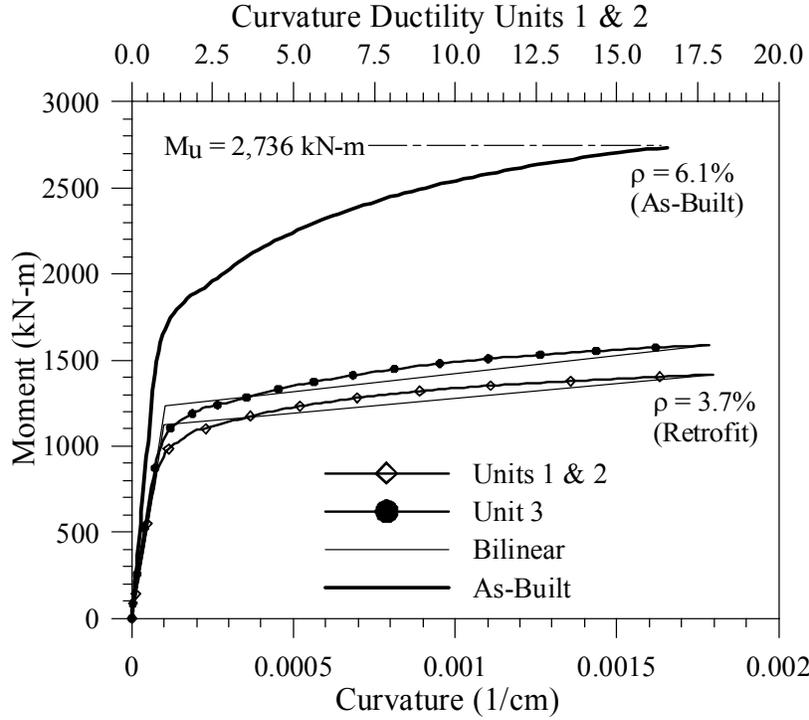
Figure 0-4. Unit 3 Moment-Curvature

Table 0-1. Bilinear Moment Curvature

Unit No.	First yield		Theoretical Yield		Ideal		Ultimate		
	ϕ'_Y (1/m)	M'_Y (kN-m)	ϕ_Y (mm)	M_Y (kN-m)	ϕ_I (1/m)	M_I (kN-m)	ϕ_U (1/m)	M_U (kN-m)	μ_ϕ
1 & 2	0.00007	790	0.00010	1125	0.00035	1168	0.00180	1,414	18
3	0.00008	903	0.00010	1232	0.00038	1290	0.00179	1,588	

1.18. JOINT PRINCIPLE STRESS DETERMINATION

Due to the additional pre-stress in the transverse direction, a principle stress analysis was implemented for a 3-dimensional stress cube, as shown in Figure 0-5. For a 3-D analysis the principle stresses are obtained by solving the determinant of the following stress matrix in terms of the scalar λ

$$\begin{vmatrix} \sigma_{xx} - \lambda & \tau_{xy} & \tau_{xz} \\ \tau_{yx} & \sigma_{yy} - \lambda & \tau_{yz} \\ \tau_{zx} & \tau_{zy} & \sigma_{zz} - \lambda \end{vmatrix} = 0 \qquad (0\text{-}1)$$

Where λ are the three principle stresses, σ_{xx} is zero because there is no pre-stressing in the longitudinal direction of the bent cap, σ_{yy} is just f_a and is the stress due to the axial load, σ_{zz} is the stress due to the transverse stress force, τ_{xy} is equal to v_j and is the shear stress due to the applied

- 35 -

column moment, and τ_{xz} and τ_{zy} are assumed zero or negligible due to the unidirectional applied column bending moment and that the applied pre-stress forces do not result in any significant shear stresses in these planes.
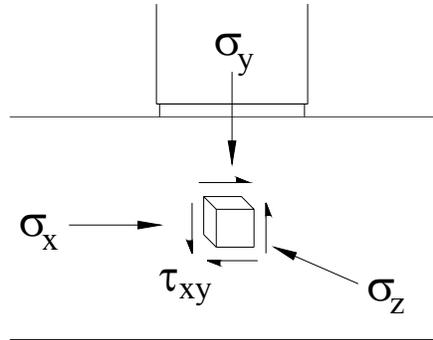
Figure 0-5. 3-D Stress Cube

As such, the determinant of Eq. (0-1) reverts to Eq. (0-12), which indicates that pre-stressing in the transverse direction has no effect on the joint principle compressive, p_c, and tensile, p_t, stresses in the longitudinal direction but only increases the joint principle compression stress in the transverse direction.

As before, with an applied axial load on the column equal to 710 kN and referring to Eq. (0-9) the axial stress, f_a, is 0.82 MPa. Given the column's predicted ultimate moment capacity of 1,588 kN-m (see Table 0-1), the shear force in the joint, V_h, is

$$V_h = \frac{M_c^F}{d} \approx \frac{M_c^F}{0.8h_b} = \frac{1588\,kN-m}{0.8 \times 0.895\,m} = 2,218\,kN \qquad (0\text{-}2)$$

Referring to Section 1.12, the joint shearing stress, v_j, is then

$$v_j = \frac{V_h}{b_{je}D_c} = \frac{2218\,kN}{0.826\,m \times 0.584\,m} = 4.60\,MPa \qquad (0\text{-}3)$$

As a last step, using the results from Eqs. (0-9) and (0-3), the principle stresses are then given by

$$p_c, p_t = \frac{f_a}{2} \pm \sqrt{\frac{f_a^2}{4} + v_j^2} = \frac{0.82}{2} \pm \sqrt{\frac{0.82^2}{4} + 4.60^2} = 5.02, -4.21(MPa) \qquad (0\text{-}4)$$

As before, normalizing the results of Eq. (0-4) in terms of the specified nominal concrete strength, f'_c, of 34.5 MPa yields the normalized principle compressive, p_c, and tensile stresses, p_t, of $0.15f'_c$ and $0.72\sqrt{f'_c}$.

As before, joint principle tensile stresses, p_t, were then computed using the entire moment curvature envelope based on the retrofitted column section shown in Figure 0-4, and the normalized principle compressive and tensile stresses at ultimate were $0.15 f_c'$ and

$0.72\sqrt{f_c'}$ respectively. The principle tensile stresses were then normalized and plotted versus the curvature of the column as shown in Figure 0-6. Again the principle tensile stresses, p_t, exceed the limits stipulated by Eq. (0-7) and full joint shear reinforcement was required for design of the joint. It is important to note that although pre-stressing in the transverse direction does not lead to a reduction in the principle tensile stresses or demand in the joint, these stresses without a doubt will increase the bond strength of the column longitudinal reinforcement and ultimate the joint shear capacity. This suggests that a different moment rotation capacity should be proposed for units retrofitted according to the design details illustrated in this section.
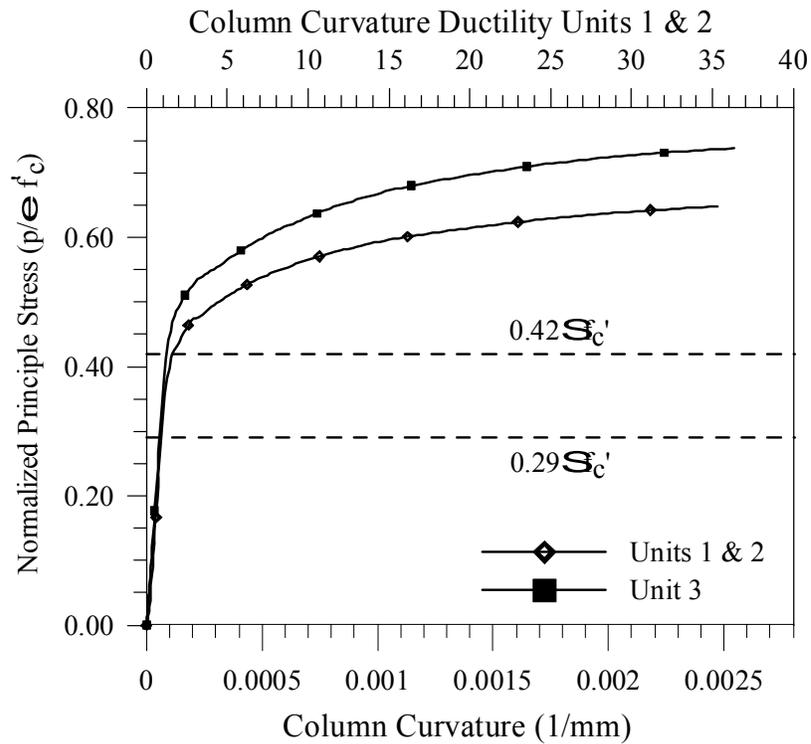
Figure 0-6. Unit 3 Principle Stresses

1.19.   CONSTRUCTION OF UNIT 3 UPGRADE SECTION

As before, the first step in the construction of the upgrade section consisted of cutting a portion of the steel shell and the designated column longitudinal bars similar to the procedure shown in Figure 0-20. As specified, in this unit, the gap region was reduced to 13 mm.

As in Unit 2, the horizontal and vertical headed reinforcement were embedded in predrilled holes, as shown in Figure 0-7 and Figure 0-8. Installation of the headed reinforcement followed the same procedure outlined in Section 1.14. After installation of the headed reinforcement the pre-stress rods were installed and stressed by tightening a nut at each end of the rods. The stressed joint for Unit 3 is shown in Figure 0-3. Then, the retrofit longitudinal and vertical steel was tied in place similar to Figure 0-22 and Figure 0-24, followed by forming and casting the upgrade section (see Figure 0-9). The completed Unit 3 during testing is shown in Figure 0-10.
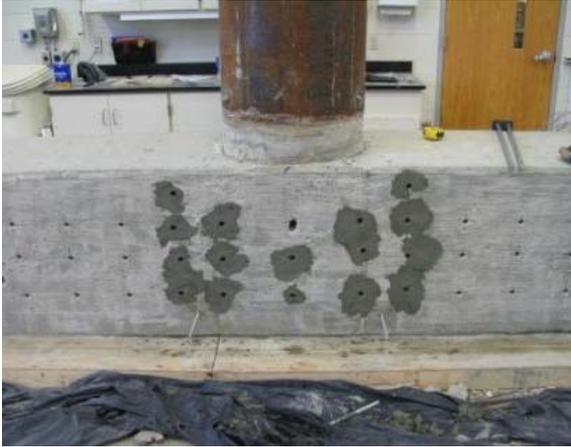
Figure 0-7. Pre-Drilled Holes

Figure 0-8. Installed Headed Reinforcement

Figure 0-9. Unit Before Casting of Upgrade Section
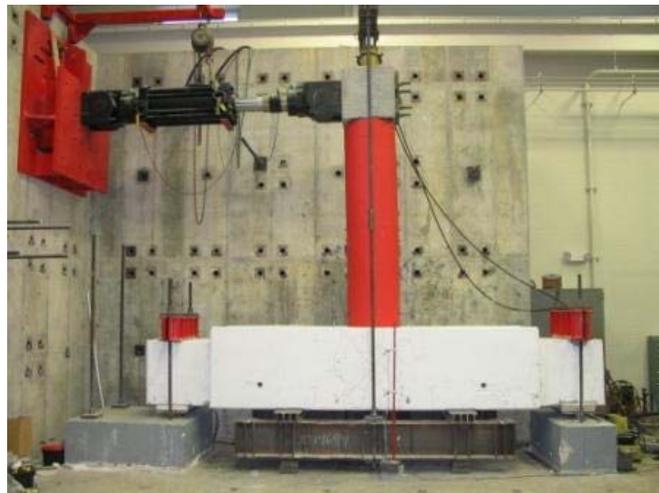
Figure 0-10. Completed Test Unit

For each test unit, strain gauges were placed on the reinforcing steel, linear variable differential transducers (LVDT's) were affixed to the joint, and load cells were placed to measure the axial force in the column. The actuator used had an internal LVDT and load cell to measure the lateral displacement and force applied to the load stub atop the column. All instruments were connected to a data acquisition system that took data at preset time intervals. A detailed description of the instrumentation used is presented in the next three sections.

1.20. STRAIN GAUGES

Strain gauges were placed on the reinforcing steel of the as-built and the retrofit section, as shown in Figure 0-1 through Figure 0-7. Instrumentation of these reinforcement consisted of electric resistance strain gages produced by Tokyo Sokki Kenkyujo Co., Ltd. These strain gauges have a gage length of 5mm and a gage resistance of $120\pm0.3\Omega$.

1.20.1. Column Section

A description of the strain gauges mounted on the column reinforcement is discussed in this section. As shown in Figure 0-1, a total of 12 gauges were applied on the column longitudinal reinforcement, and 6 and 8 strain gauges were positioned vertically and horizontally in the steel shells, respectively.
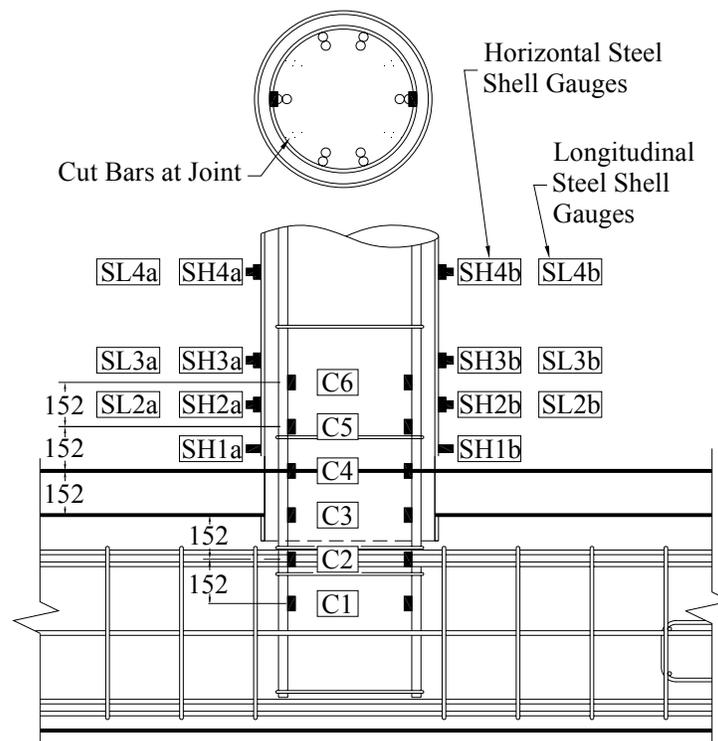
Figure 0-1. Column Reinforcement and Steel Shell Strain Gauges

1.20.2. Bent Cap As-Built Section

A description of the strain gages mounted on the bent cap as-built section reinforcement is discussed in this section. As shown in Figure 0-2, a total of 16 gauges were applied on the as-built section longitudinal reinforcement, and as shown in Figure 0-3, 6 strain gauges were positioned on the as-built section stirrups.
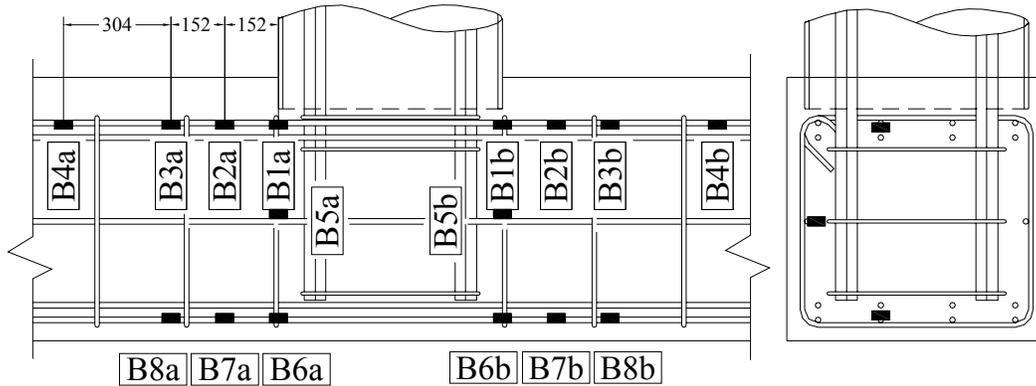
Figure 0-2. As-Built Bent Cap Strain Gauges
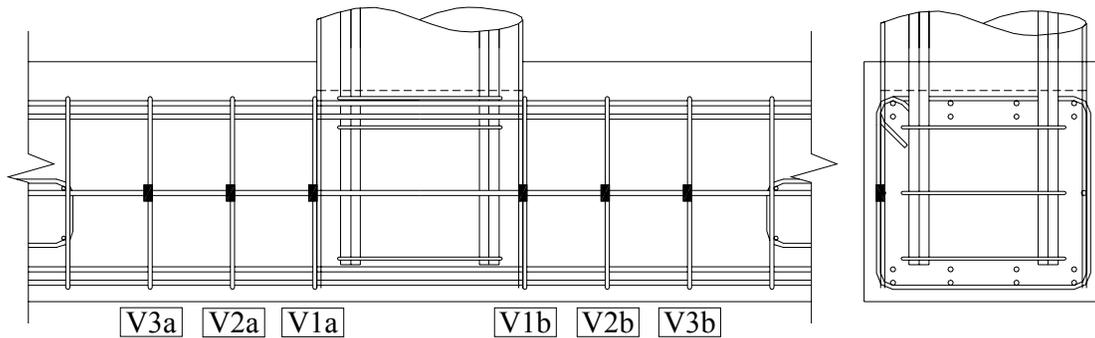
Figure 0-3. As-Built Bent Cap Shear Strain Gauges

1.20.3. Bent Cap Retrofit Section

A description of the strain gauges mounted on the bent cap upgrade section reinforcement is discussed in this section. As shown in Figure 0-4, a total of 16 gauges were also applied on the new section longitudinal reinforcement, and as shown in Figure 0-5, Figure 0-6, and Figure 0-7 15 strain gauges were positioned on the as-built section stirrups, 16 strain gauges were positioned on the horizontal headed reinforcement and 6 strain gauges were positioned on the vertical headed reinforcement.
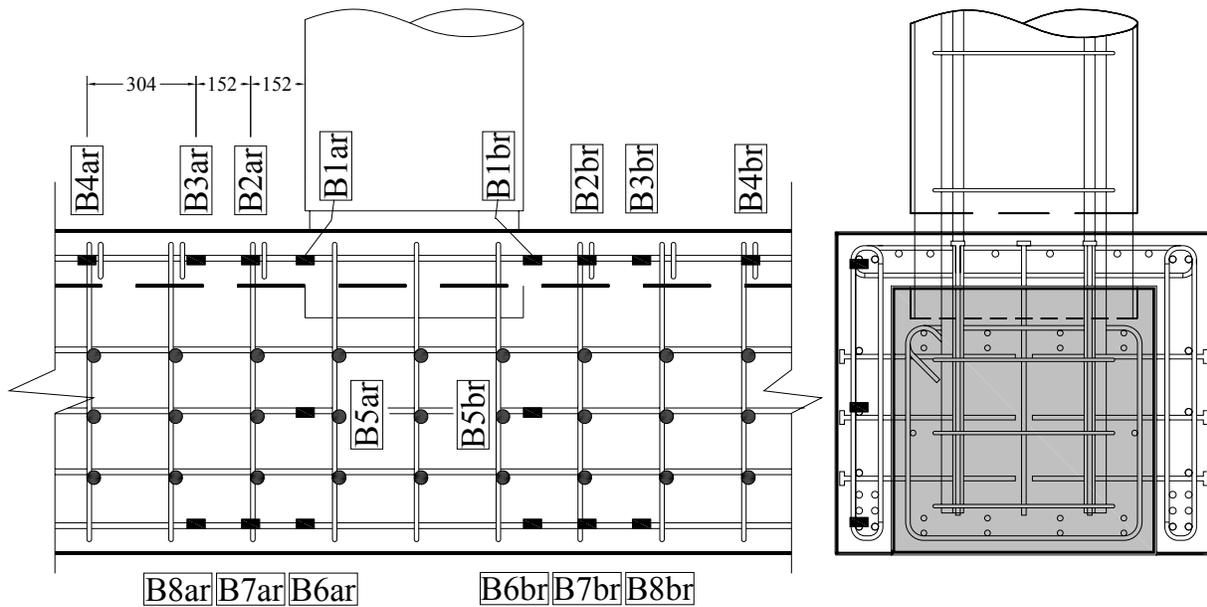
Figure 0-4. Retrofit Bent Cap Strain Gauges
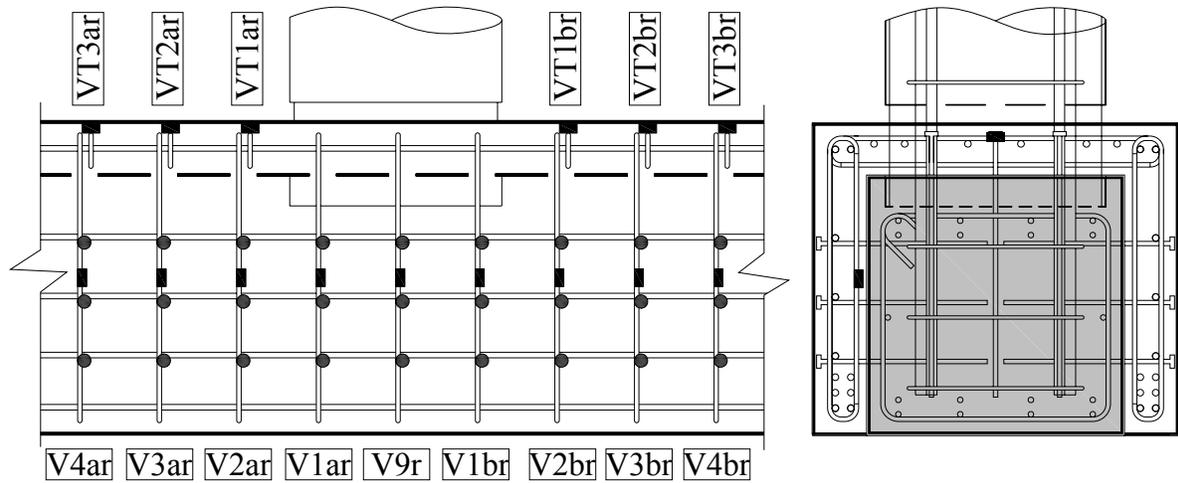
Figure 0-5. Retrofit Bent Cap Shear Strain Gauges
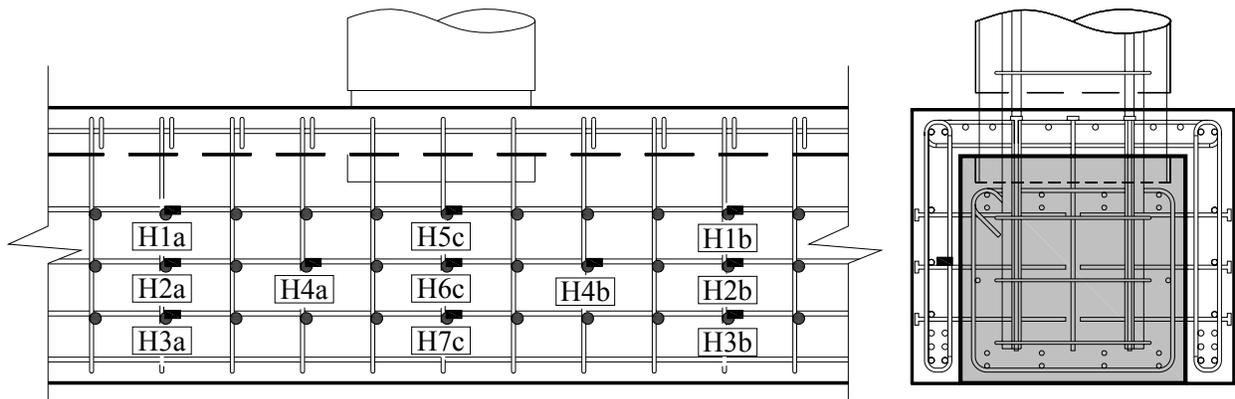
Figure 0-6. Retrofit Transverse Headed Reinforcement Strain Gauges
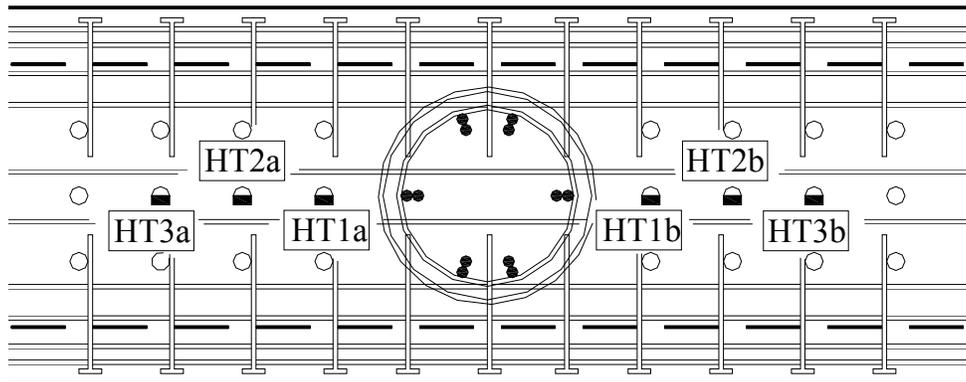
Figure 0-7. Retrofit Vertical Headed Reinforcement Strain Gauges

1.21. LOAD CELLS

Two load cells were placed on top the reaction beam used to apply the axial load into the column as shown in Figure 0-8. The axial load was held constant by a hydraulic pump with a control valve applying a constant pressure to the hydraulic jack placed on top of the column.
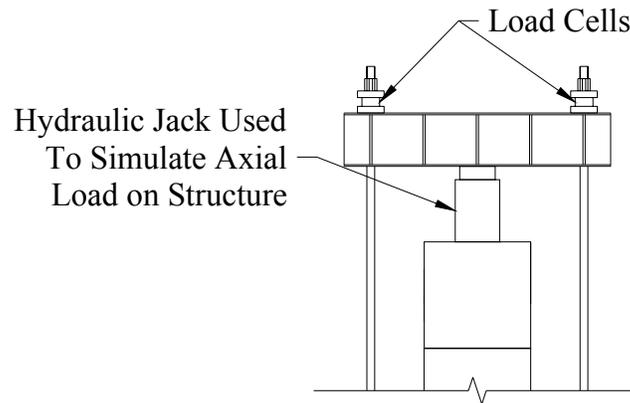
Figure 0-8. Load Cells for Axial Load

1.22. LVDT'S

A total of 14 LVDT's were placed across the joint to measure the joint shear as shown in Figure 0-9. The deformations from LVDT's JHt, JHb, JVb, JVa, J1, and J2 were used to calculate the joint shear deformations and strains according to Figure 0-10.
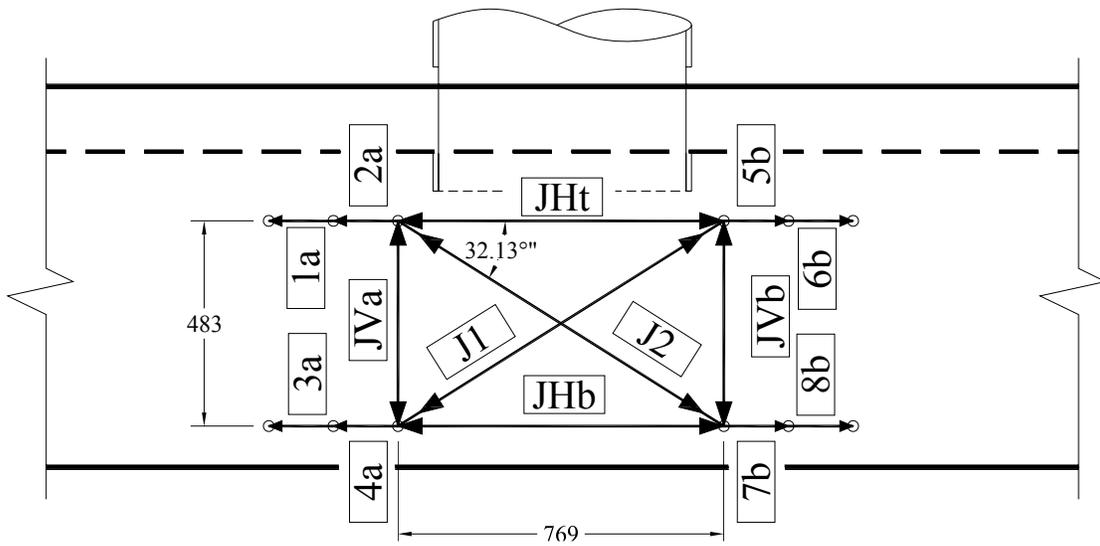
(a) Schematic

(b) Test Setup Installation

Figure 0-9. Joint LVDT's
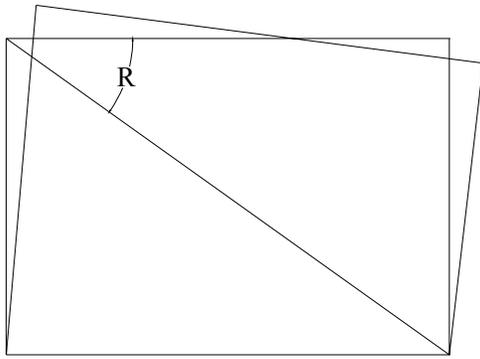
(a) Overall Deformation
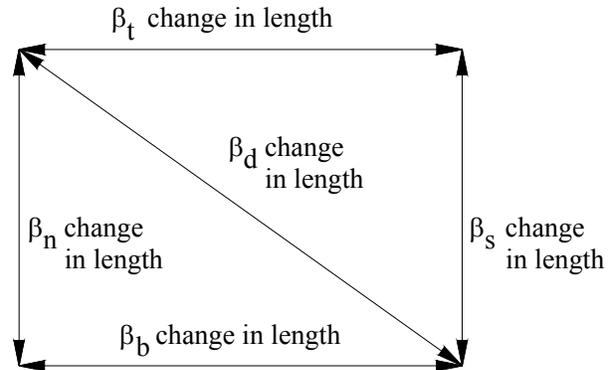
(b) Measured Deformations
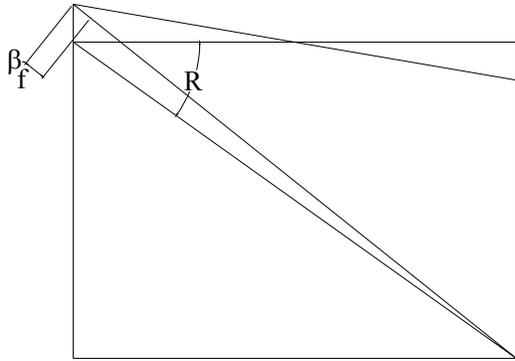
(c) Flexural Deformation
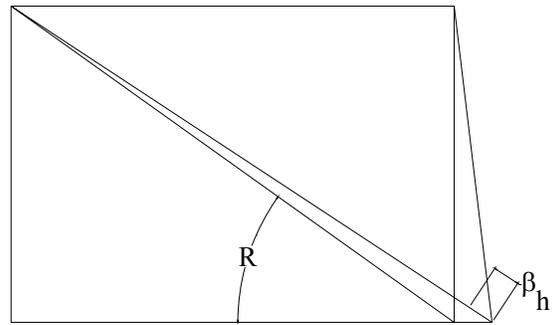
(d) Horizontal Deformation Due to Cracks
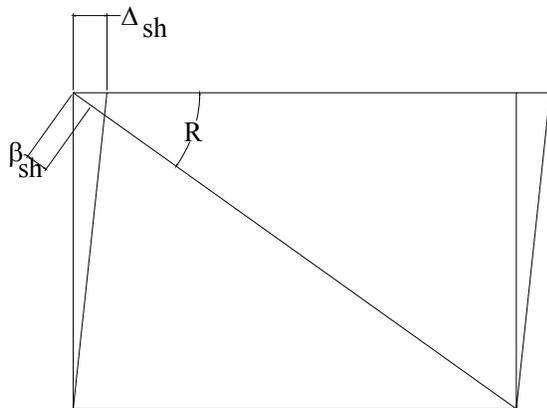
(e) Shear Deformation

$\beta_{sh} = \beta_d - \beta_f - \beta_h$

and hence : $\quad \Delta_{sh} = \beta_{sh} / \cos(R)$

where : $\quad \beta_f = \{ (\beta_n + \beta_s) / 2 \} \sin(R)$

and : $\quad \beta_h = \{ (\beta_t + \beta_b) / 2 \} \cos(R)$

Figure 0-10. Joint Strain Calculation

1.23. One-Component Nonlinear Giberson Model

The theoretical column top lateral deflection was established based on variables depicted in Figure 0-4, and according to the following expression:

$$\Delta V_i = \left(\frac{1}{K_{C,i}} + \frac{(L_c + H_b/2)^2}{K_{B,i}} \right)^{-1} \times \Delta D_i \tag{0-1}$$

Where ΔV_i and ΔD_i are the incremental column lateral load and top deflection, respectively, $K_{C,i}$ is the instantaneous tangential bending stiffness for the column bending response, and $K_{B,i}$ is the instantaneous tangential rotational stiffness of the bent cap contribution to the column top deflection expressed by Eq. (0-2). Furthermore in Eq. (0-1), the center of rotation of the bent cap was set at a distance of $H+H_b/2$, where H_b is the depth of the bent cap. The stiffness terms for the column and the bent cap were developed based on the one-component nonlinear Giberson model (Carr, 2000; Cheng, 2001). However, because of the test unit layout, this model was simplified for a base rotation due to the plastic hinge formation at one end only. As such, it was feasible to decouple the modes of deformation in the joint region in terms of plastic hinge plus bent cap rotation. In Eq. (0-1), the column and bent cap stiffness, $K_{C,i}$ and $K_{B,i}$, are, respectively:

$$K_{C,i} = \frac{3\, r_{i,C}\, EI'_C}{L_C^2 \left[L_C\, r_{i,C} + 3\, L_{p,C} \left(1 - r_{i,C} \right) \right]}$$

$$K_{B,i} = \frac{12\, r_{i,B}\, EI'_B}{\left[L_B\, r_{i,B} + 6\, L_{p,B} \left(1 - r_{i,B} \right) \right]} \tag{0-2}$$

Referring to Figure 0-4, L_C is the column height measured from the centerline of the applied lateral load to the bent cap interface (i.e. $L_C = 2.72$ m), L_B is the length of the bent cap measured between supports blocks A and B (i.e. $L_B = 4.57$ m), and for the as built units $L_{p,C}$ and $L_{p,B}$ are the column and bent cap plastic hinge lengths and were computed based on the expressions developed by Priestley *et al.* (1995), which are given by the member height, rebar diameter and yield strength. In addition, $r_{i,C}$ and $r_{i,B}$ are the column and bent cap instantaneous stiffness ratios, and EI_C' and EI_B' are the column and bent cap secant yield stiffness obtained from the column and bent cap moment curvature analyses. These quantities were further evaluated based on:

$$r_{i,C} = \frac{\Delta M_{i,c}/\Delta\phi_{i,C}}{EI'_C} \qquad r_{i,B} = \frac{\Delta M_{i,B}/\Delta\phi_{i,B}}{EI'_B}$$

$$\text{and}$$

$$EI'_C = \frac{M_{Y,C}}{\phi_{Y,C}} \qquad EI'_B = \frac{M_{Y,B}}{\phi_{Y,B}} \tag{0-3}$$

In Eq. (0-3) when the column is in the elastic range r_i is one, and the expression for $K_{C,i}$ reverts to the bending stiffness of a cantilever member given by $EI'_C/3L_C^3$. The procedure given by Eq. (0-1) can be used without the need to compute in advance the yield and ultimate conditions, which makes it suitable for the seismic assessment of system with multiple members with hinging at one end only. Hinging at both ends is a significantly more complex approach and was not covered in this research.

Another attractive feature of the approach given by Eq. (0-1), is that the procedure is easily implemented for systems with multiple members responding within the inelastic range and for displacement control analysis, which were necessary conditions for this research program because the bent cap is likely to experience inelastic actions. Furthermore, in the Section 0 it will be shown that the influence of the inelastic deformations in the joint region will be easily handled with this approach.

1.24. FORCE-DISPLACEMENT RESPONSE

Using the moment curvature analyses for the column and the bent cap previously outlined in Sections 0 and 0 and using the model developed based on Eq. (0-1), the corresponding predicted force-displacement responses for Units 1, 2 and 3 was performed and results of this analysis are shown in Figure 0-1.
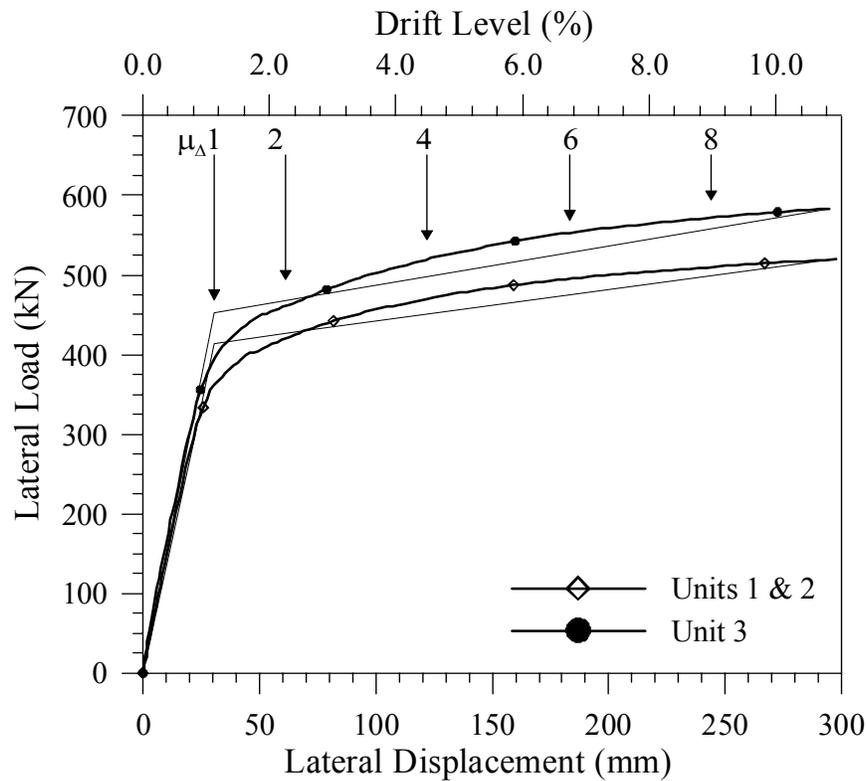

Figure 0-1. Predicted Force-Displacement Response of Units 1, 2 and 3

Table 0-1 outlines values from this analysis at first yield, and other performance levels. From the moment curvature analyses described in Section 1.10.1, and Figure 0-3 first yield of the section was defined at yielding of the column longitudinal reinforcement. The ideal capacity was defined at the moment that develops a strain of ε_c=0.5 mm/m in the extreme compression fibers of the columns. Allowing for low cycle fatigue of the column longitudinal reinforcement due to cyclic loading and recognizing that the steel shell provides adequate resistance to prevent buckling of the column longitudinal reinforcement, rupture of these bars was predicted at a strain of 7%, which was based on previous laboratory tests. Numerical results at these performance levels are outlined in Table 0-1. Numerical analysis also indicates that the maximum expected displacement ductility capacity for the three tests units is within 9 and 10 with drift levels exceeding 10. These values indicate that the gap region was within values that can lead to displacement ductility levels that can ensure a safe seismic performance of RC bridge bents retrofitted according to the design details previously described.

Table 0-1. Bilinear Force Deformation

Unit No.	First yield		Theoretical Yield		Ideal		Ultimate		
	Δ'_Y (mm)	V'_Y (kN)	Δ_Y (mm)	V_Y (kN)	Δ_I (mm)	V_I (kN)	Δ_U (mm)	V_U (kN)	μ_Δ
1 & 2	21.4	290	30.5	413	69.1	429	297.5	520	9.8
3	22.1	332	30.2	453	72.4	474	295.0	584	

1.25. LOADING PROTOCOL

Following the development of the load deformation response for the three test units the loading protocol was outlined for these units. In order to maintain a direct comparison all the three test units were loaded to the same load and displacement levels. Loading of the test units consisted of first applying the simulated gravity load followed by the cyclic lateral loads, which are described next.

The gravity load of the superstructure was simulated by a 710 kN axial load that was applied to the column by means of a hydraulic jack and the loading fixture shown in Figure 0-1. After applying the simulated gravity load, the units were tested according to the reversed cyclic loading protocol shown in Figure 0-2.

As discussed in Sections 0, 0, and 0, throughout testing, the three test units supported the applied gravity load. In the initial stages of testing, the three test units were loaded in force control with single initial cycles up to first yielding of the column longitudinal reinforcement. After first yielding, three cycles were applied in displacement control at each intermediate displacement

corresponding to the displacement ductility levels of 1, 1.5, 2, 4, and 6. At the displacement ductility level of 8, five cycles were applied to further investigate at any level of joint degradation under multiple reversed cyclic loading.

$$\Delta_{\mu 1} = \frac{\left(\left|\Delta^T_{y1}\right| + \left|\Delta^T_{y2}\right|\right)}{2} \frac{V_Y}{V_Y'} \tag{0-4}$$

where $\Delta_{\mu 1}$ is the lateral displacement at $\mu_\Delta = 1$, V_Y is the lateral force at the theoretical yield, Δ^T_{y1} and Δ^T_{y2} are, respectively, the experimental lateral deflections recorded at first yield in the push and pull directions of loading. For Unit 1, in the push and pull directions these lateral deflections were recorded at 28.86 mm and 24.66 mm, respectively. Bilinear approximation of Unit 1 is presented in Figure 0-1. Thus, the lateral displacement of the test unit at the displacement ductility level of $\mu_\Delta = 1$ was 38.10mm. It is important to emphasize that this number is different than the computed yield deflection presented in Table 0-1, which for Units 1 and 2 the yield deflection was 27.12 mm and for unit 3 the yield deflection was 26.86 mm. However, the same force and ductility levels were used for testing of Units 2 and 3 for a direct comparison of the test results.
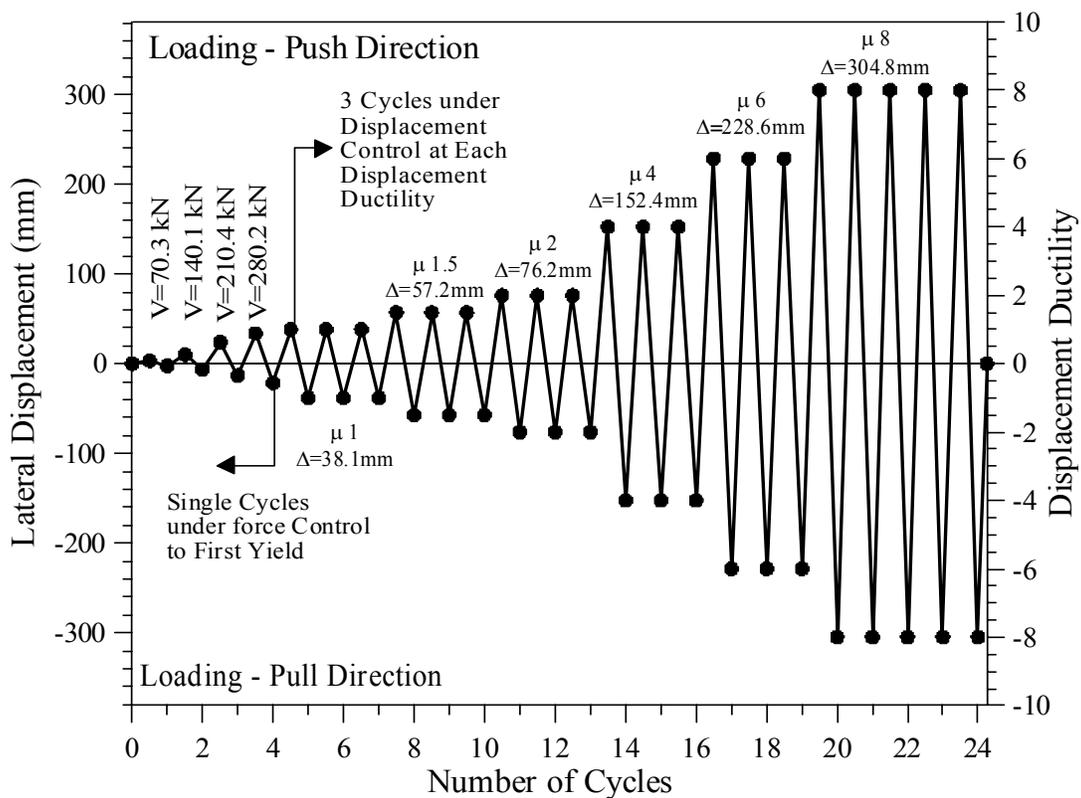

Figure 0-2. Loading Protocol Sequence

This section presents observations recorded during testing, including load deformation and strain profiles for the column and bent cap reinforcement. The reversed cyclic loading protocol was previously described in detail in Section 1.25 and shown in Figure 0-2.

1.26. GENERAL TEST OBSERVATIONS

1.26.1. Force Control Load Cycles

Following application of the 710 kN axial load, the column was loaded during the first four reversed cycles in force control up to the theoretical first yield of the column longitudinal reinforcement. Theoretical yielding was previously defined in Section 1.10.1. Up to this load level, single fully reversed cycles were applied at $0.25V_y$, $0.50V_y$, $0.75V_y$, and $1.00V_y$ corresponding to the lateral loads of 70.3, 140.1, 210.4, and 280.2 kN. At each peak cycle the load was held constant while damage was assessed and major observations were recorded for post-test evaluation.

During these four force controlled cycles, inception of first cracking was detected during loading to $0.50V_y$. Micro-cracks were recorded at the interface between the column and the bent cap and within the steel shell gap region. Next at $0.75V_y$, these cracks propagated entirely around the column footprint and remained within widths smaller than 2mm. Then, as shown in Figure 0-1 and Figure 0-2, at $1.00V_y$ cracks propagated into the bent cap in a pattern emanating perpendicular to the column footprint. This crack pattern is indicative of onset of yielding of the column longitudinal reinforcement at the bent cap interface and development of yielding penetration into the joint region. This observation by itself indicates strong correlation to the predicted response, indicating yielding of the longitudinal reinforcement at this load level. As such, testing was continued and the theoretical displacement at ductility level 1 was calculated according to Eq. (0-4).

Figure 0-1. Bent Cap Cracking at 1.00V_y

Figure 0-2. Bent Cap Cracking at 1.00 V_y

1.26.2. Displacement Control Load Cycles

After these four cycles the loading pattern was changed to displacement control as outlined in Section 1.25. At each peak displacement ductility level, testing was paused on the first and third cycles to visually inspect and record any damage to the test unit. The recorded damage at each ductility level is described in greater detail. It is important to emphasize that the ductility levels described in this section do not correlate directly to those defined during the post-test evaluation and different ductility levels were defined, as described in Section 1.47.

- *1.0 μ_Δ [38.1 mm]:* During the first cycle to this displacement ductility level onset of joint shear cracking and flexural cracking of the bent cap was recorded, with the crack pattern recorded in Figure 0-3. It was also recorded that previously marked cracks increased in width along with onset of spalling of the cover concrete within the steel shell gap region as shown in Figure 0-4.

- *1.5 μ_Δ [57.2 mm]:* Additional joint shear crack were recorded including extension of previous cracks as shown in Figure 0-5. An increase of strain penetration cracks occurred as shown in Figure 0-6 along with further crushing of the column cover concrete.

- *2.0 μ_Δ [76.2 mm]:* Increase in the number of cracks and elongation of previous cracks was recorded in the joint as seen in Figure 0-7. Separation of the cover concrete in the bent cap top surface further indicate continued strain penetrations into the bent cap (see Figure 0-8). At this damage level, further crushing and spalling of the column cover concrete were also recorded

indicating development of the plastic hinge. These two observations further confirm that up to this displacement level the joint was capable of sustaining the imposed joint shear stresses.

- *4.0 μ_Δ [152.4 mm]:* At each successive cycle at ductility level 4, there was a loss of strength in the column combined with accumulated damage at the interface between the bent cap and column. There were no additional joint shear cracks and only minimal extensions of the existing cracks were recorded in Figure 0-9. The concrete blocks on either side of the column lifted and the first line of headed reinforcement prevented further extension of these cracks into the bent cap as shown in Figure 0-10. The joint shear cracks remained within small widths as shown in Figure 0-11. At this level there was also further crushing of the column concrete cover as shown in Figure 0-12.

- *6.0 μ_Δ [228.6 mm]:* At this level the column strength continued to decrease; however, joint shear cracks neither extended further or increased in width as shown in Figure 0-13. Additional crushing of the column cover concrete was also recorded as shown in Figure 0-14. Onset of cracking on the underside of the bent cap was also observed indicating the typical pullout cone that is generally indicative of anchorage failure of the column longitudinal reinforcement. Further cycles accentuated the cracking and spalling of the cover concrete on the underside of the bent cap as shown in Figure 0-15. Then as the longitudinal bars were pulled from within the joint core under reversed cyclic loading the steel shell was not as effective in preventing buckling of this reinforcement. As such during the last cycle at this level buckling of the main column longitudinal bar was observed as shown in Figure 0-16. Although joint shear failure is likely to be attributed at this displacement level, complete failure of the test unit has not yet developed and even at this level the unit is capable of sustaining the imposed axial load and some level of lateral load.

- *8.0 μ_Δ [304.8 mm]:* There was a continual loss in capacity at this ductility level. The column bars that had previously buckled finally fractured under low cycle fatigue, as shown in Figure 0-18. Cracking continued on the underside of the bent cap was observed and large blocks separated from the bent cap as shown in Figure 0-19. However, cracks on the side of the bent remained within widths smaller than 3 mm with the corresponding cracking pattern shown in Figure 0-20. This observation suggests that joint damage was concentrated within the as-built section.

After the test's completion all loose concrete was removed and the test unit was further inspected to evaluate the main failure mode. The extent of damage to the bent cap was confined to the first row of headed reinforcement as shown in Figure 0-21. On the underside of the bent cap it was recorded that a wide open crack extended in the longitudinal direction of the bent cap. This indicates splitting of the bent cap and potential dilation of the bent cap in the transverse direction. This indicates also that the transverse reinforcement through the bent cap was not

effective in preventing this dilation and continuous reinforcement should be provided instead, as outlined in Section 0 while describing the design of Unit 2.
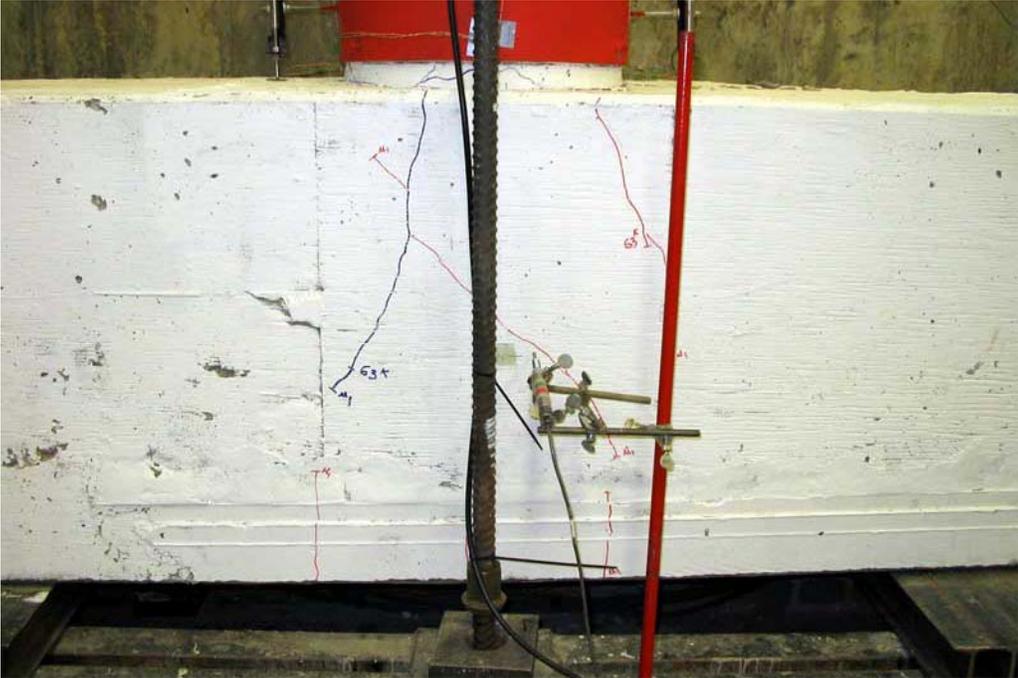
Figure 0-3. Joint Cracking at 1.0 μ_Δ

Figure 0-4. Bent Cap Cracking at 1.0 μ_Δ
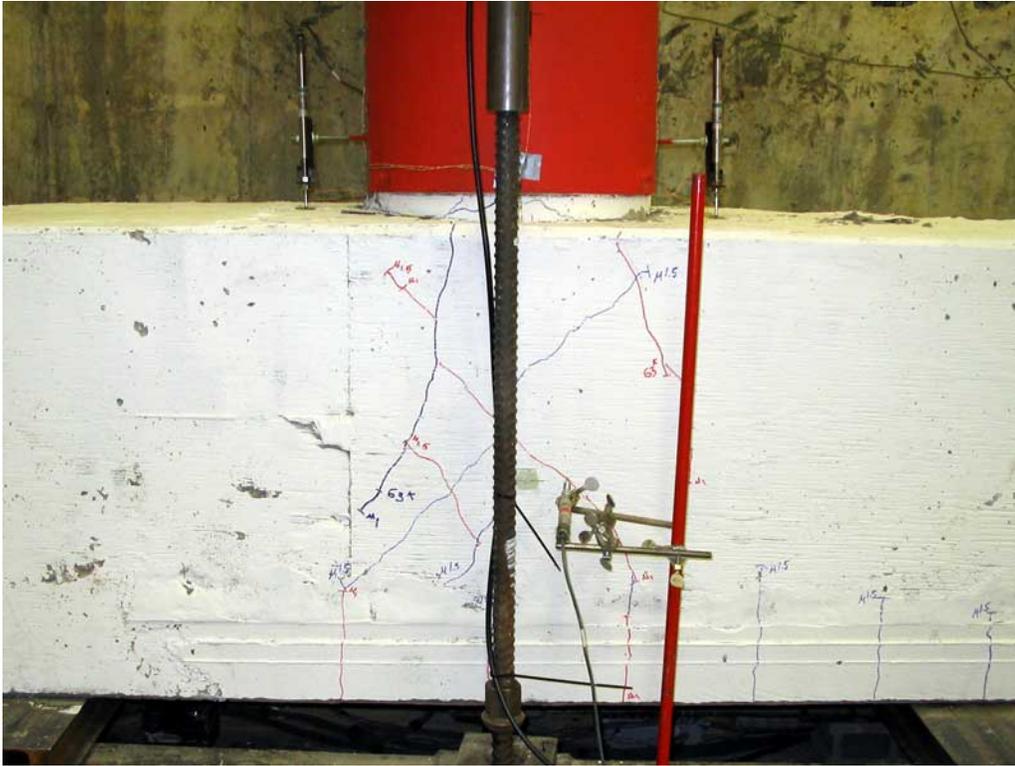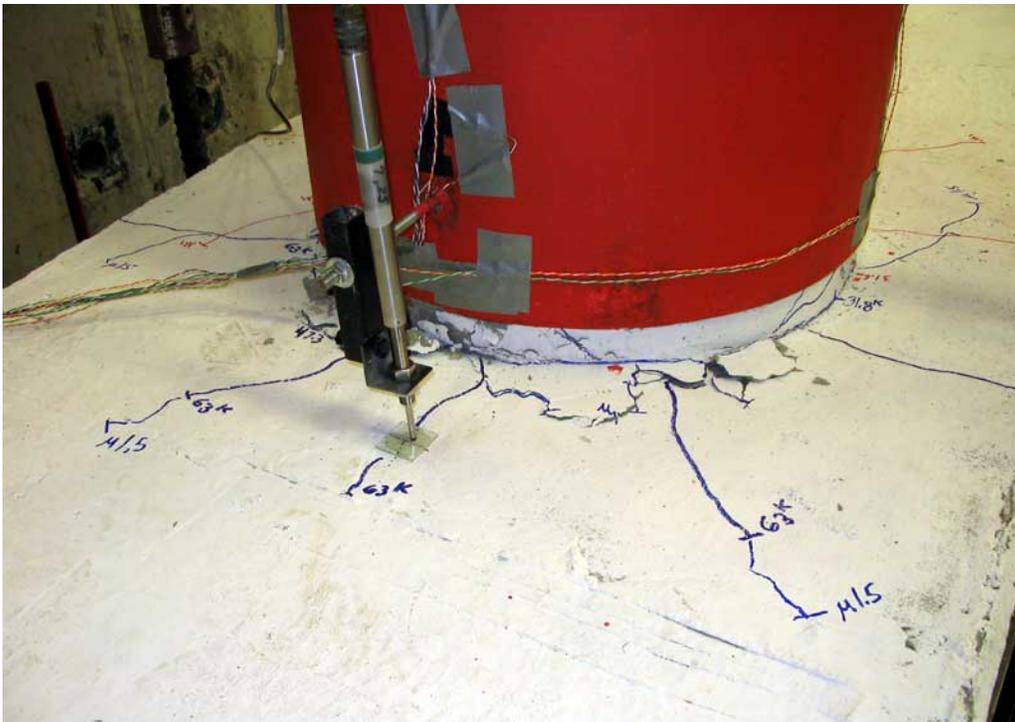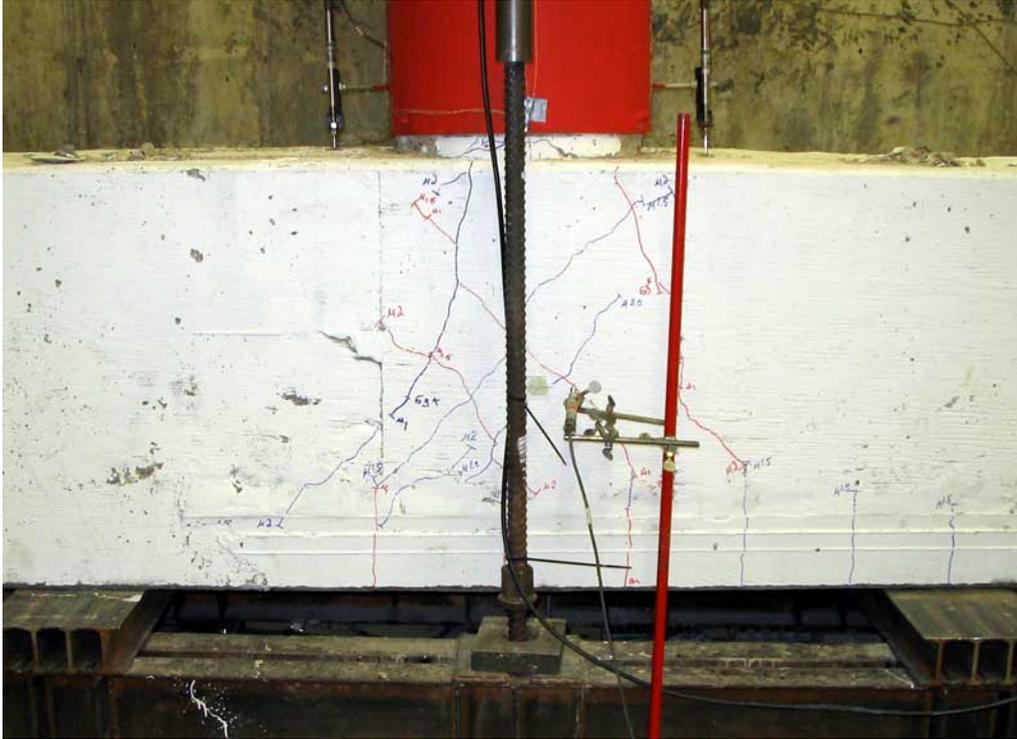
Figure 0-5. Joint Cracking at 1.5 μ$_\Delta$

Figure 0-6. Bent Cap Cracking at 1.5 μ$_\Delta$

Figure 0-7. Joint Cracking at 2.0 μ$_\Delta$

Figure 0-8. Bent Cap Cracking at 2.0 μ$_\Delta$
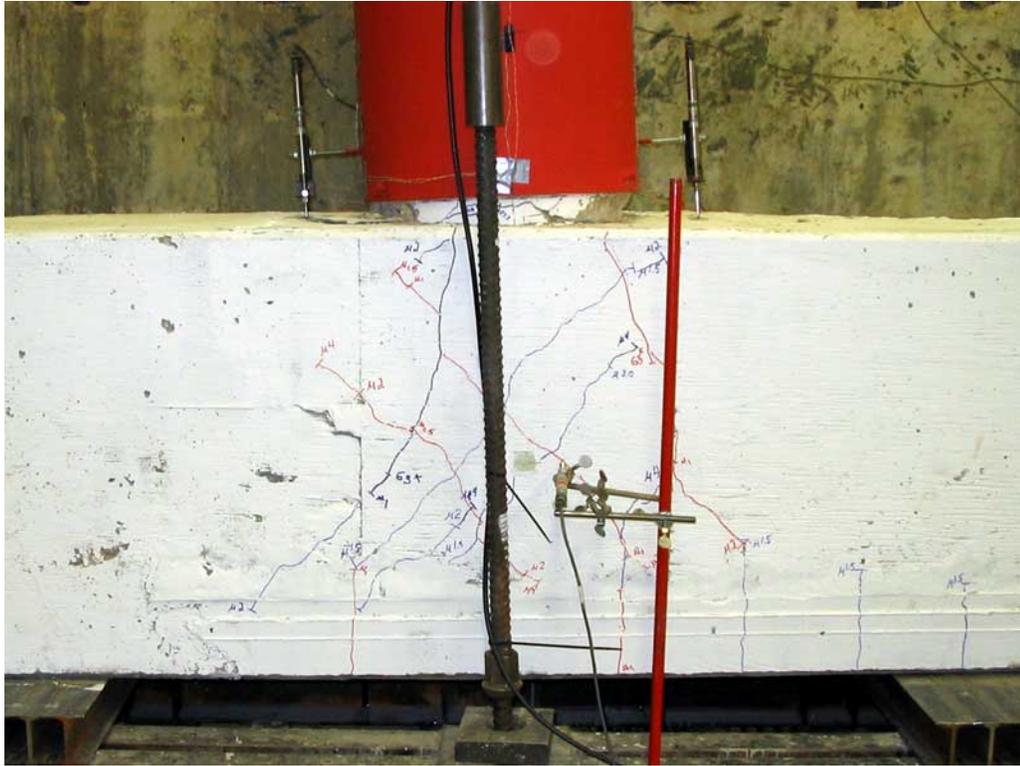
Figure 0-9. Joint Cracking at 4.0 μ_Δ

Figure 0-10. Bent Cap Cracking at 4.0 μ_Δ
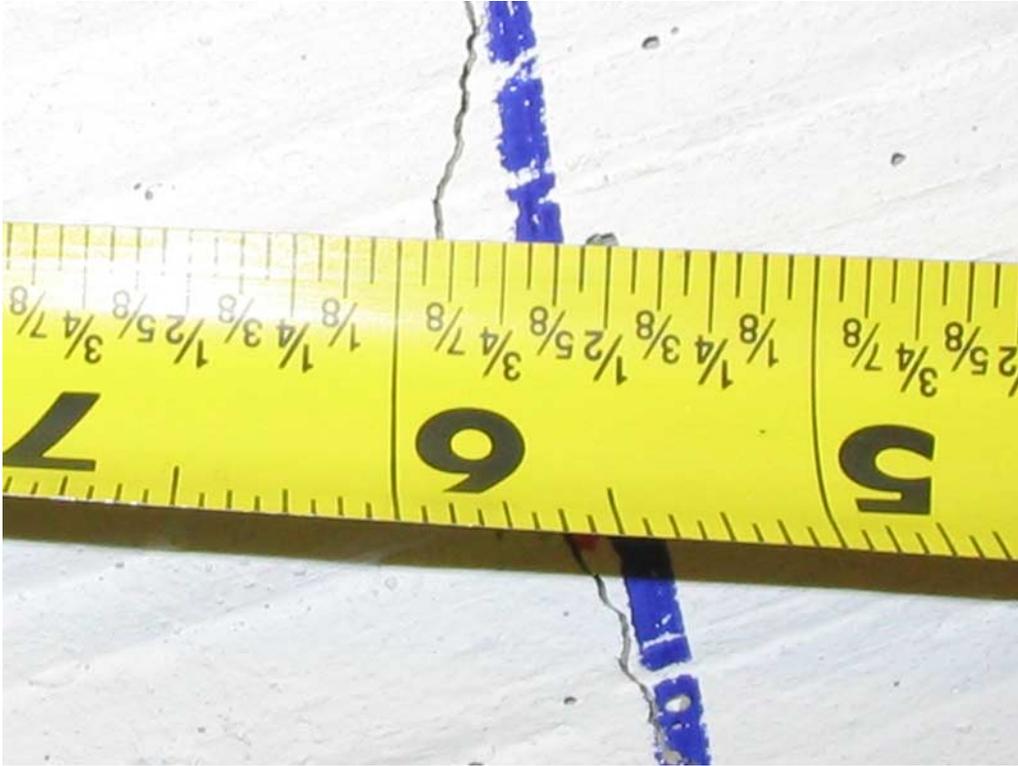
Figure 0-11. Joint Crack Width at 4.0 μ_Δ

Figure 0-12. Column Concrete Crushing at 4.0 μ_Δ
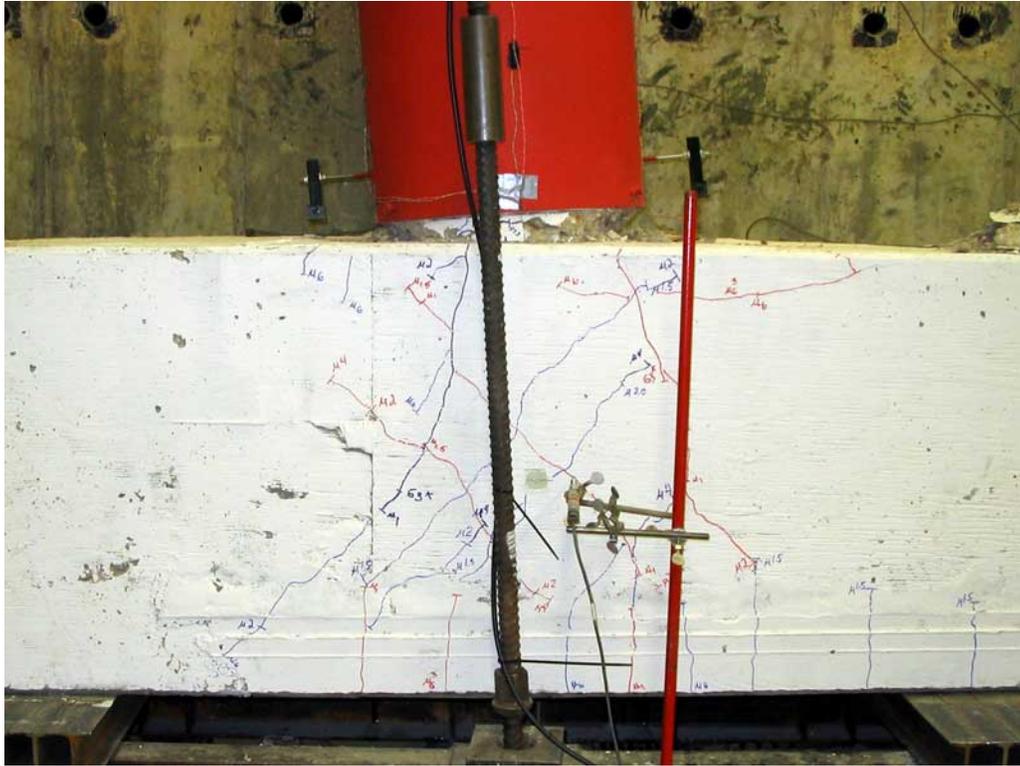
Figure 0-13. Joint Cracking at 6.0 μ_Δ

Figure 0-14. Column Concrete Crushing at 6.0 μ_Δ

Figure 0-15. Bent Cap Bottom Cracking at 6.0 μ_Δ

Figure 0-16. Column Longitudinal Bar Buckling at 6.0 μ_Δ

Figure 0-17. Bent Cap Cracking at 8.0 μ_Δ

Figure 0-18. Column Longitudinal Bar Fracture at 8.0 μ_Δ

Figure 0-19. Bent Cap Bottom Spalling at 8.0 μ_Δ
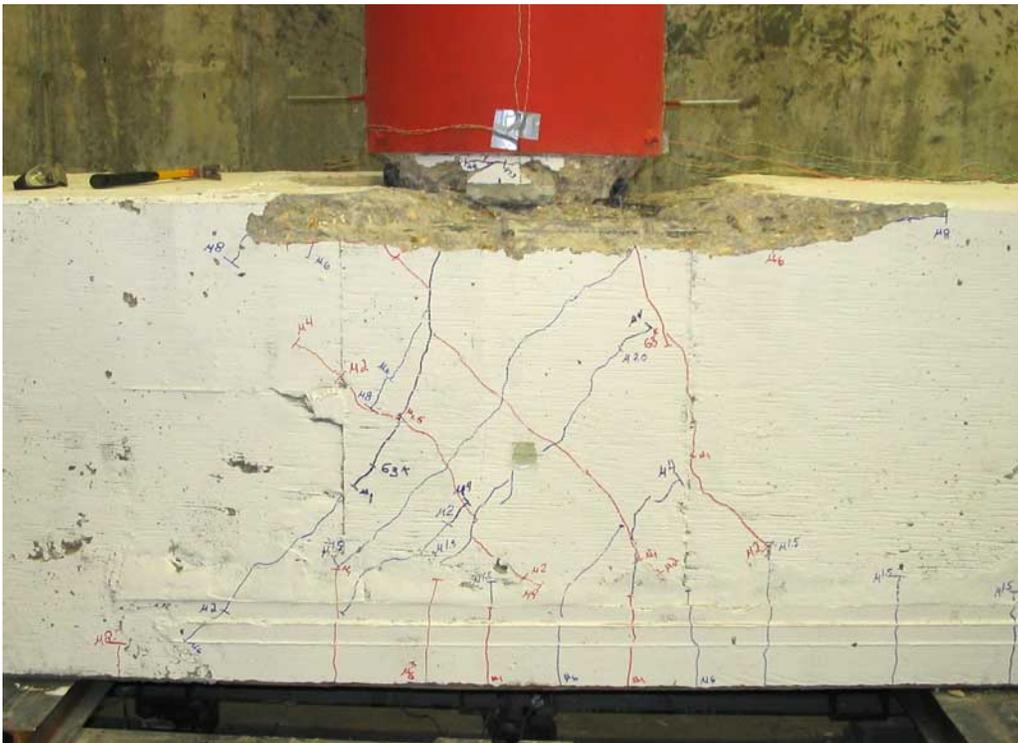
Figure 0-20. Joint Cracking at 8.0 μ_Δ

Figure 0-21. Bent Cap Ultimate Damage

1.27. LOAD DEFORMATION RESPONSE

The pre and post-test theoretical and experimental load vs. deformation curves for Unit 1 are shown in Figure 0-22. Development of the pre test analysis curve was previously outlined in Section 1.23 and the post-test analysis is outlined in Section 1.51, which also describes the post-testing investigation for the three test units. After testing, the displacement at ductility level one was rectified to reflect directly the test results. Based on a direct investigation of the test results the new displacement at ductility level one was set at 31.5 mm, leading to the ductility levels shown in the figure below.

In Unit 1 the maximum registered lateral load was recorded during loading to the first cycle at the displacement of 152.4 mm. At this cycle, in the push and pull directions the lateral loads were +421 and -442 kN, respectively. Between the first and second cycles, a drop in the lateral load of approximately 17% was recorded, and between the second and third cycles the drop in the lateral load was only 5%, indicating stability in the response of the test unit at this displacement level. During loading to the next displacement level or 228.6 mm, there was a continuous degradation in the strength of the test unit during subsequent cycles and significant pinching in the hysteretic response of the test unit. The first significant drop in the lateral load capacity of the test unit below the theoretical yield load level was observed at this displacement

level, which occurred during the second cycle. Before this displacement ductility level, the hysteretic response of the test unit was reasonably stable with significant amounts of energy dissipation capacity. However, it is important to emphasize that during loading to the first cycle at 228.6 mm the lateral load was nearly the same as the load registered to the third cycle at 152.4 mm. This indicates that load transfer within the joint region was still within limits capable of sustaining load levels within 80% of the maximum registered lateral load for displacement ductility levels less than 5. As such the ductility level 4 was selected as the limiting ductility level for assessment and design using this retrofit procedure.
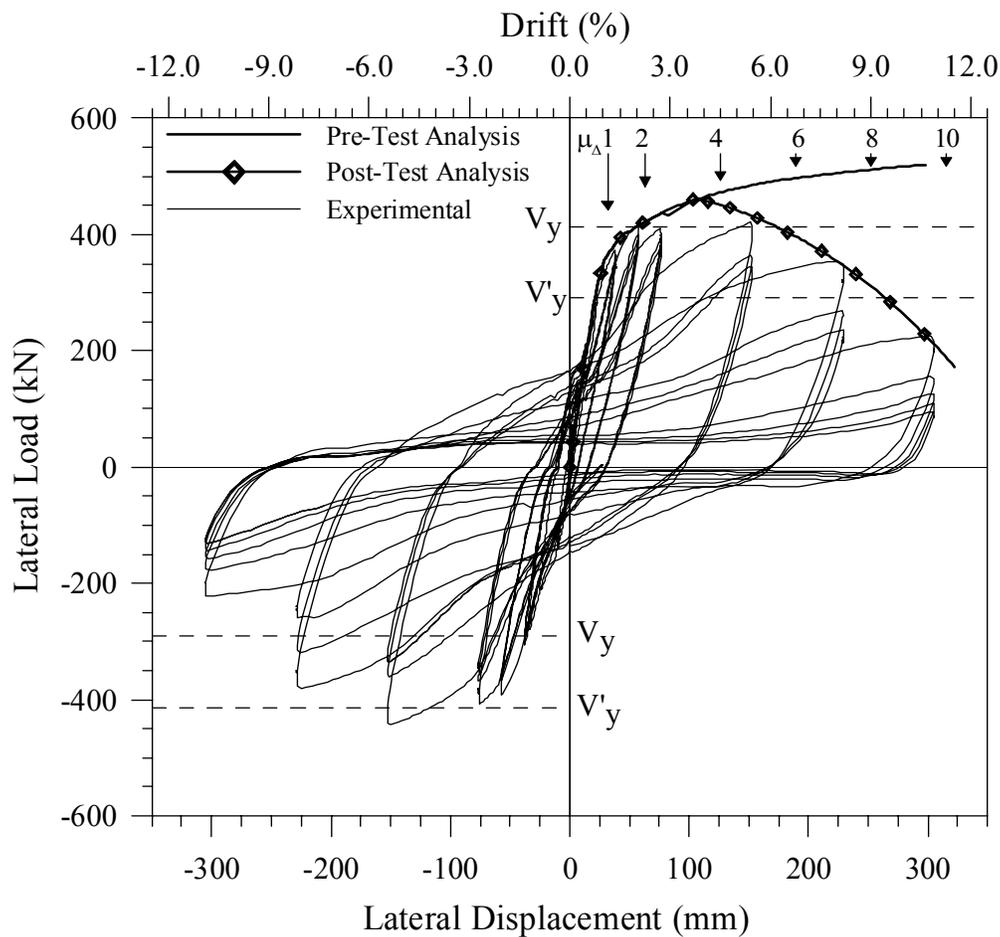
Figure 0-22. Unit 1 - Load Displacement Response

During the second cycle to 228.6 mm, cracks and then spalling of a concrete wedge were observed on the underside of the bent cap immediately below the column footprint. This indicates that severe joint degradation under reversed cyclic loading had initiated, which is also evidenced by the drop in the lateral load during subsequent cycles. However, this damage level did not lead to complete loss in the lateral and axial load capacity of the test unit. In fact, during the first cycle to the displacement of 304.8 mm, low cycle fatigue of one of the column

longitudinal rebar was detected, which shows that the joint had reserve capacity to prevent complete pull-out of the column longitudinal bars. Also, the three cycles at the displacement ductility level of 228.6 mm exhibited considerable levels of energy dissipation capacity.

During the subsequent cycles at the displacement 304.8 mm, large blocks of concrete separated from the bottom of the bent cap. Through visual inspection it was possible to distinguish a wide open crack running in the longitudinal direction and along the mid-width of the bent cap indicating splitting of the bent cap. This was accompanied by significant drop in the lateral load capacity indicating partial pullout failure of the column longitudinal reinforcement in addition to low cycle fatigue.

1.28. LOAD VS. CURVATURE RESPONSE

Figure 0-23 shows the measured lateral load versus the computed curvatures at the column to the bent cap interface. The diagram depicted in this figure indicates a good correlation between the pre-test analysis and the experimental test results during the initial stages of testing. However, after peak load there is a considerable deviation between these two curves. These can be attributed to the fact that during the initial stages of testing most of the deformations are due to curvature along the length of the column, and at later stages of testing most of the column top deflection is a result of large rotations originating solely from within the joint region.
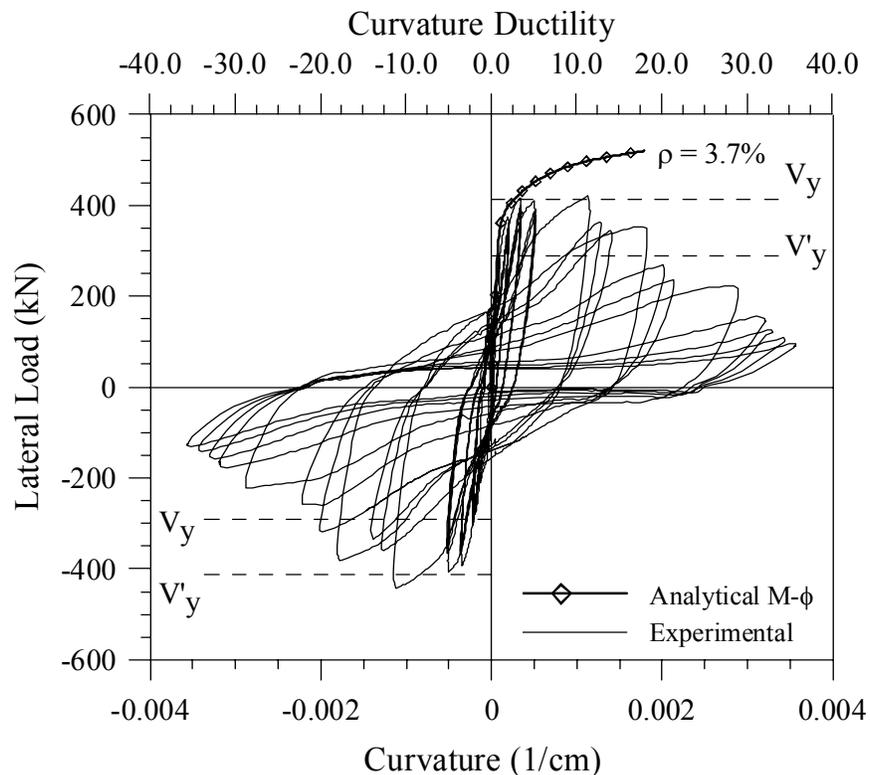

Figure 0-23. Unit 1 – Load versus Curvature Response

Using these experimental results it was possible to back calculate any potential rotations within the joint region and propose models that can account for the contribution of the joint rotation on the column top deflection. This issue is further discussed in Section 0.

Curvatures presented in Figure 0-23 represent average values and were computed according to the expression:

$$\phi_{ave} = \frac{\Delta_1 - \Delta_2}{W_{cur} \times h_{cur}} \tag{0-1}$$

Where Δ_1 and Δ_2 are the relative vertical displacements between the adjacent curvature rods in the extreme faces on opposite sides of the pile section, W_{cur} is the horizontal distance between the pair of linear potentiometers and h_{cur} is the vertical distance between the adjacent linear potentiometers. During computations of curvatures at the pile cap interface the height of the linear potentiometer cell h_{cur} include an additional term to account for tensile strain penetration into the bent cap by including the strain penetration length into the curvature cell height h_{cur} according to the expression:

$$h_{cur} = h + 0.0022\, d_b\, f_s \tag{0-2}$$

Where d_b is the column main bar diameter and f_s is the column main bar stress obtained from the reinforcement strains obtained from the next section data. In the early stages of the testing procedure strain levels in the inner core reinforcement are minimum and f_s should be used instead of f_y because tensile strain penetrations are negligible. Then at later stages of testing f_y was used.

1.29. COLUMN LONGITUDINAL REINFORCEMENT STRAINS

Strains presented in this section and subsequent sections are indicated as positive when the bars are subjected to a tensile strain and negative when the bars are subjected to compressive strains. The strain histories of the column longitudinal reinforcement gauges at the interface of the column and bent cap for side "A" and side "B" are shown in Figure 0-24 and Figure 0-25, respectively. The yield strain of the column longitudinal reinforcement occurred at $\pm 2{,}740\mu\varepsilon$ as determined from tensile testing as indicated in the material properties Table 0-2. The strain profiles for each side of the column are shown in Figure 0-26 and Figure 0-27. The onset of yielding of the main column longitudinal bars occurred at $\mu 1.0$ for each side of the column, which are within the predicted levels.
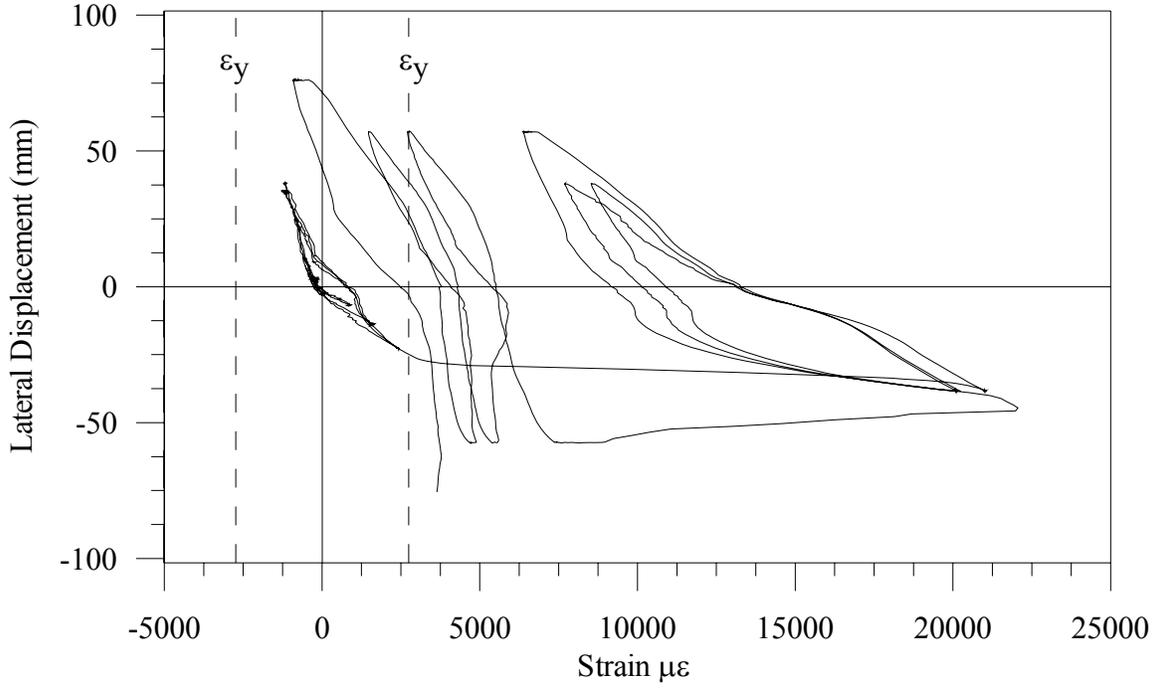
Figure 0-24. Strain Gauge History – C4a
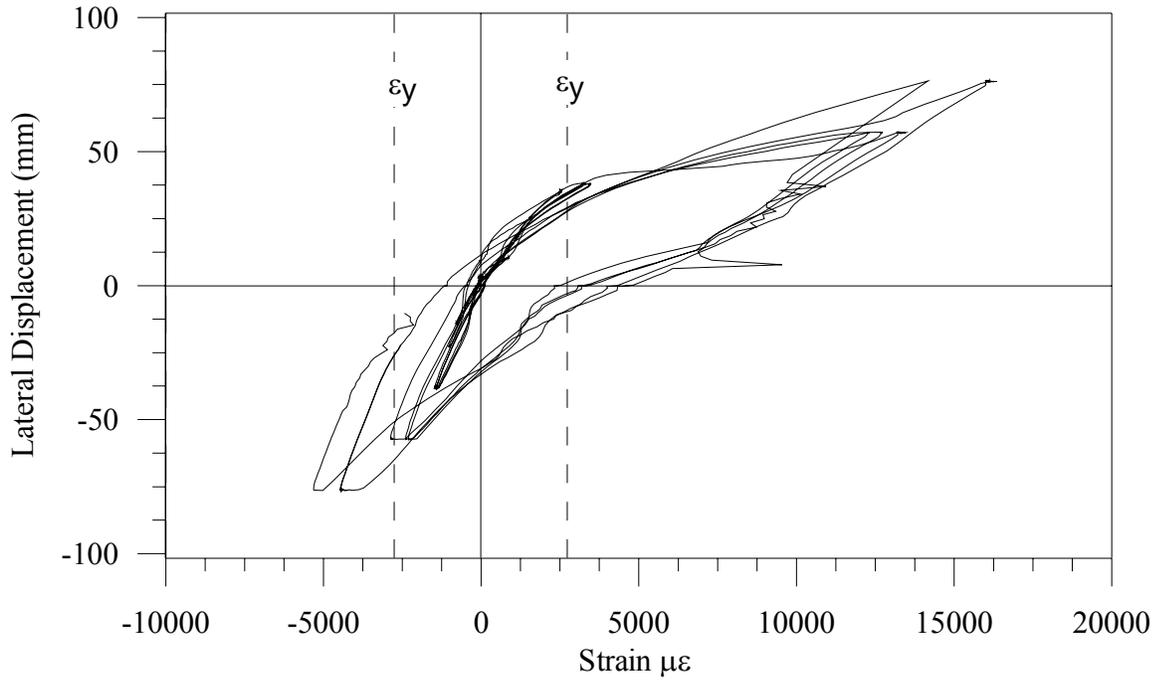
Figure 0-25. Strain Gauge History – C4b
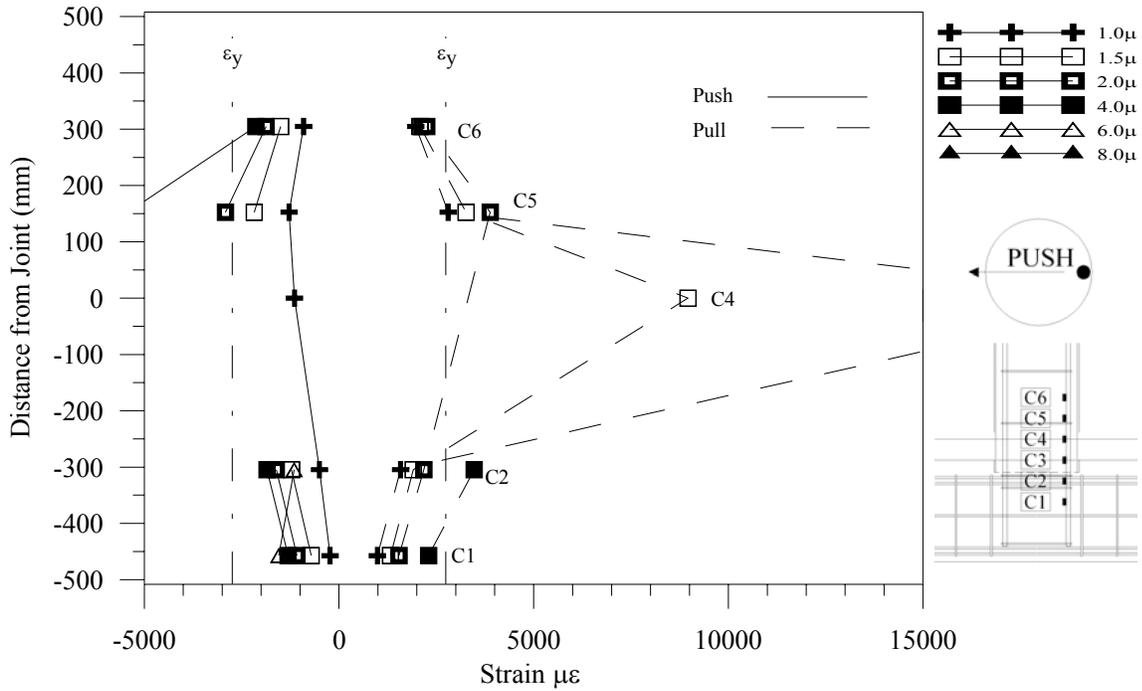
Figure 0-26. Strain Gauge Profile – Side "A"
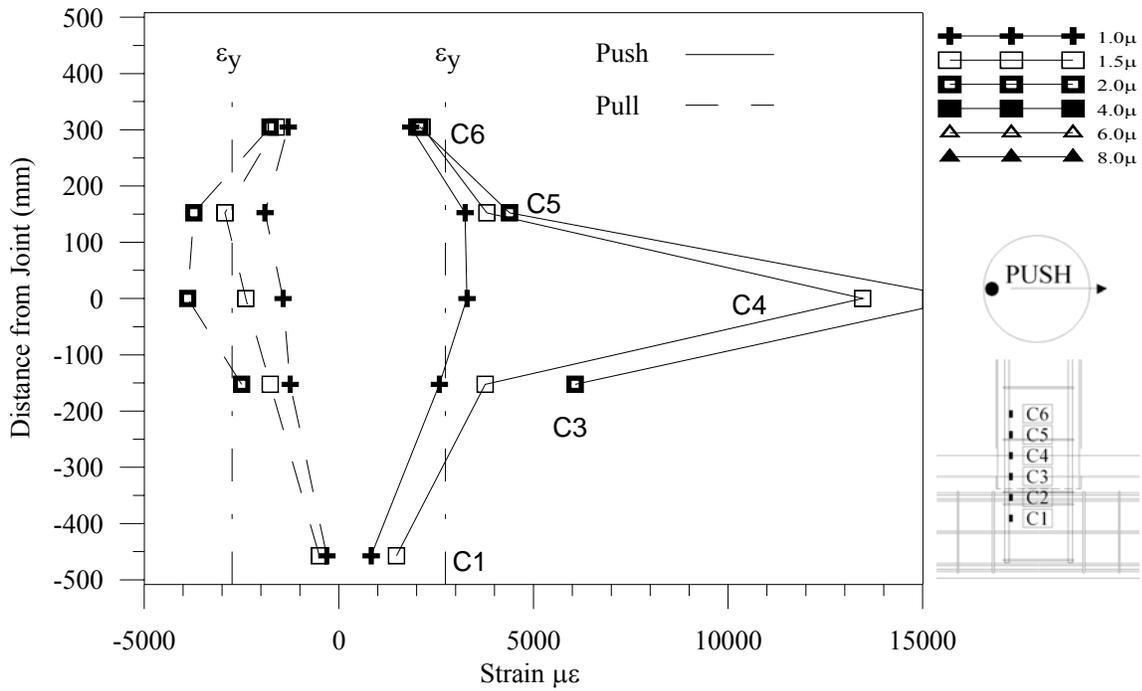
Figure 0-27. Strain Gauge Profile – Side "B"

1.30. JOINT SHEAR REINFORCEMENT STRAINS

The strain gauges from the shear reinforcement are presented in this section. The yield strain of the as-built shear reinforcement occurred at $\pm2,191\mu\varepsilon$ and the yield strain of the retrofit shear reinforcement occurred at $\pm2,340$ as determined from tensile testing. Figure 0-28 and Figure 0-29are the strain profiles for the stirrups in the as-built concrete and the stirrups in the retrofit concrete, respectively. The stirrups stayed below the yield point indicating that joint shear did not occur in the longitudinal plane of the bent cap.

Through the initial stages of testing, there was not any significant amount of strain in the shear reinforcement for both the original steel and the retrofit steel indicating that there was not any shear cracks as was observed during testing. Through the later stages of testing, both the original steel and the retrofit steel had a achieved approximately the same level of strain. This is a strong indication that composite action developed between the as-built and retrofit sections. The retrofit stirrup at the centerline of the column had approximately twice the strain as the stirrups at the column face. The original concrete did not have shear reinforcing at the centerline of the column as the retrofit did. Past the column face, the strain in the stirrup quickly decreases indicating that the shear strains are primarily confined within an area h/2 away from the centerline of the column as indicated by joint shear cracks staying within this region.
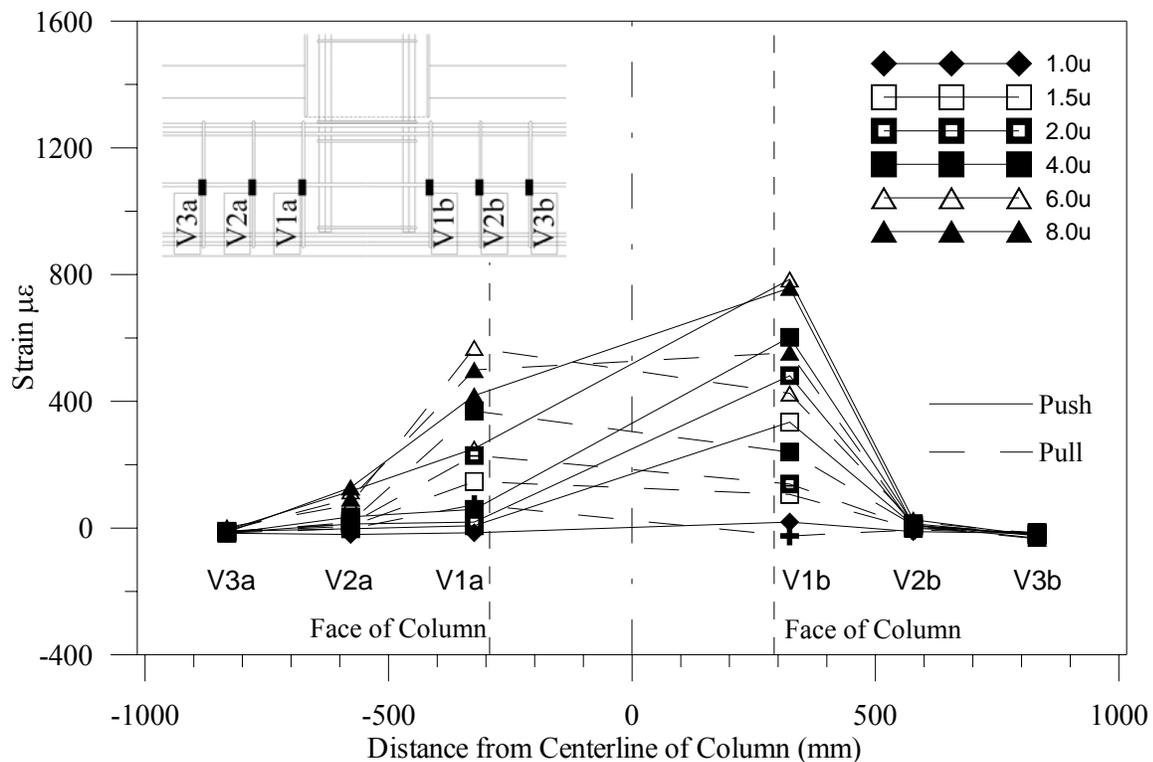

Figure 0-28. As-Built Strain Gauge Profile
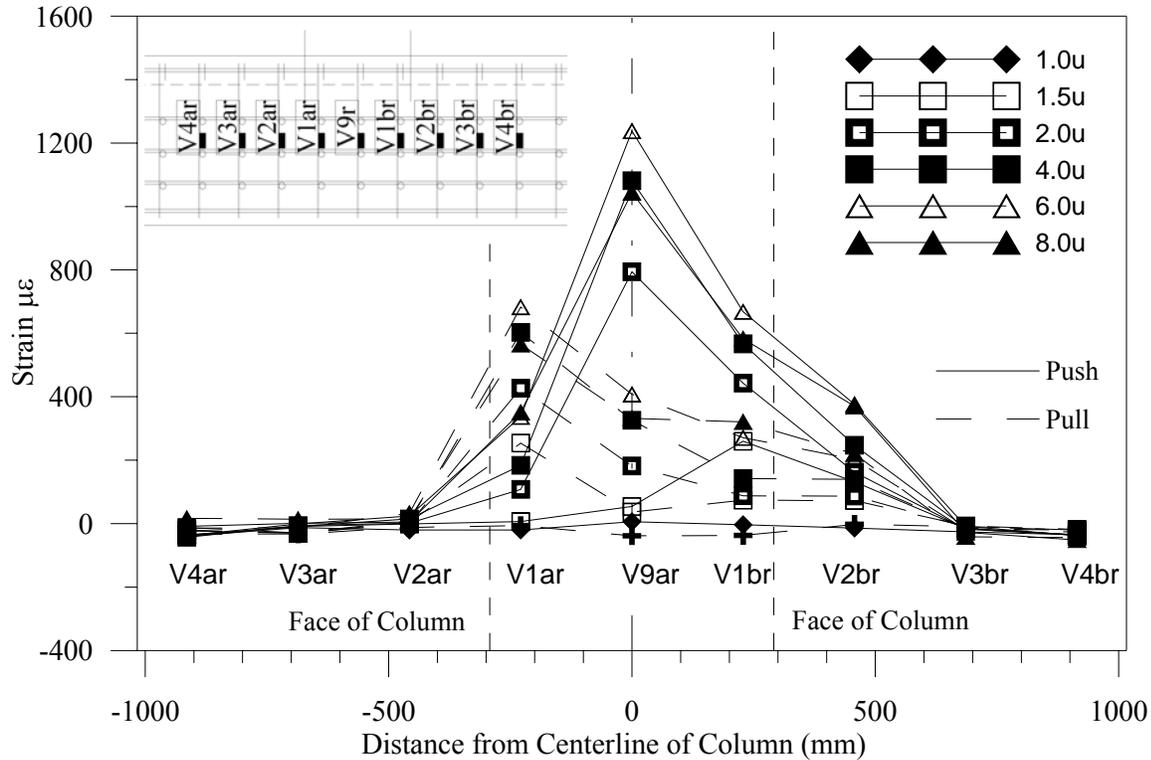
Figure 0-29. Retrofit Strain Gauge Profile

1.31. BENT CAP LONGITUDINAL REINFORCEMENT STRAINS

The following section presents the strain in the cap beam longitudinal steel. The yield strain for the original longitudinal steel is 2,807 με. The yield strain for the retrofit longitudinal steel is 2,544 με. For both the original and retrofit steel, the steel did not yield, indicating that the cap beam stayed elastic. For similar locations, the strain in both the retrofit steel and the original steel had strain levels that were very close indicating that the entire beam acted as one unit.

After ductility level four, the applied lateral load decreased and hence, the moment applied to the bent cap decreased. However, the strain in the longitudinal reinforcement at the bottom of the bent cap continued to increase as shown in Figure 0-30 and Figure 0-31. This is due to the anchorage failure of the column longitudinal bars. As the main column longitudinal bars slipped, it produced a localized stress cone, shown in Figure 0-32, that was confined by the bottom longitudinal reinforcement causing it to have an increase in strain even though there was not an increase in moment. As the distance from the face of the column increases, the strain decreases showing that the strain is influenced less by the confining resistance to the column longitudinal bars pushing on the block and more so due to the stresses from the flexure in the cap beam.
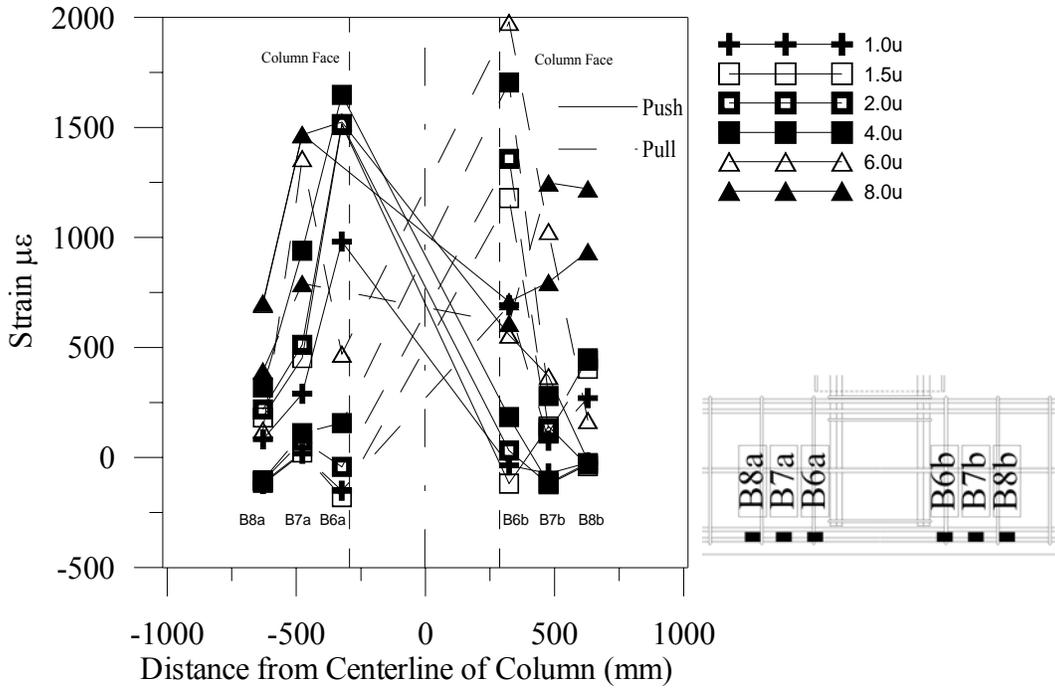
Figure 0-30. As-Built Strain Gauge Profile
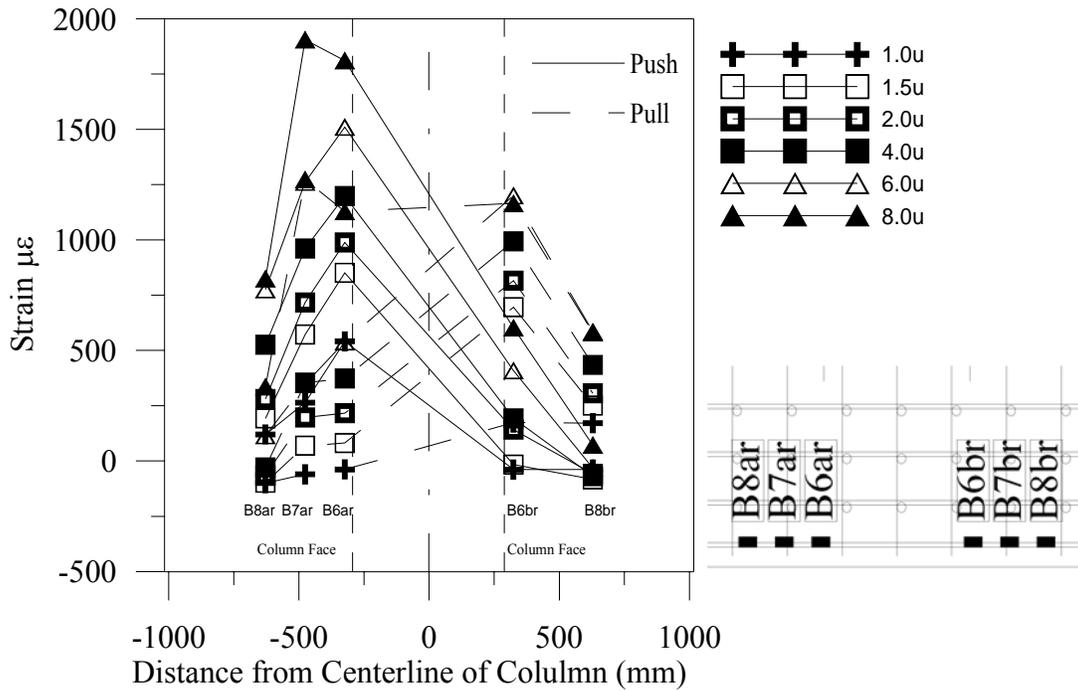
Figure 0-31. Retrofit Strain Gauge Profile
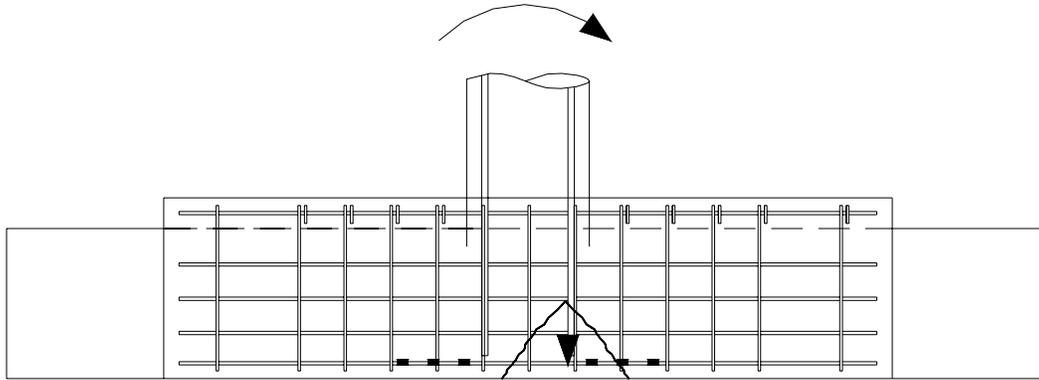
Figure 0-32. Confinement of Column Anchorage Failure

1.32. JOINT SHEAR ANALYSIS

Referring to Figure 0-22 and based on a post-test investigation it is reasonable to infer that the loss in strength was a result of joint shear failure. However, it is important to emphasize that the joint shear cracks marked on the sides of the bent cap were rather small to justify any level of joint shear degradation. Due to the proper detailing of the reinforcement in the longitudinal plane of the bent cap, the shear deformations stayed small as shown in Figure 0-33 corresponding to the joint shear cracks staying small. Joint shear deformations were computed based on the mathematical methodology presented in Figure 0-10 and using experimental data obtained from the devices shown in Figure 0-9. Based on the information shown on the figure below it was possible to construct the information shown in Figure 0-34.
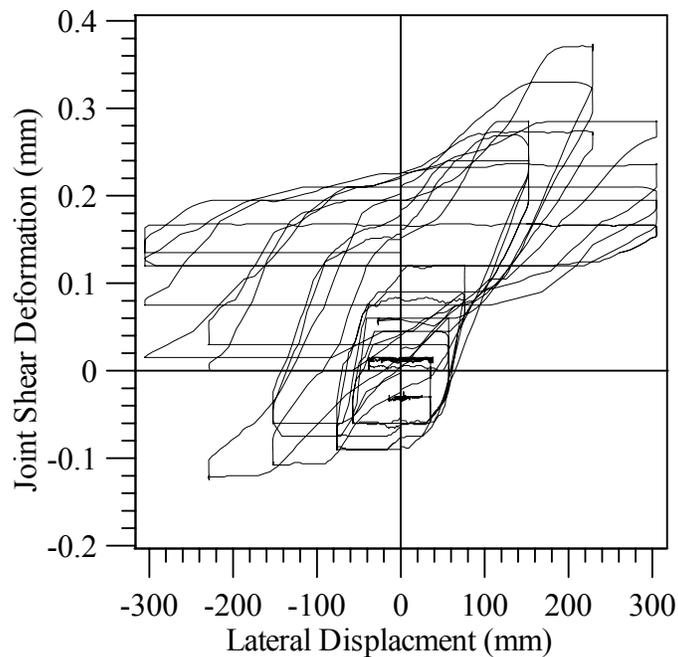
Figure 0-33. Joint Shear Deformation

Priestley (1993) developed a model for joint behavior using principle tensile stresses and joint shear strains that were obtained from tests conducted for unreinforced concrete joints. Based on his work Priestley developed a trilinear model which comprises of an initial joint stiffness based on the shear modulus of concrete, G_c, and is linear until cracking occurs at $0.29/\sqrt{f_c'}$. The second slope of the joint stiffness model is based on the joint reinforcing steel stiffness of the cracked section where it peaks at $0.42/\sqrt{f_c'}$ and at a corresponding strain of 0.007. Finaly, the third slope is based on a linear decent to an ultimate strain of 0.01 at zero principle tensile stress (Priestley 1993). In another model proposed by Mazzoni (2004) the second slope stays linear past $0.42/\sqrt{f_c'}$ until $0.62/\sqrt{f_c'}$.

In Figure 0-34 is shown the joint shear strain versus the principle tensile stress for Unit 1, along with the models for the "weak" and "intermediate" joints. Based on these results it is clear that for most part during testing the test data stays above stays above the "weak" joint limit until there is a loss in principle tensile stress, at which point the joint strain also decreased indicating an elastic response of the joint. The elastic behavior of the joint shear strains indicates that joint shear failure did not occur in the longitudinal direction of the bent cap. Post-test investigation has revealed that joint shear failure was likely due to the transverse headed reinforcement not being continuous, allowing a longitudinal crack to form near the middle of the bent cap as shown in Figure 0-35 , which led to the bent cap splitting and partial anchorage failure of the column longitudinal bars. As such, in the design of Unit 2 the transverse reinforcement going through the joint was positioned continuous as described in Section 0. In Section 1.50 a different joint model for each of the three test units is proposed and described in further detail using the data extracted from the curves shown in Figure 0-22 and Figure 0-23. These new models were then used in Section 1.51 to develop the post-test analysis for the three test units.

As discussed previously, the transverse joint strain should be limited to 1500$\mu\varepsilon$ to provide adequate confinement of the joint. The strain across the entire joint could not be determined for Unit 1 due to the discontinuity of the transverse reinforcement across the joint. For Unit 2, the maximum strain in the transverse reinforcement was 506$\mu\varepsilon$, as shown in Figure 0-35, well below the confinement limit. For Unit 3, the strain was not measured in the transverse direction due to the transverse reinforcement being post-tensioned threaded rods; however, the strain would be assumed to similar to Unit 2. With the transverse strain staying below the required limit, joint shear failure did not occur in the transverse direction.

Anchorage failure of the column longitudinal bars did occur as indicated by the breaking away of the bottom concrete on the bent cap of Unit 1 and 3 during testing as shown in Figure 0-35 and **Error! Reference source not found.**, respectively. While blocks of concrete did not break away for Unit 2, anchorage failure cannot be ruled out due to the cracking on the bottom of the bent cap as shown in Figure 0-23 indicating a similar response to Unit 1 and 3. While anchorage failure is not expected in bridge tee joints unless significant inelastic stresses are developed in the beam longitudinal reinforcement at the column faces (Sritharan 2003), this did occur even though adequate anchorage length was provided. In addition to providing a minimum required anchorage length, it must also be ensured that the column bars are extended into the joint as close to the top beam bars (the bottom of this test set-up due to the Units being inverted) as possible. If this condition is not satisfied, adequate clamping of the column bars into the joint strut will not occur and nodal failure can develop despite satisfying the minimum anchorage length requirement. (Sritharan 2003) In this retrofit scheme, only the as-built bent cap longitudinal reinforcement is within the region of the column reinforcement as shown in Figure 0-1, Figure 0-1, and Figure 0-1 for Unit 1, 2, and 3 respectively. While adequate clamping of the outer most column longitudinal reinforcing might have occurred due to the concentration of the bent cap retrofit reinforcement being near by, clamping of the center longitudinal bar did not occur leading to the anchorage failure and loss of capacity of the column at higher ductility levels.
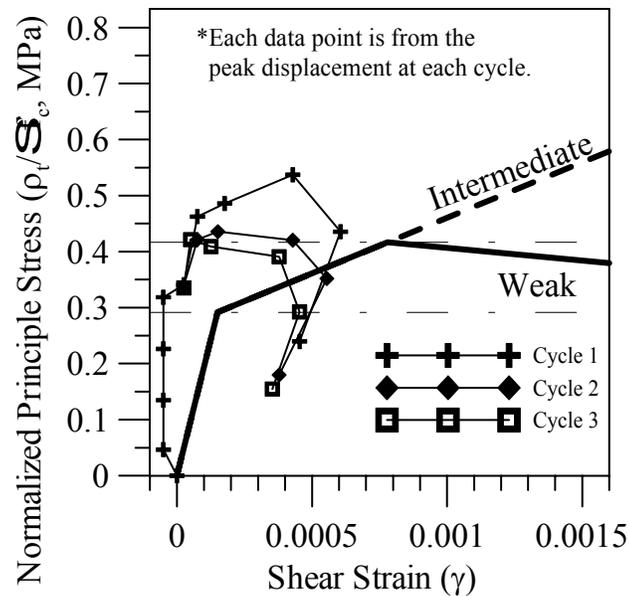

**Figure 0-34. Unit 1 Principle Tensile Stress vs. Joint Shear Strain**
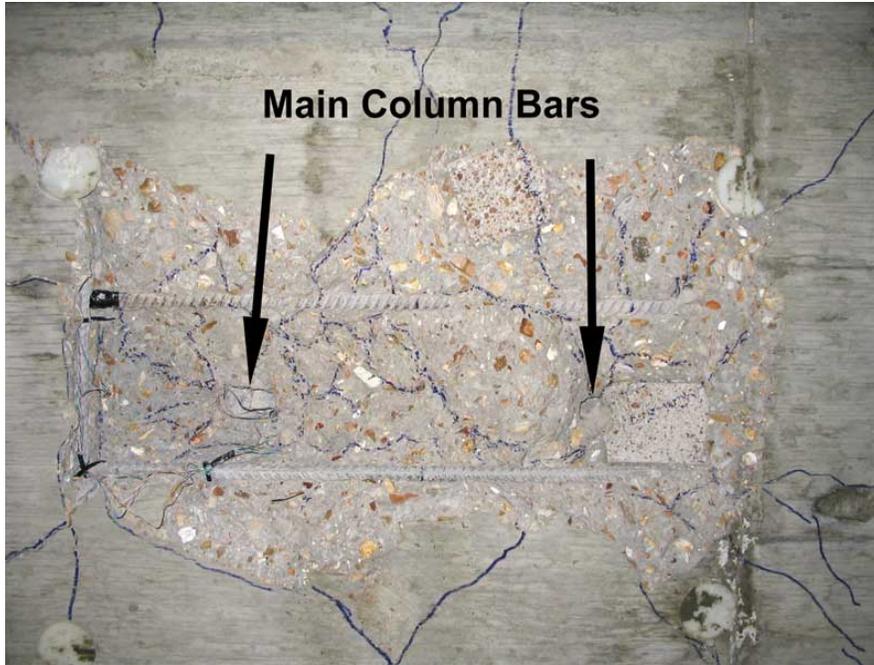
Figure 0-35. Underside of Bent Cap Cracking Pattern

This section presents observations made during experimental testing, including force-deformation and reinforcement strain profiles for the column and bent cap.

1.33. GENERAL TEST OBSERVATIONS

1.33.1. Force Control Load Cycles

Unit 2 was loaded using the same loading protocol as in Unit 1 (see Figure 0-2). Similar observations were recorded for these two test units up to the first four cycles in force control. As in Unit 1, inception of cracking was detected at $0.50V_y$ with micro cracks developing at the bent cap interface. At this load level a single crack was also observed on the bent cap as shown in Figure 0-1. At $0.75V_y$ additional cracks developed due to strain penetration along with cracking at the interface of the base of the column and the bent cap as shown in Figure 0-2. At $1.00V_y$ extension of the strain penetration cracks were recorded (see Figure 0-3) along with onset of joint shear cracking as shown in Figure 0-4.
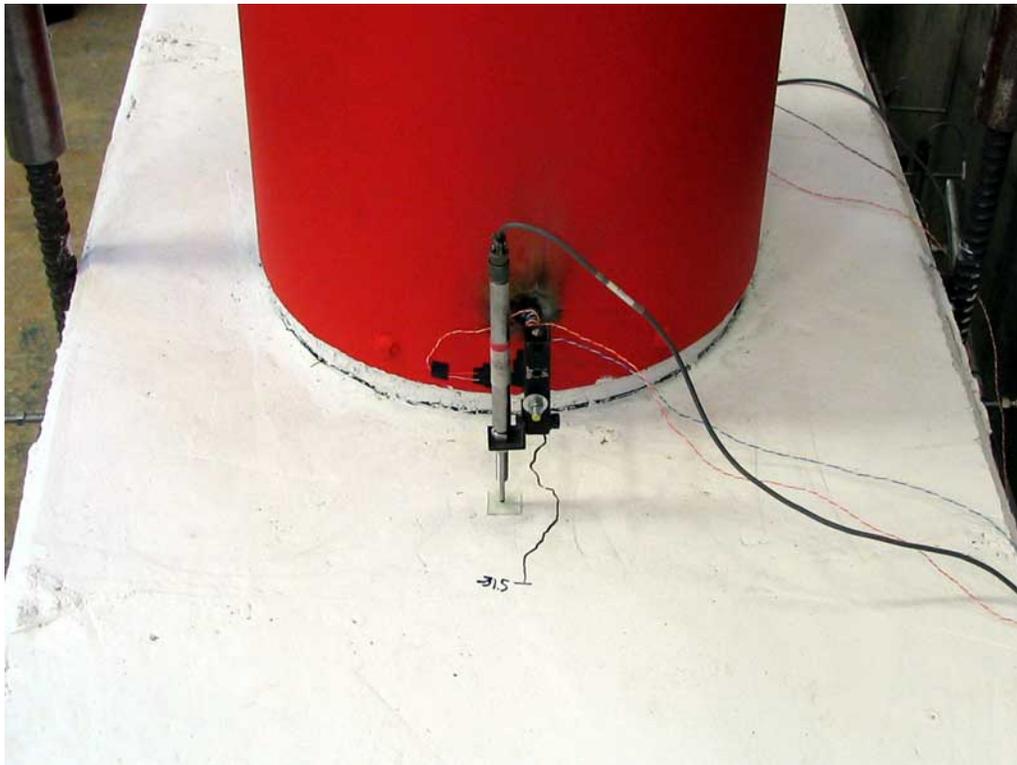

Figure 0-1. Bent Cap Cracking at $0.50V_y$
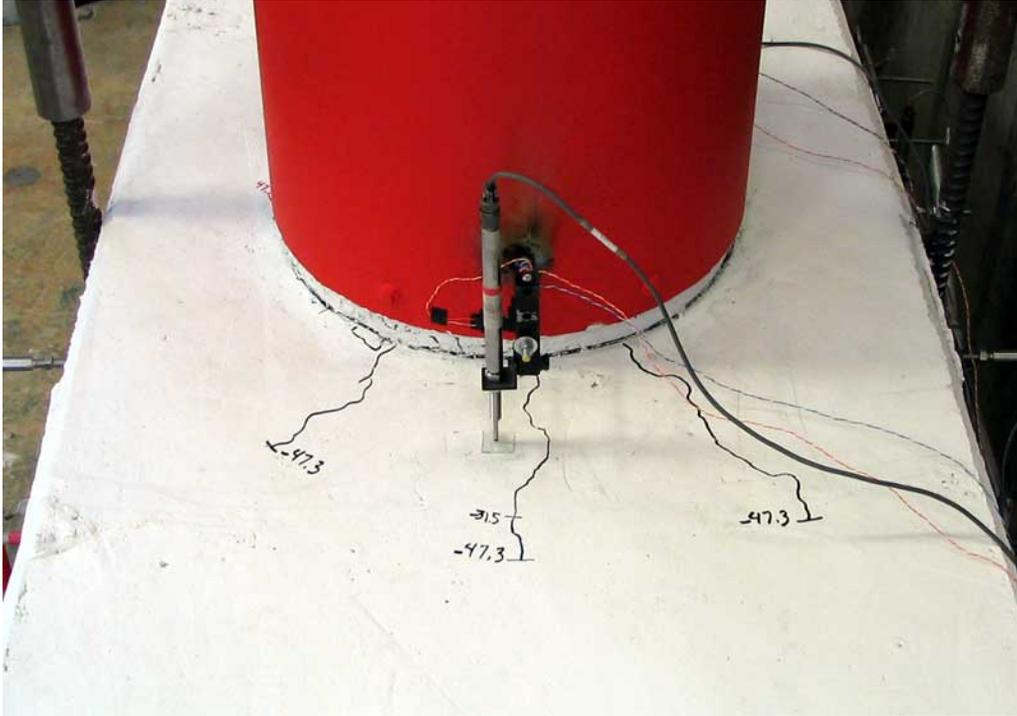
Figure 0-2. Bent Cap Cracking at 0.75V$_y$
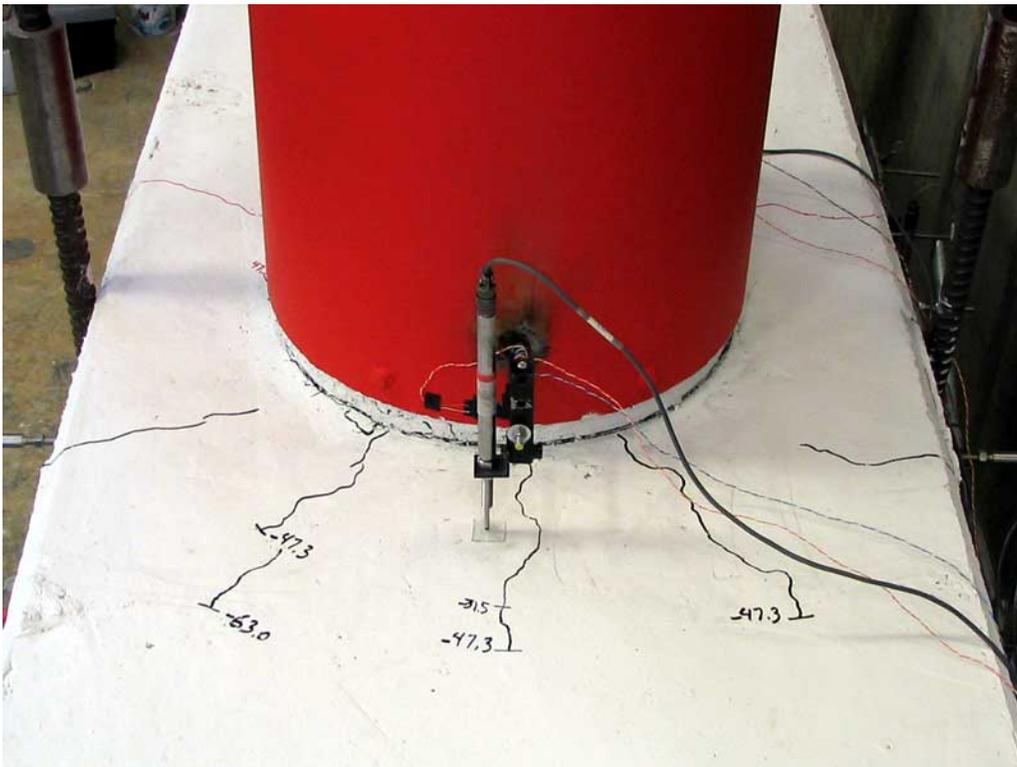
**Figure 0-3. Bent Cap Cracking at 1.00V$_y$**
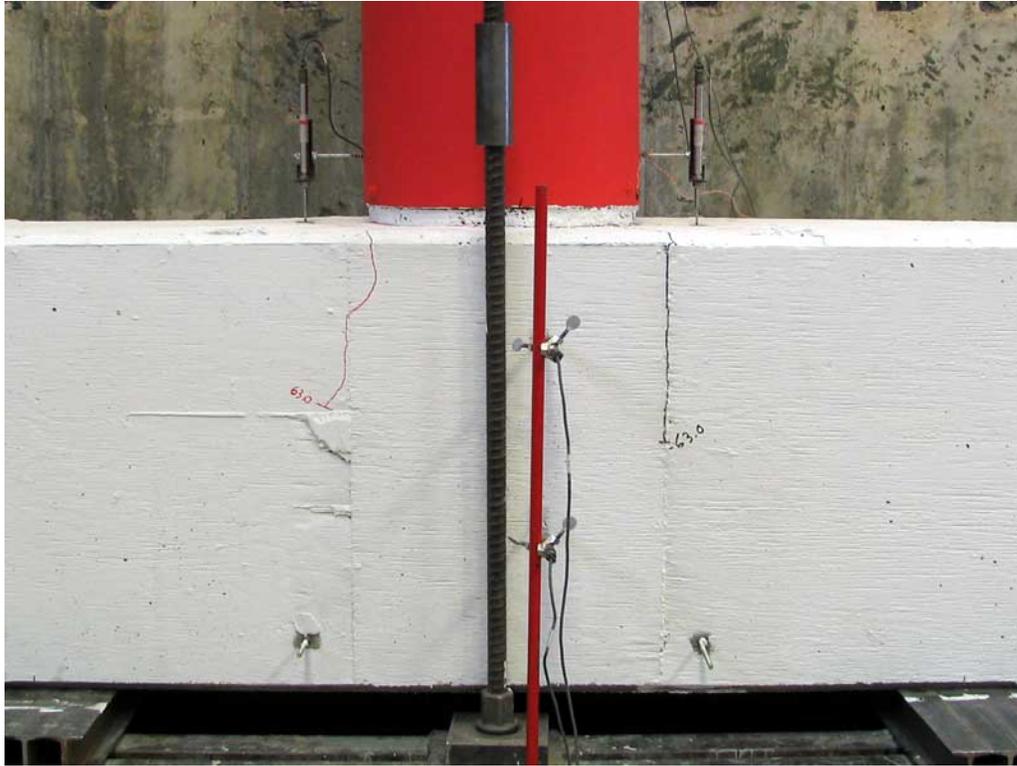
Figure 0-4. Joint Cracking at 1.00V$_y$

1.33.2. Displacement Control Load Cycles

After the force control load cycles the loading pattern was changed to displacement control as outlined in Section 1.25. As before, after reaching the peak at each displacement ductility level testing was paused on the first and last cycles to visually inspect and record damage to the unit.

- *1.0 μ_Δ [38.1 mm]:* Onset of joint shear cracking was observed in the joint region as shown in Figure 0-5. Strain penetration cracks around the column extended and onset of spalling of the cover concrete in the gap region was observed as shown in Figure 0-6.

- *1.5 μ_Δ [57.2 mm]:* There was additional joint shear cracking including extension of previous cracks along with additional flexural cracking as shown in Figure 0-7. An increase of strain penetration was observed by the increased cracking of the bent cap near the column as shown Figure 0-8.

- *2.0 μ_Δ [76.2 mm]:* Additional joint shear cracking was observed along with the extension of existing joint shear cracks as shown in Figure 0-9. Further cracking and lifting of the concrete next to the column due to the strain penetration was observed along with the onset of crushing of the column concrete as shown in Figure 0-10.

- *4.0 μ_Δ [152.4 mm]* –After the fist cycle at ductility level 4.0, there was a loss of moment capacity in the column. There were no additional joint shear cracks and only minimal extensions of the existing cracks as shown in Figure 0-11. The strain penetration blocks on each side of the

column lifted and the first line of headed reinforcement prevented cracking further into the bent cap as shown in Figure 0-12.

- *6.0 μ_Δ [228.6 mm]:* There was loss in moment capacity at this ductility level. At the second and third cycles, there were significant drops in stiffness and capacity. There were no additional joint shear cracks and the existing cracks did not extend further and remained within small widths as shown in Figure 0-13. Additional crushing of the column concrete was observed along with buckling and fracture of one of the column longitudinal bars on the last cycle as shown in Figure 0-14.

- *8.0 μ_Δ [304.8 mm]:* There was a continual decrease in capacity at this ductility level. Additional fracture of the main column longitudinal reinforcement was observed and detected during loading to this ductility level. Cracks propagated on the underside of the bent cap (see Figure 0-15), however, these cracks remained within small widths and no blocks were separated from the bent cap as occurred in Unit 1. In conclusion, joint shear cracks on the sides of the bent cap remained within small widths (see Figure 0-16), along with further crushing of the column cover concrete was observed as shown in Figure 0-17.

As before, after testing all loose concrete was removed. In comparison to Unit 1 damage to the bent cap was significantly smaller, as shown in Figure 0-18. The field welded hoops that were placed below the interface of the bent cap and column were effective in preventing buckling of the column longitudinal reinforcement at low ductility levels; however, they could not prevent entirely buckling to the column longitudinal reinforcement as shown in Figure 0-19 and Figure 0-20. As such, in design practice it is recommended to reduce the steel gap region and install additional transverse reinforcement to further prevent buckling of the longitudinal reinforcement. These issues were addressed during design of Unit 3 in Section 0, and will be further discussed in Section 1.54.
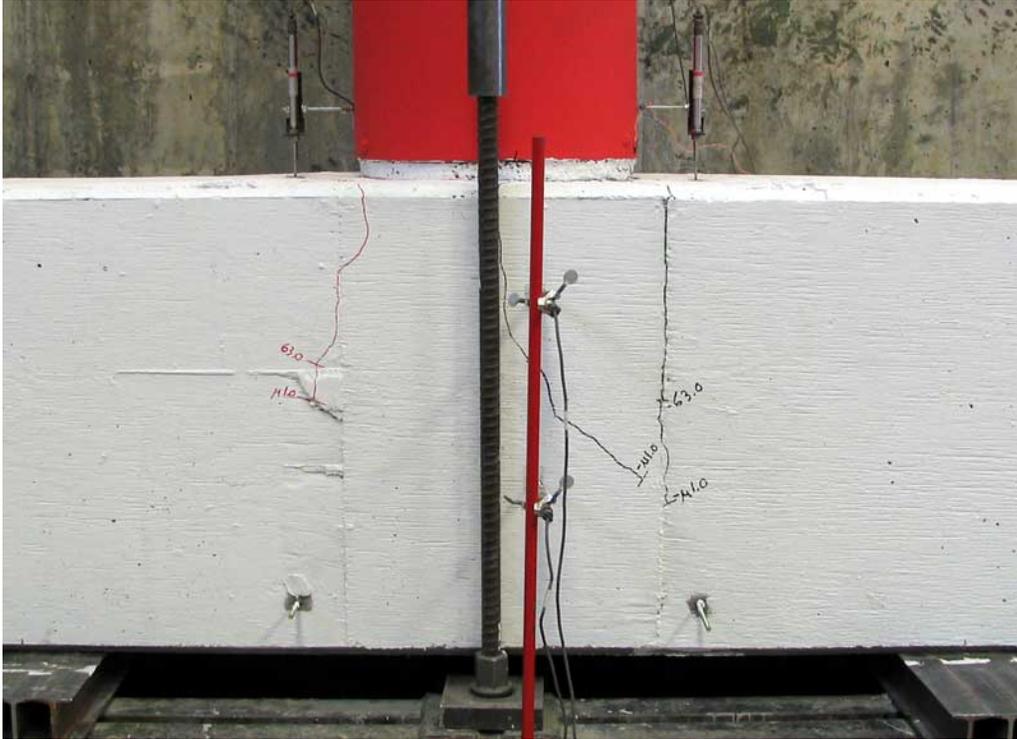
Figure 0-5. Joint Cracking at 1.0 μ_Δ
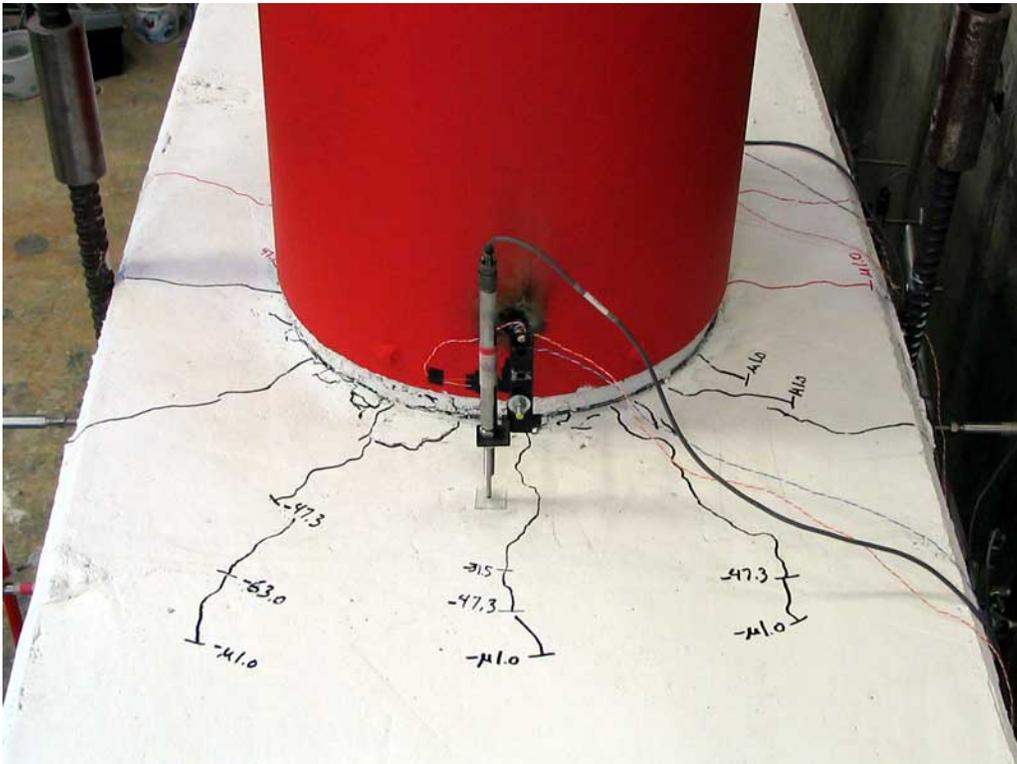
Figure 0-6. Bent Cap Cracking at 1.0 μ_Δ

Figure 0-7. Joint Cracking at 1.5 μ_Δ

Figure 0-8. Bent Cap Cracking at 1.5 μ_Δ
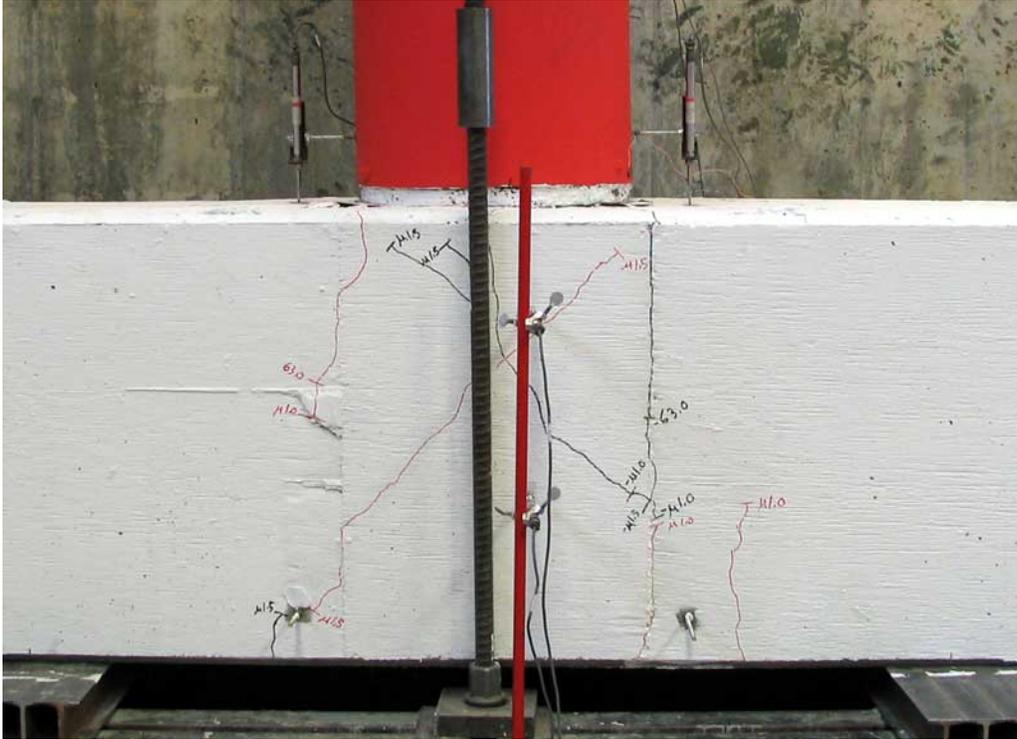
Figure 0-9. Joint Cracking at 2.0 μ$_\Delta$
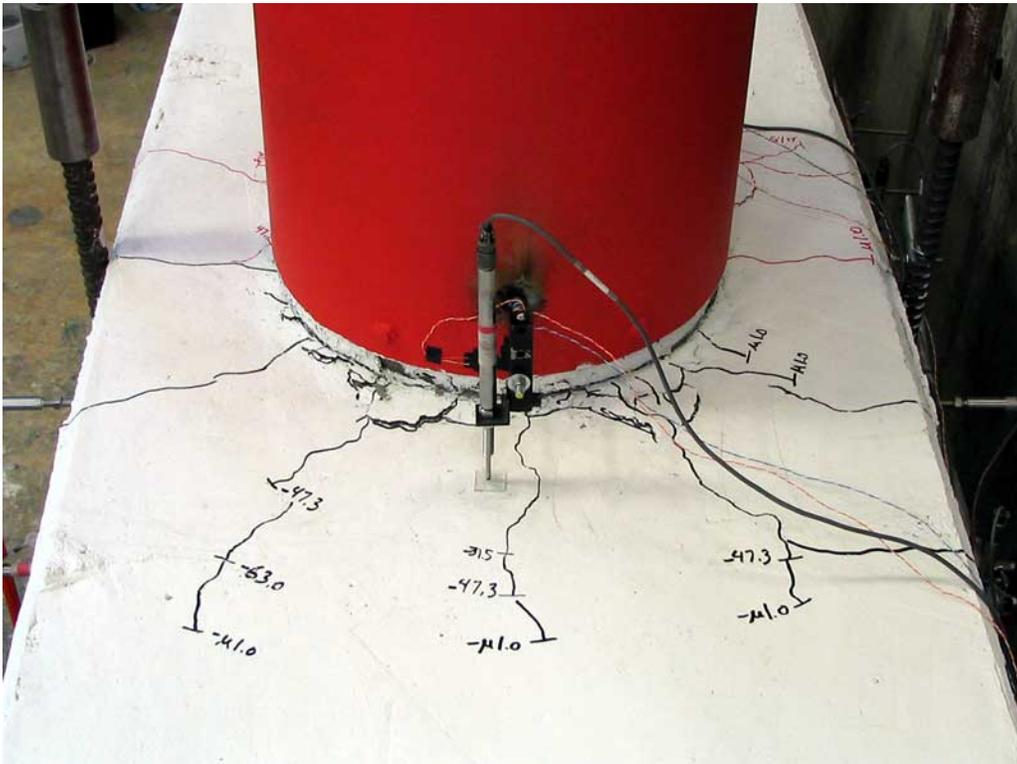
Figure 0-10. Bent Cap Cracking at 2.0 μ$_\Delta$
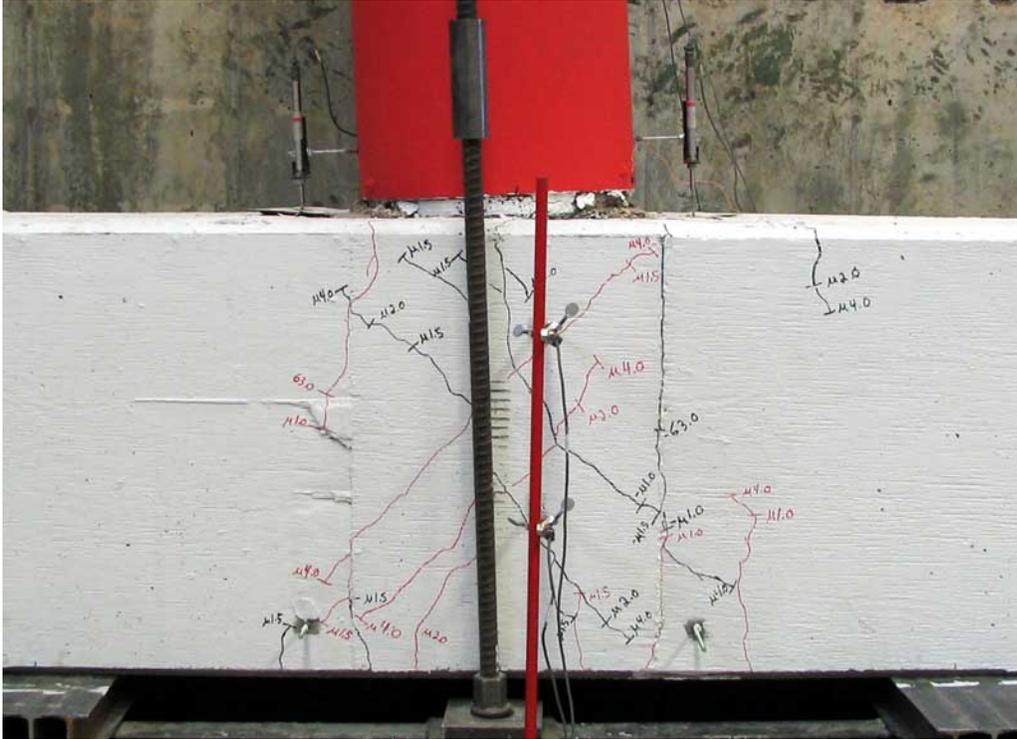
Figure 0-11. Joint Cracking at 4.0 μ_Δ
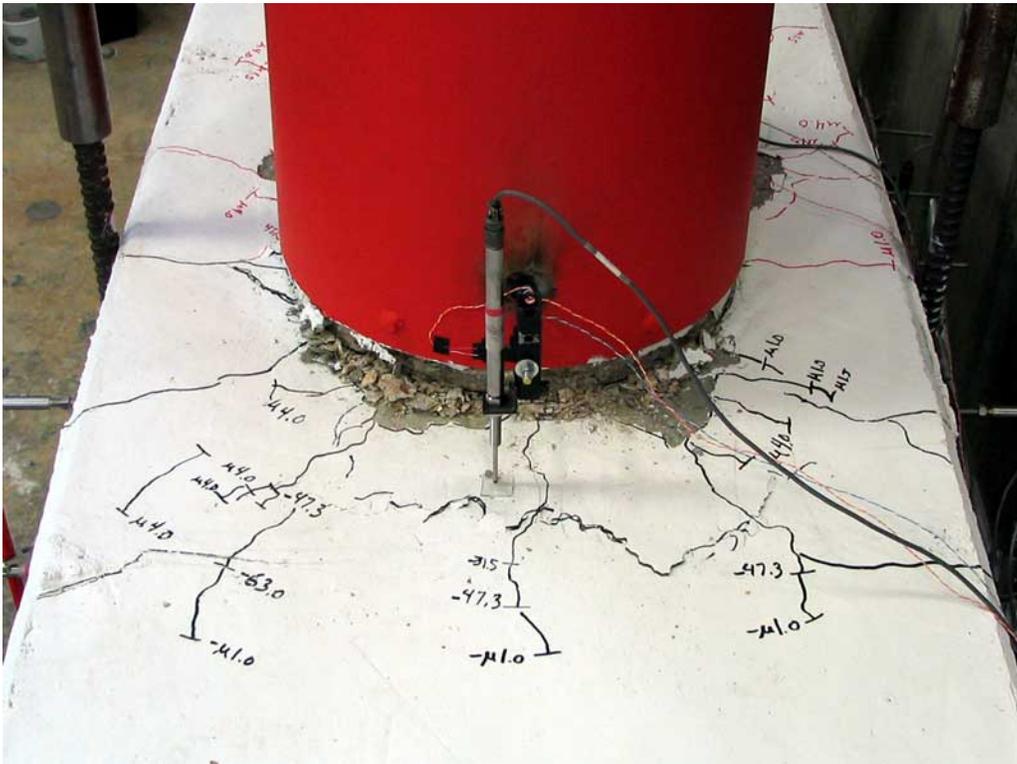
Figure 0-12. Bent Cap Cracking at 4.0 μ_Δ
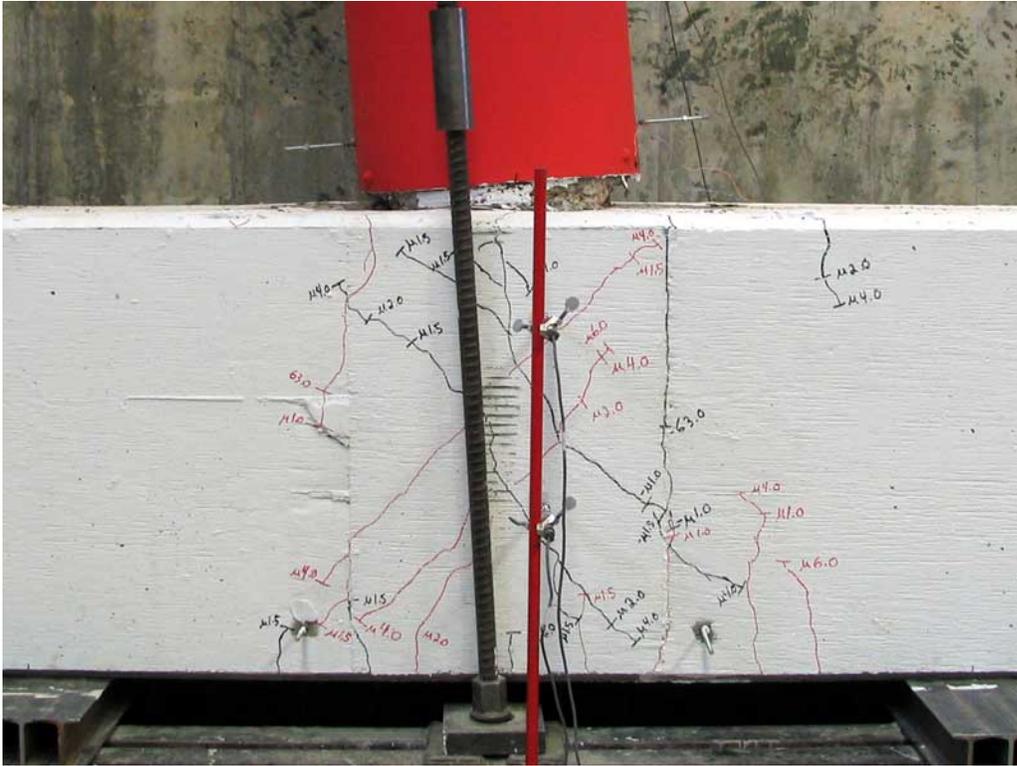
Figure 0-13. Joint Cracking at 6.0 μ_Δ
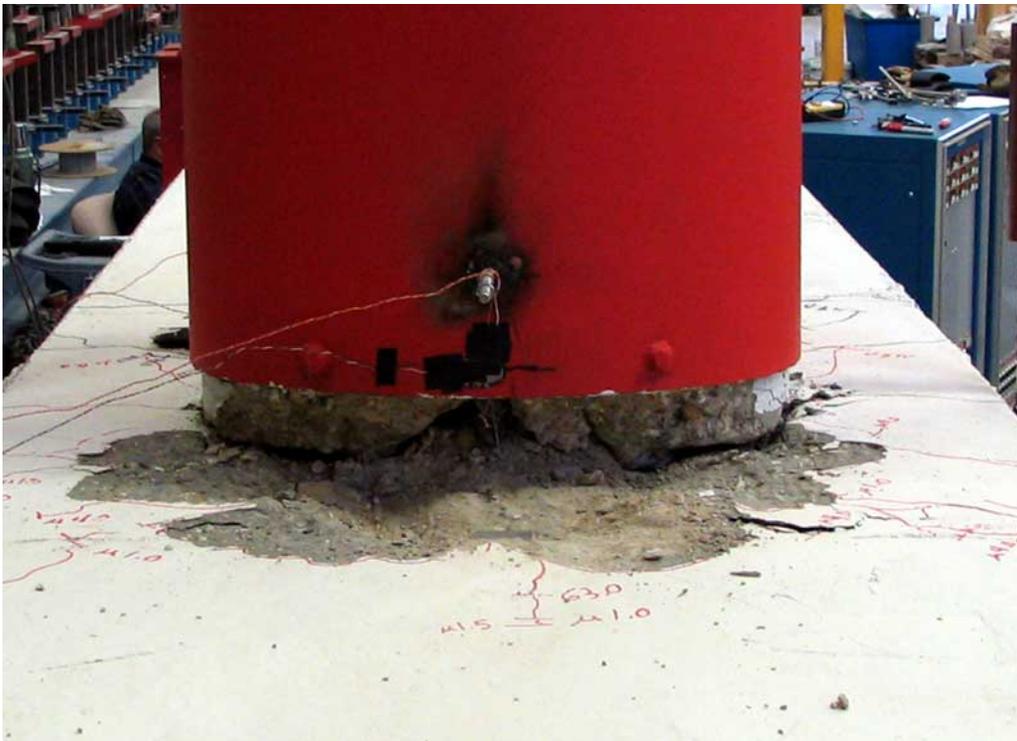
Figure 0-14. Bent Cap Cracking at 6.0 μ_Δ

Figure 0-15. Bottom Cracking at 8.0 μ_Δ
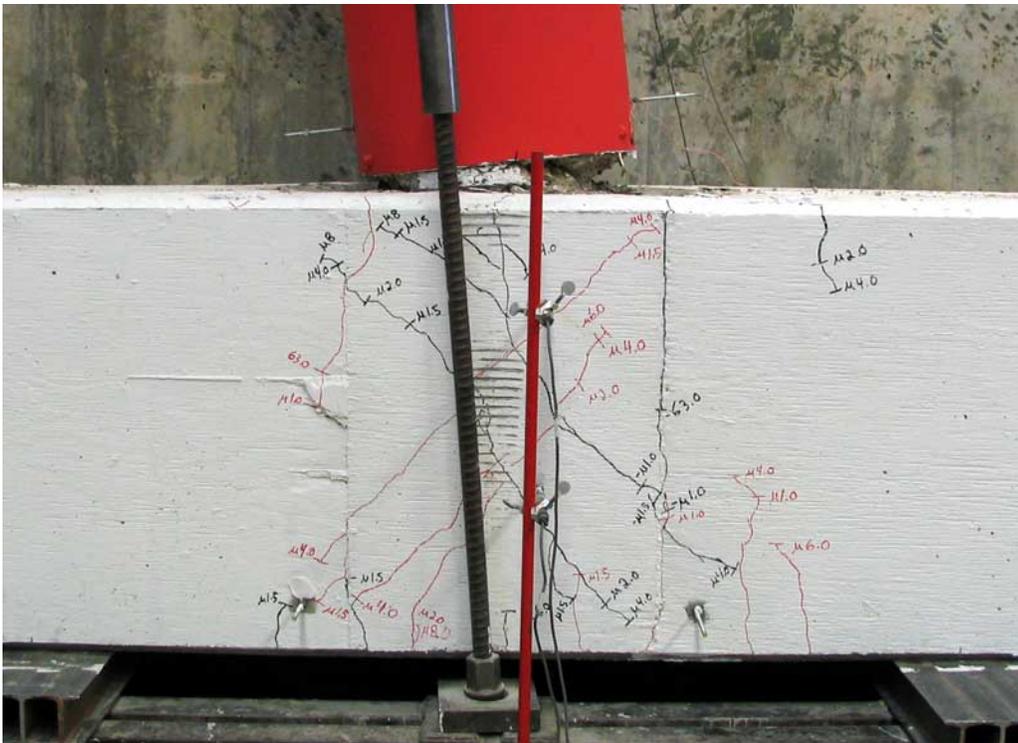
Figure 0-16. Joint Cracking at 8.0 μ_Δ

Figure 0-17. Column Crushing at 8.0 μ_Δ

Figure 0-18. Final Damage

Figure 0-19. Hoop Buckling Side "A"

Figure 0-20. Hoop Buckling Side "B"

1.34. LOAD DEFORMATION RESPONSE

Unit 2 was also tested under the loading protocol shown in Figure 0-2. The load vs. deformation response of Unit 2 is shown in Figure 0-21 along with the same features as those described for Unit 1. From an observation of the load vs. deformation for these two test units may lead to the general conclusion that the revised design details employed in the construction of Unit 2 does not translate in a significant improvement in the seismic response. However, further evaluation of the response of Unit 2 showed an improvement in the seismic response of this test unit in terms of damage comparisons and load degradation at higher ductility levels, which are described in further extent in Section 1.47. As in Unit 1, based on a direct investigation of the test results the new displacement at ductility level one was set at 35.1 mm.
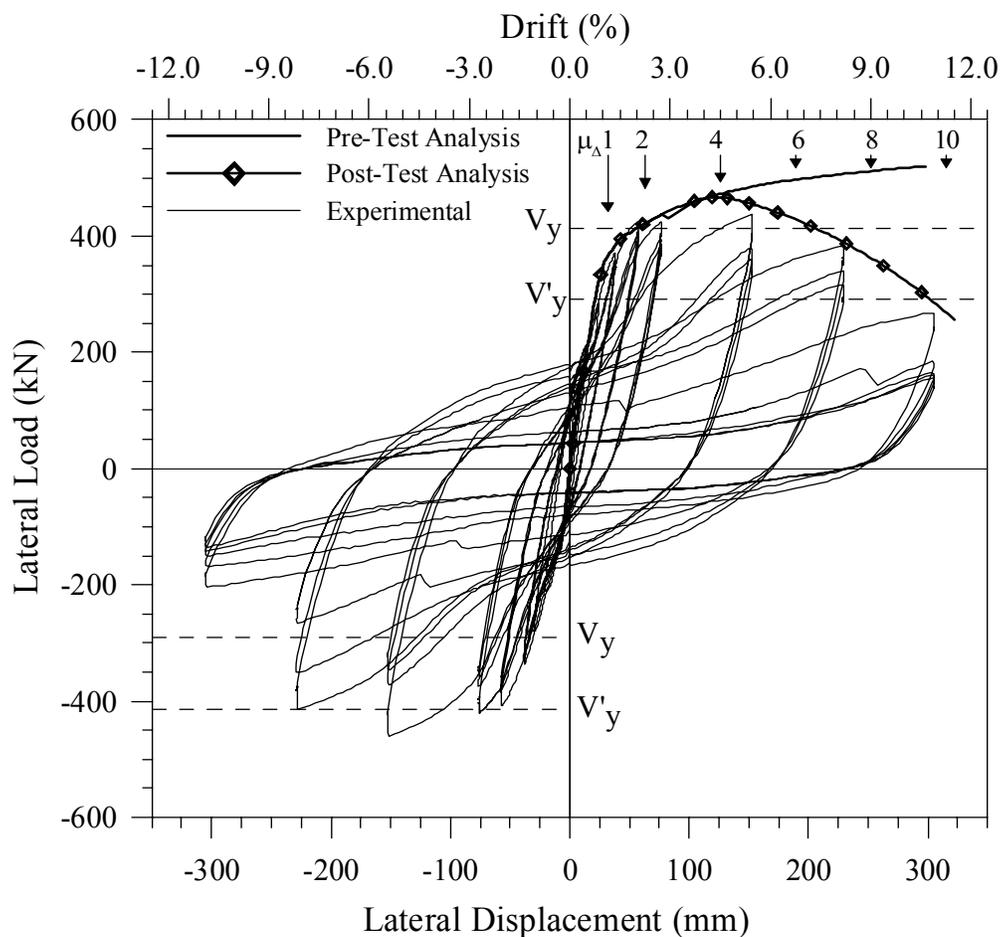
Figure 0-21. Unit 2 – Load Displacement Response

In Unit 2 the maximum registered lateral load was also recorded during the first cycle to the displacement of 152.4 mm. In the push and pull directions the registered lateral loads were +440 and -460 kN, respectively, which are slightly higher than those registered in Unit 1. Between the first and second cycles the drop in the lateral load was the same as in Unit 1 or approximately

17%, and between the second and third cycles the drop in the lateral load was 5%, indicating stability in the response of this unit. Comparisons of load degradation at higher ductility levels are also described in further detail in Section 1.47.

Unlike Unit 1, the first significant drop in the lateral load capacity of the test unit below the theoretical yield load level was not observed until the first cycle at the displacement of 304.8 mm. In Unit 1 similar levels of load degradation were observed at the displacement level of 228.6 mm, which is one of the main differences in the response of these two units. As before, the unit exhibit significant levels of strain penetration around the column but this was limited to the first row of vertical headed reinforcement. Compared to Unit 1 the levels of strain penetration and damage extended much further in the bent cap (see Figure 0-22). In total, four column longitudinal bars buckled and fractured due to low cycle fatigue during displacement ductility levels 6 and 8 indicating reserve capacity in the joint against pullout of the column reinforcement. Cracking due to joint shear was minimal and all joint shear cracks were small as shown in Figure 0-22. Some level of cracking occurred on the underside of the bent cap but was significantly smaller than in Unit 1 as shown in Figure 0-23, which indicates also an improvement in the seismic response of the test unit.
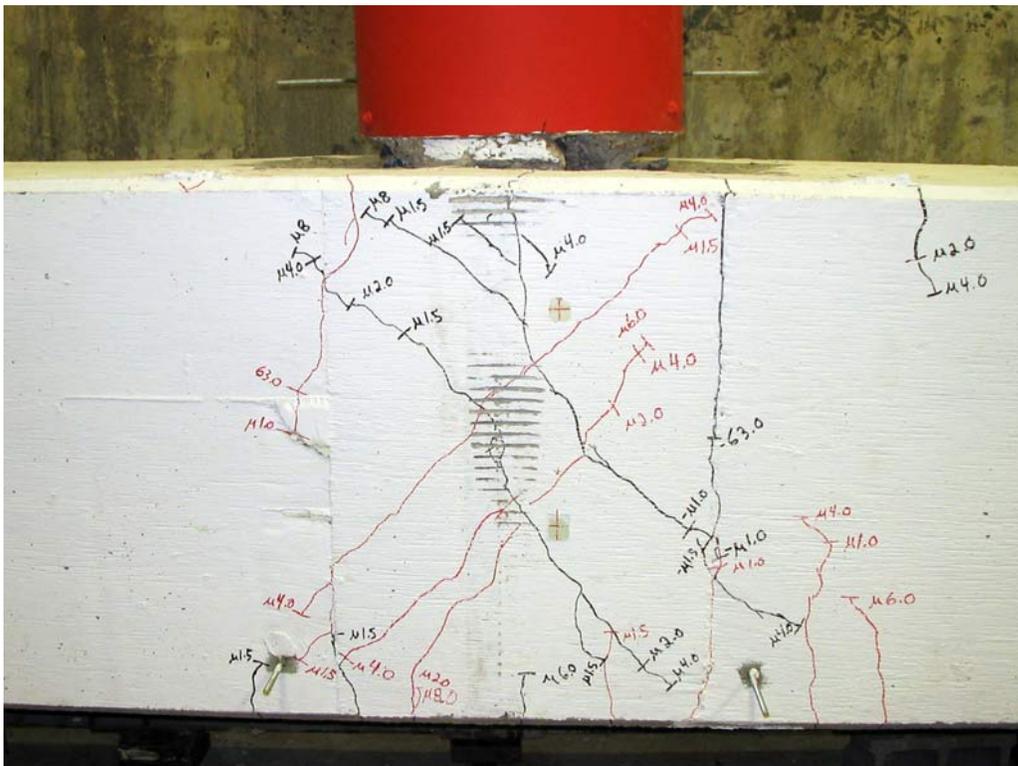
Figure 0-22. Unit 2 Joint Shear Cracks
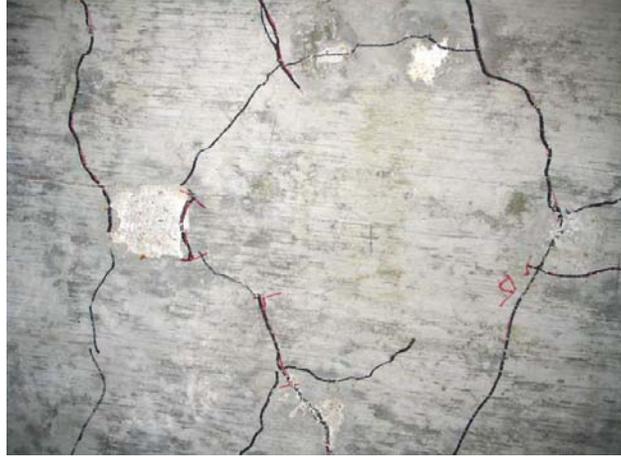
Figure 0-23. Cracking on Underside of Bent Cap

1.35. LOAD VS. CURVATURE RESPONSE

Figure 0-24 shows the measured lateral load versus the computed curvatures at the column to the bent cap interface for Unit 2. As in the previous Unit 1, the diagram depicted in this figure also indicates a good correlation between the pre-test analysis and the experimental test results during the initial stages of testing. However, after peak load there is a considerable deviation between these two curves. As in Unit 1, this can be attributed to large rotations originating solely from within the joint region.
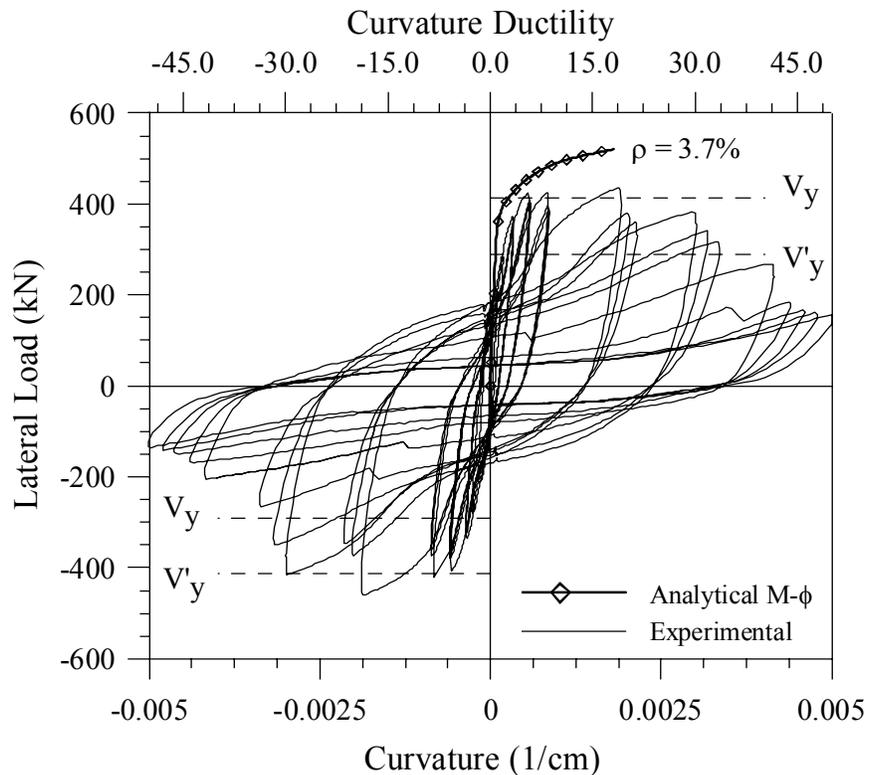
Figure 0-24. Unit 2 – Load versus Curvature Response

1.36.   COLUMN LONGITUDINAL REINFORCEMENT STRAINS

The strain histories of the column longitudinal reinforcement gauges at the interface of the column and bent cap for side "A" and side "B" are shown in Figure 0-25 and Figure 0-26, respectively. The yield strain of the column longitudinal reinforcement occurred at ±2,740με as determined from tensile testing.

The strain profiles for each side of the column are shown in Figure 0-27 and Figure 0-28. The onset of yielding of the main column longitudinal bars occurred at μ1.0 for each side of the column.
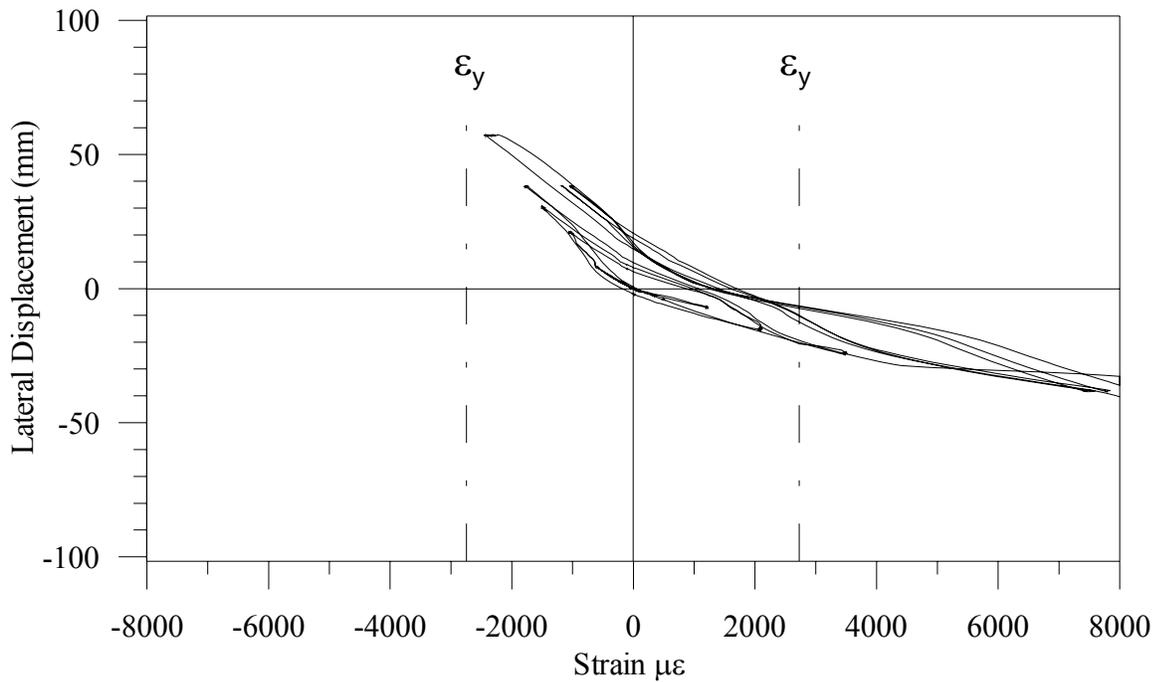
Figure 0-25. Strain Gauge History – C4a
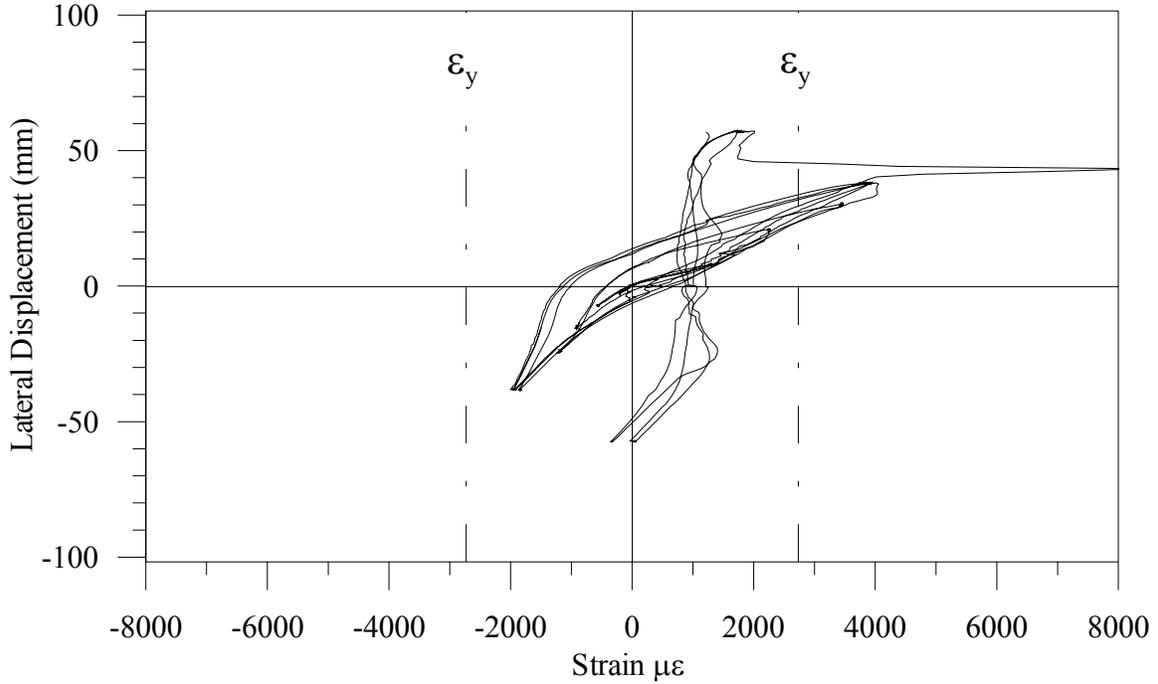
Figure 0-26. Strain Gauge History – C4b
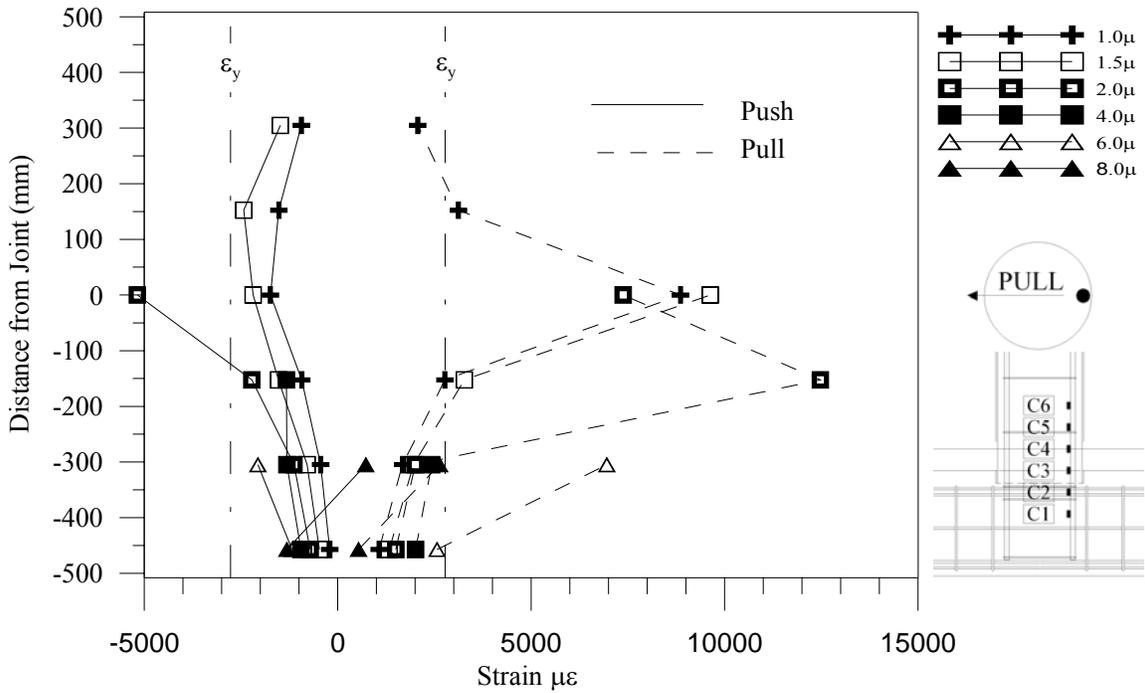
Figure 0-27. Strain Gauge Profile – Side "A"
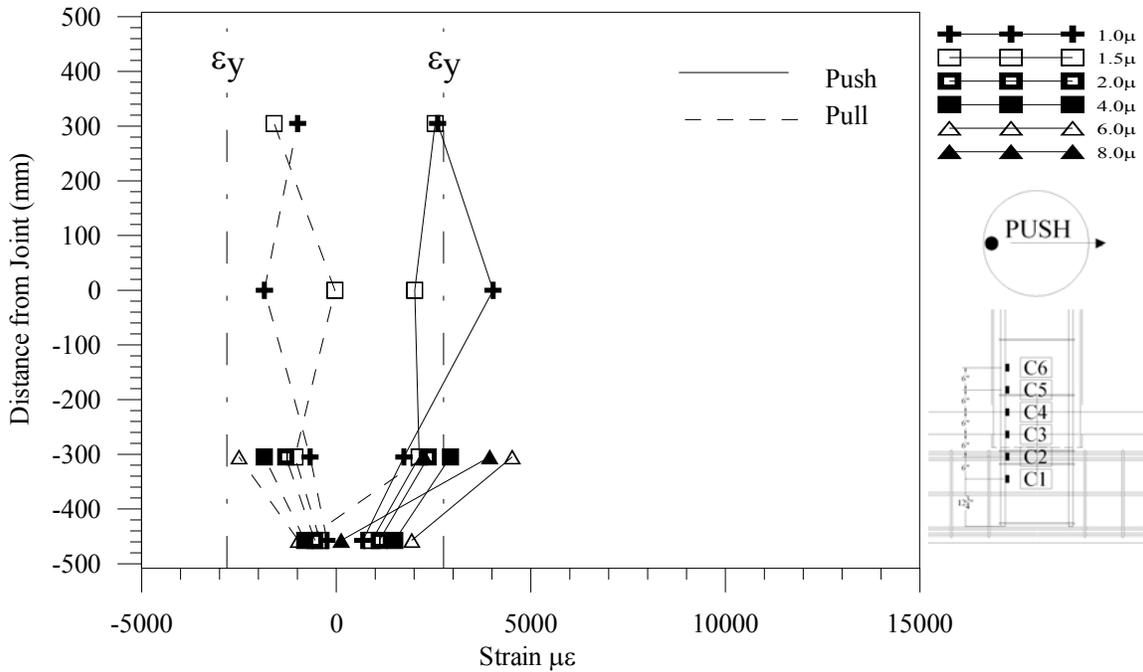
Figure 0-28. Strain Gauge Profile – Side "B"

1.37. JOINT SHEAR REINFORCEMENT STRAINS

The strain gauges from the shear reinforcement are presented in this section. The yield strain of the as-built shear reinforcement occurred at $\pm2,191\mu\varepsilon$ and the yield strain of the retrofit shear reinforcement occurred at $\pm2,630$ as determined from tensile testing. Figure 0-29 and Figure 0-30 are the strain profiles for the stirrups in the as-built concrete and the stirrups in the retrofit concrete, respectively. The stirrups stayed below the yield point indicating that joint shear did not occur in the longitudinal plane of the bent cap.

Through the initial stages of testing, there was not any significant amount of strain in the shear reinforcement for both the original steel and the retrofit steel indicating that there was not any shear cracks as was observed during testing. Through the later stages of testing, both the original steel and the retrofit steel had a achieved approximately the same level of strain. This is a strong indication that composite action developed between the as-built and retrofit sections. Past the column face, the strain in the stirrup quickly decreases indicating that the shear strains are primarily confined within an area h/2 away from the centerline of the column as indicated by joint shear cracks staying within this region.
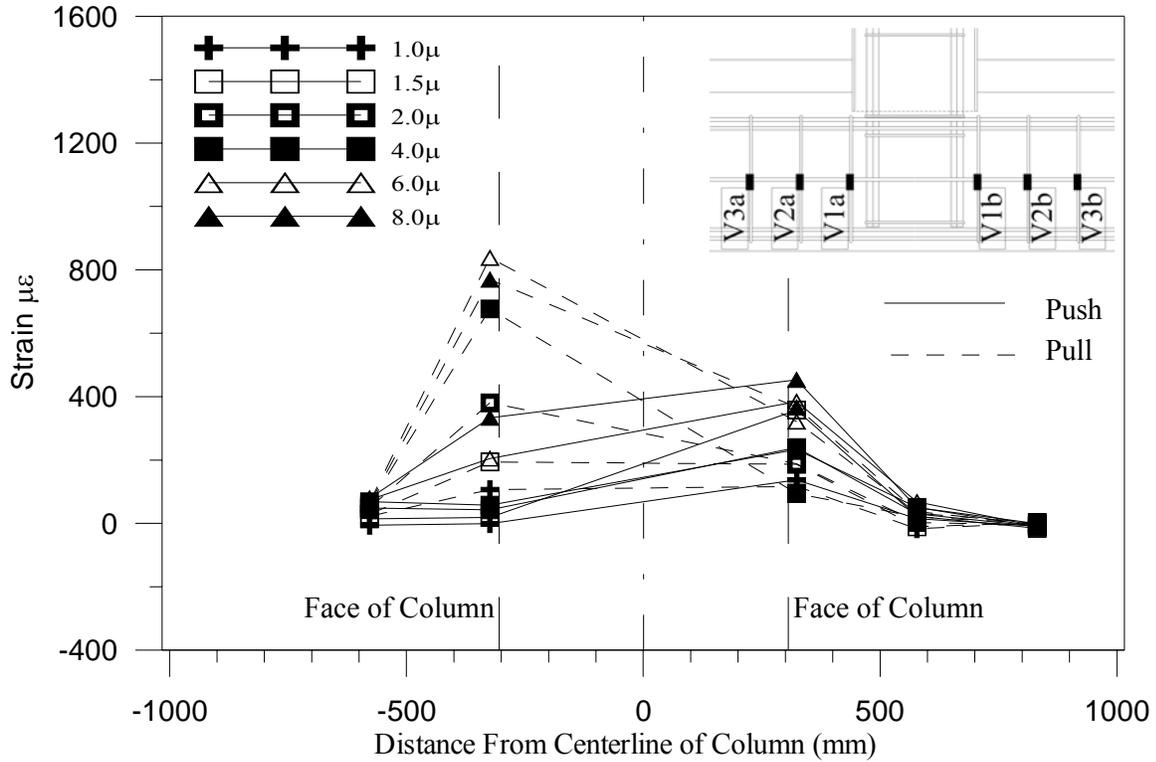
Figure 0-29. As-Built Strain Gauge Profile
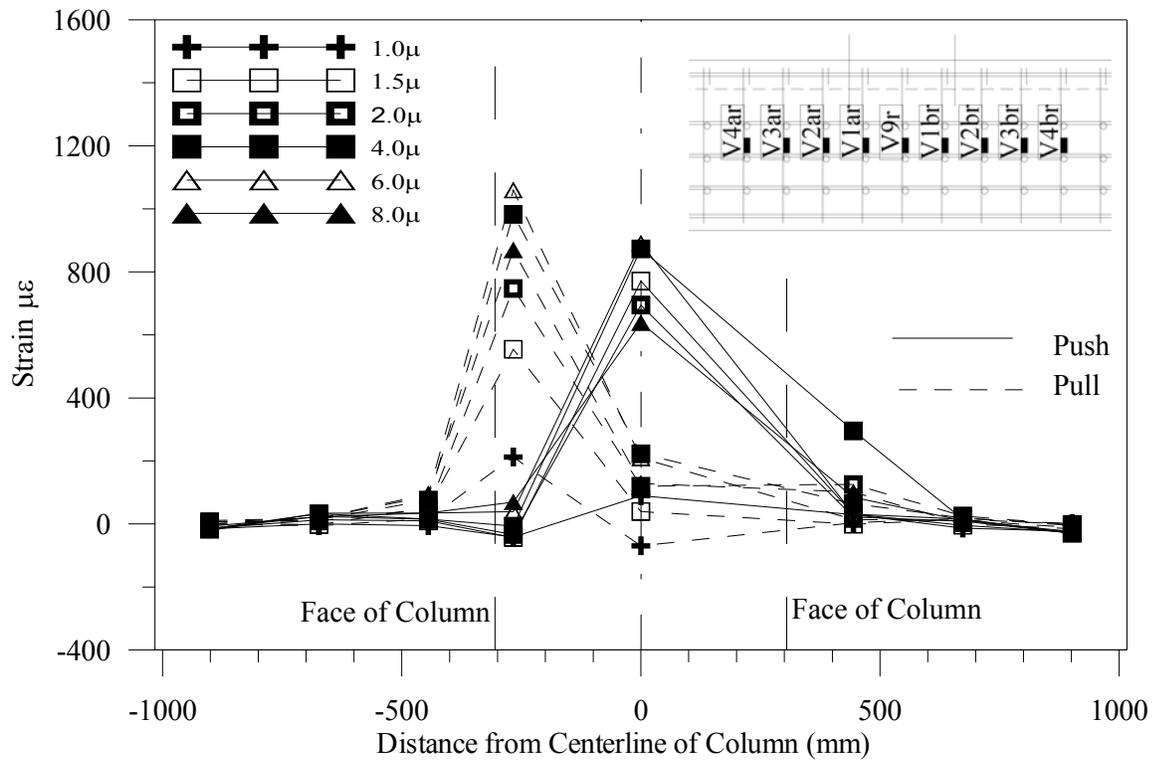
Figure 0-30. Retrofit Strain Gauge Profile

1.38. BENT CAP LONGITUDINAL REINFORCEMENT STRAINS

The following section presents the strain in the cap beam longitudinal steel. The yield strain for the original longitudinal steel is 2,807 με. The yield strain for the retrofit longitudinal steel is 2,604 με. For both the original and retrofit steel, the steel did not yield, indicating that the cap beam stayed elastic. For similar locations, the strain in both the retrofit steel and the original steel had strain levels that were very close indicating that the entire beam acted as one unit.
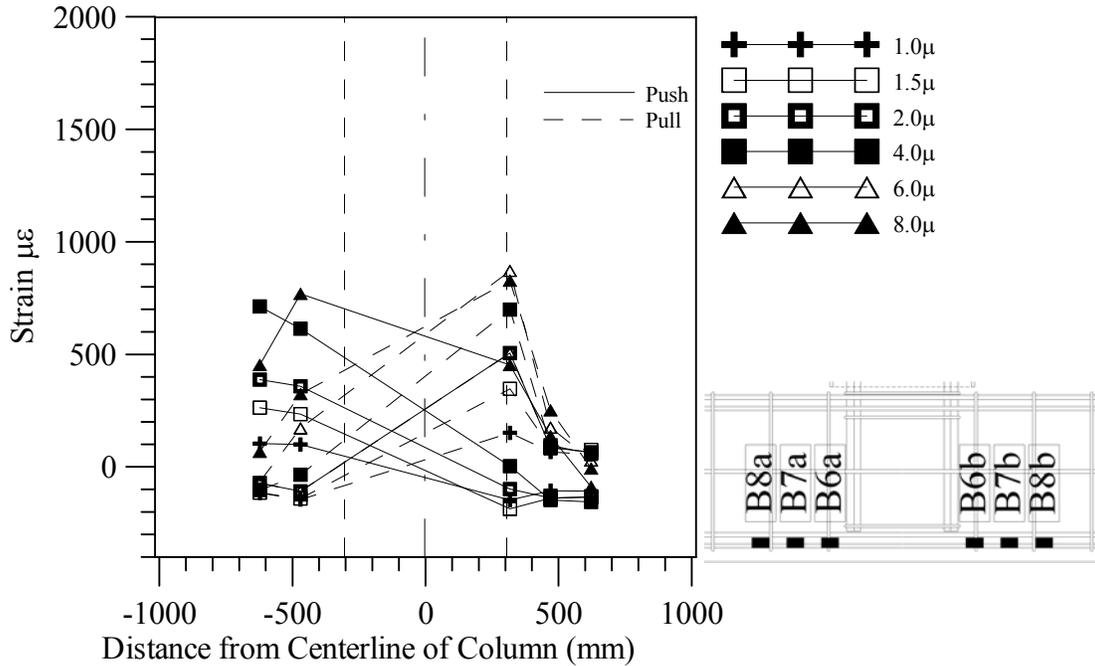
Figure 0-31. As-Built Bent Strain Gauge Profile
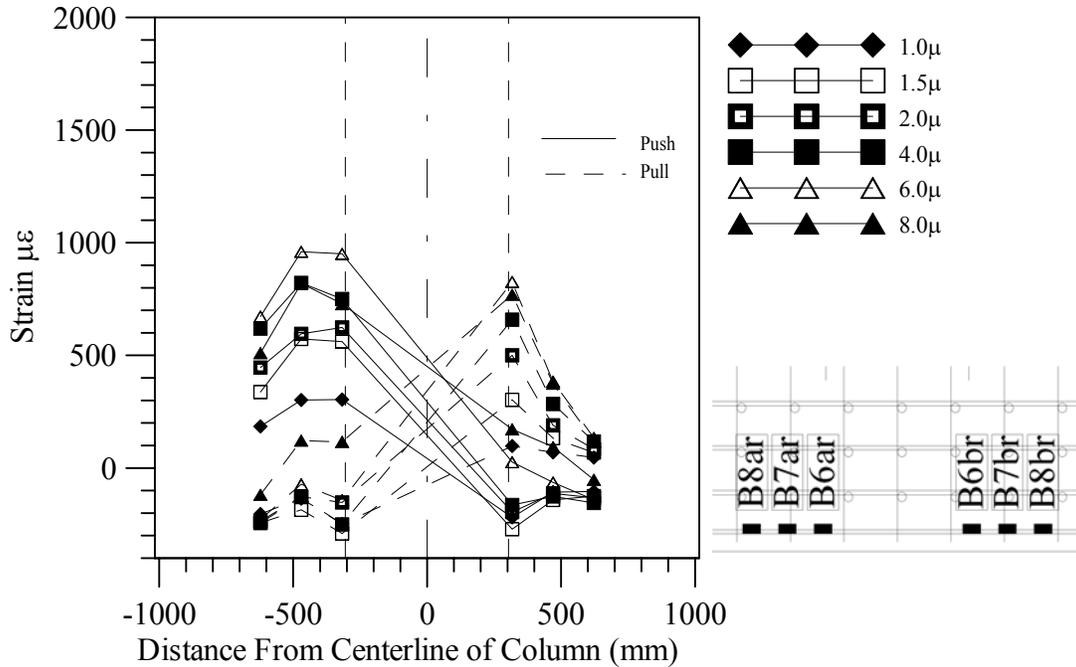
Figure 0-32. Retrofit Strain Gauge Profile

1.39. JOINT SHEAR ANALYSIS

Joint shear failure did occur as indicated by the degradation of the load and loss of capacity shown by the load vs. deformation curve in Figure 0-21. The shear deformation, shown in Figure 0-33, is larger than the first Unit. The continuous transverse headed reinforcement provided a mechanism to prevent the splitting failure as occurred in the first test Unit, preventing excessive transverse dilation and hence controlling the cracking and splitting of the bent cap.

The maximum recorded strain in the bent cap top transverse reinforcement was $1281\mu\varepsilon$ while the maximum strain in the transverse headed reinforcement was $506\mu\varepsilon$ as shown in the strain histories in Figure 0-35 and Figure 0-36, respectively, both of which are smaller than the $1,500\mu\varepsilon$ limit in the transverse direction that is recommended by Priestley (1996).

The strains in the longitudinal and shear reinforcement stayed below the yield point as shown in Figure 0-29, Figure 0-30, and Figure 0-31, Figure 0-32, respectively. This indicates that the bent cap performed as desired and preventing any permanent deformations and forcing the plastic hinge to form in the column.
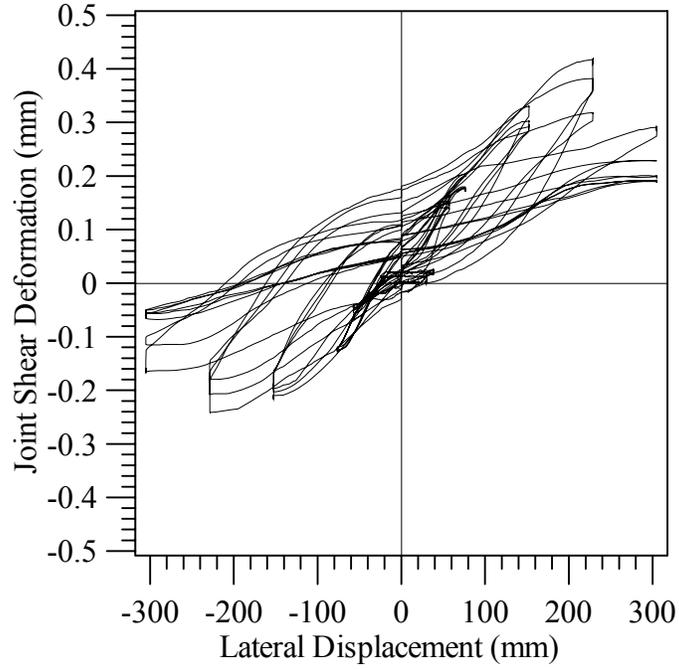
Figure 0-33. Specimen #2 Joint Shear Deformation
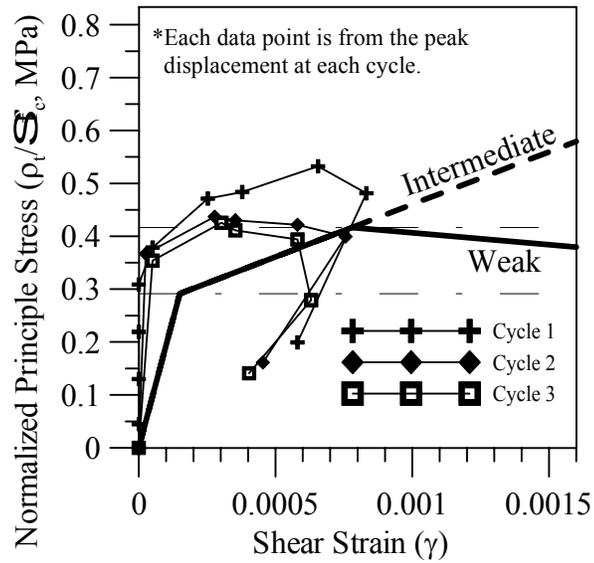
Figure 0-34. Unit 2 Principle Tensile Stress vs. Joint Shear Strain
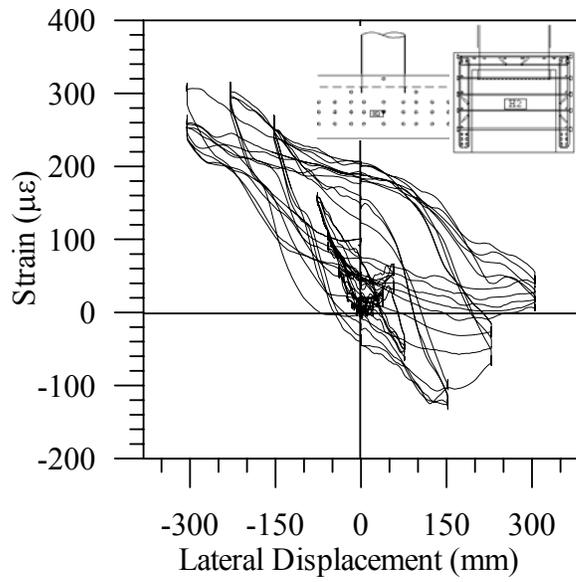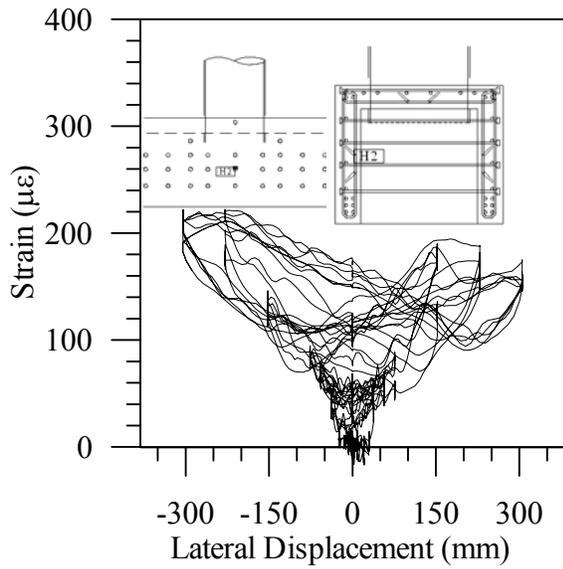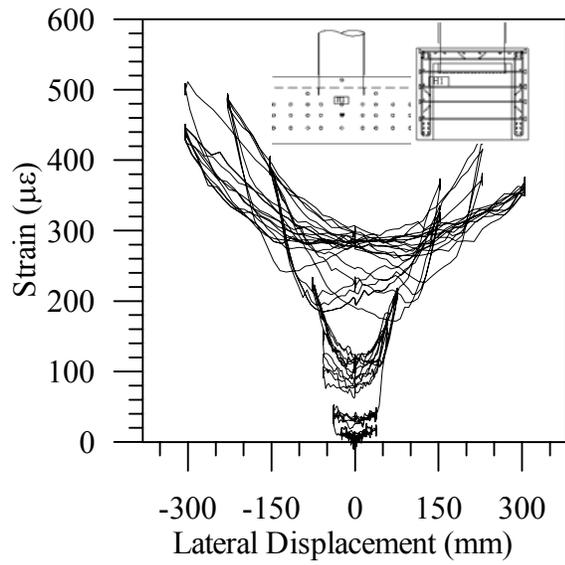
Figure 0-35. Unit 2 Headed Transverse Reinforcement Strain History
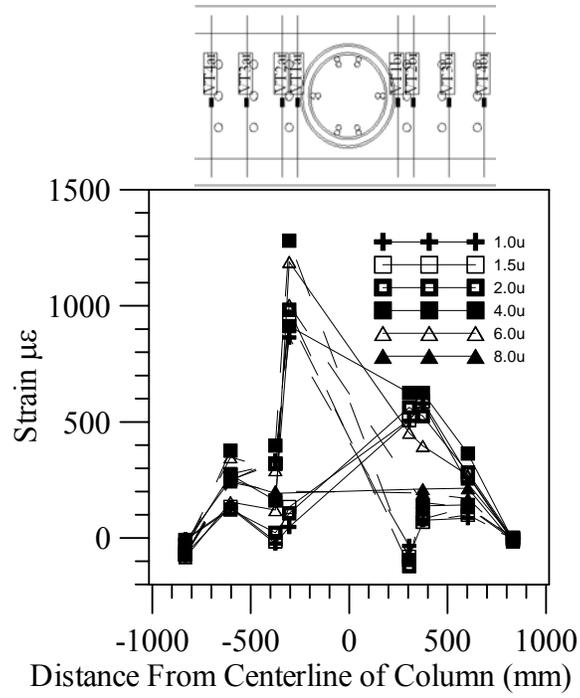
Figure 0-36. Unit 2 Top Transverse Reinforcement Strain Profile

This section presents observations made during experimental testing, including force-deformation and reinforcement strain profiles for the column and bent cap.

1.40. GENERAL TEST OBSERVATIONS

1.40.1. Force Control Load Cycles

Unit 3 was loaded in the same manner as Unit 1 and 2, using the same loading protocol as shown in Figure 0-2. Onset of cracking was detected at $1.00V_y$ with cracks forming on the bent cap top surface, which once again indicates onset of strain penetration, as shown in Figure 0-1. no other damage level was recorded for this test unit.
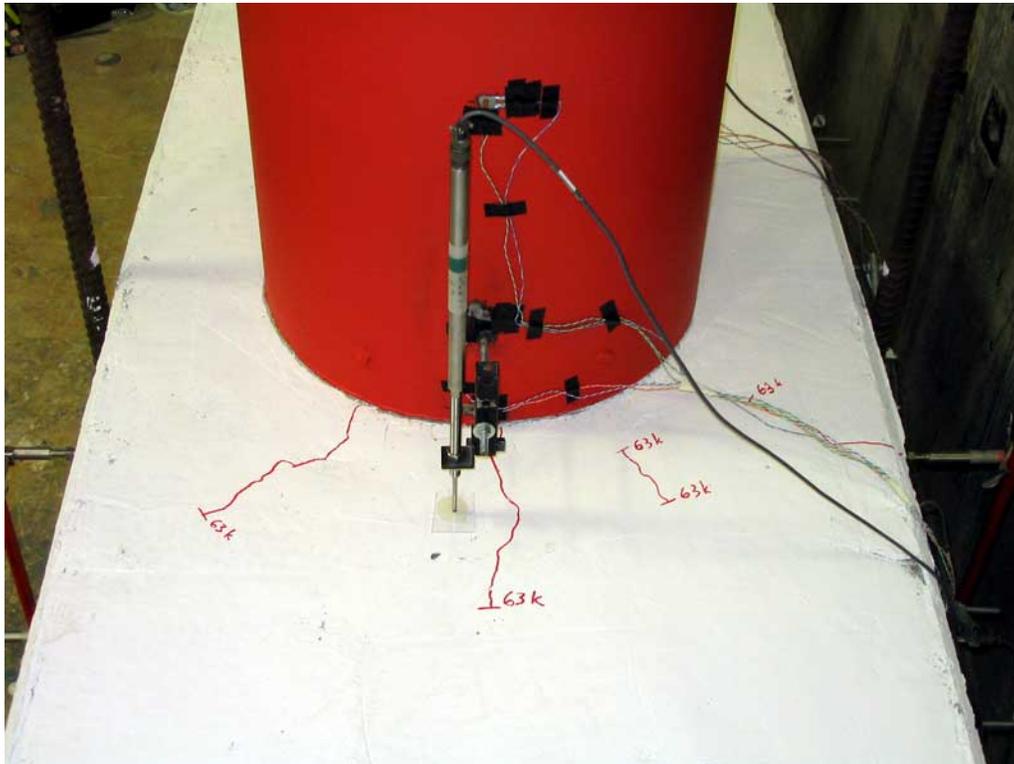
Figure 0-1. Bent Cap Cracking at $1.00V_y$

1.40.2. Displacement Control Load Cycles

After the four force control load cycles the loading pattern was changed to displacement control as outlined in Section 1.25. During the first and last cycle peak reversals and at each displacement ductility level testing was paused to visually inspect and record damage to the test unit. It is important to note that besides some minor differences nearly the same observations were recorded for the three units.

- 1.0 μ_Δ [38.1 mm]: Onset of joint shear cracking was observed in the joint region as shown in Figure 0-2. As shown in Figure 0-3, previously recorded cracks depicting strain penetration grew in width, indicating the longitudinal bars were properly anchored to the joint.

- 1.5 μ_Δ [57.2 mm]: There was additional joint shear cracking including extension of previous cracks along with the onset of flexural cracking in the bent cap as shown in Figure 0-4. Additional cracking on the bent cap due to strain penetration was minimal (see Figure 0-5).

- 2.0 μ_Δ [76.2 mm]: Additional joint shear cracking and flexural cracking was observed along with the extension of existing joint shear and flexural cracks as shown in Figure 0-6. Additional cracking and extension of existing cracks was observed on the bent cap due to strain penetration along with onset of crushing of the column cover concrete as shown in Figure 0-7.

- 4.0 μ_Δ [152.4 mm]: After the fist cycle at ductility level 4.0, there was a loss of moment capacity in the column. There were no additional joint shear cracks observed with minimal extensions of existing cracks. Additional flexural cracks were observed on the side of the joint along with extension of existing cracks as shown in Figure 0-8. Concrete blocks originating from strain penetration on either side of the column lifted and the first line of headed reinforcement prevented further cracking into the bent cap as shown in Figure 0-9.

- 6.0 μ_Δ [228.6 mm]: There was loss in moment capacity at this ductility level. The first cycle followed the stiffness of the second and third cycles of 4.0μ but there was an overall loss in capacity at 6.0μ. At the second and third cycles, there were significant drops in stiffness and capacity; however, no additional joint shear cracks or extension of existing cracks were observed as seen Figure 0-10. Additional crushing of the column cover concrete was observed along with the widening of one of the existing cracks on the surface of the bent as shown in Figure 0-11. Onset of cracking on the underside side of the bent cap was observed at this level.

- 8.0 μ_Δ [304.8 mm]: There was a continual significant loss in capacity at this ductility level. No further extension of joint shear cracks was observed and previously recorded cracks stayed within constant widths through testing. Cracking from the strain penetration extended to the side of the bent cap as indicated by the horizontal crack on the side of the bent cap as shown in Figure 0-12. Further lifting of the concrete around the column due to strain penetration was observed including the increase of one crack on each side of the bent cap as shown in Figure 0-13 and Figure 0-14. Cracking continued at the bottom and blocks started to fall off as shown in Figure 0-15.

As in the previous two test units, after testing all loose cracked concrete was removed. The extent of the damage to the bent cap was confined by the first row of headed reinforcement as shown in Figure 0-16. Reducing the gap region to 13 mm prevented excessive crushing of the column concrete as shown in Figure 0-17. This also prevented the column longitudinal reinforcement from buckling and leading to premature low cyclic fatigue and fracture. The

extent of the cracking on the underside of the bent cap is shown in Figure 0-18. Further comparisons and discussions with Units 1 and 2 is discussed in Section 0.
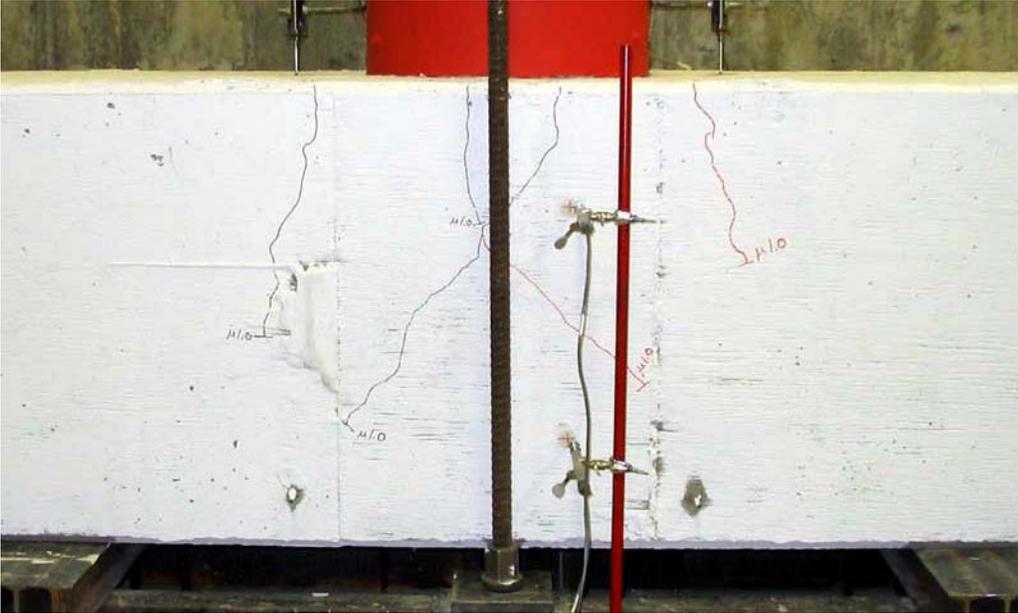
Figure 0-2. Joint Cracking at 1.0 μ_Δ
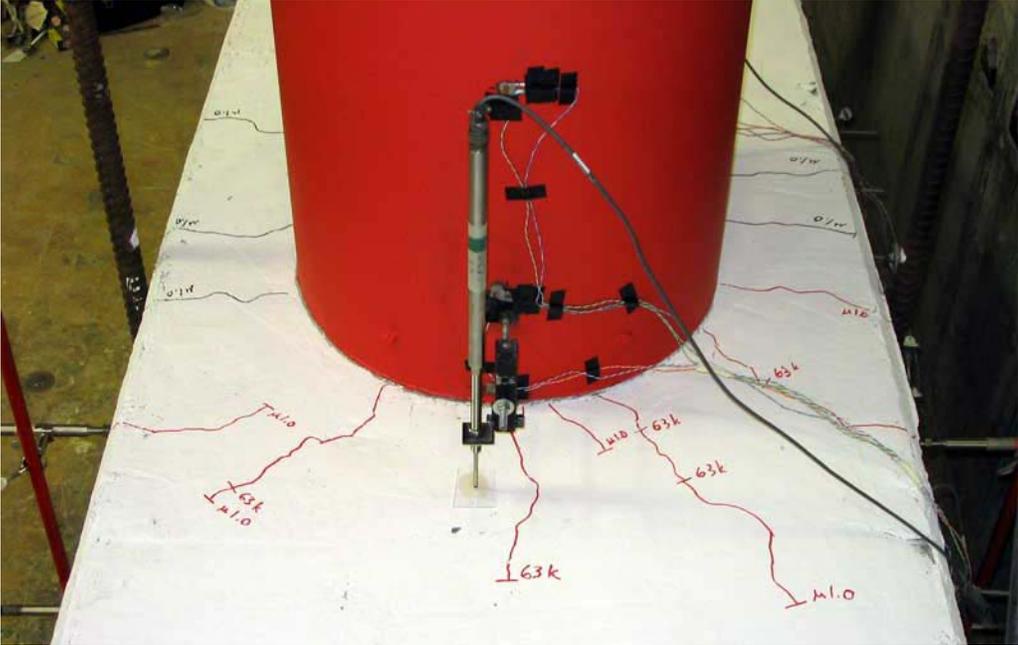
Figure 0-3. Bent Cap Cracking at 1.0 μ_Δ
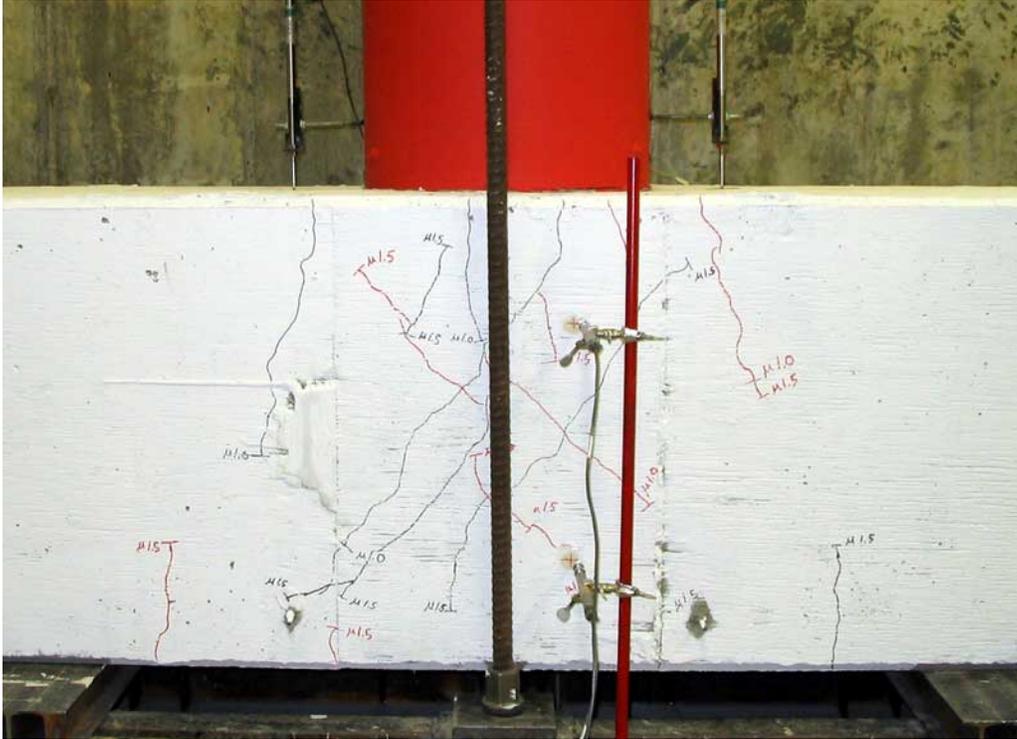
Figure 0-4. Joint Cracking at 1.5 μ_Δ
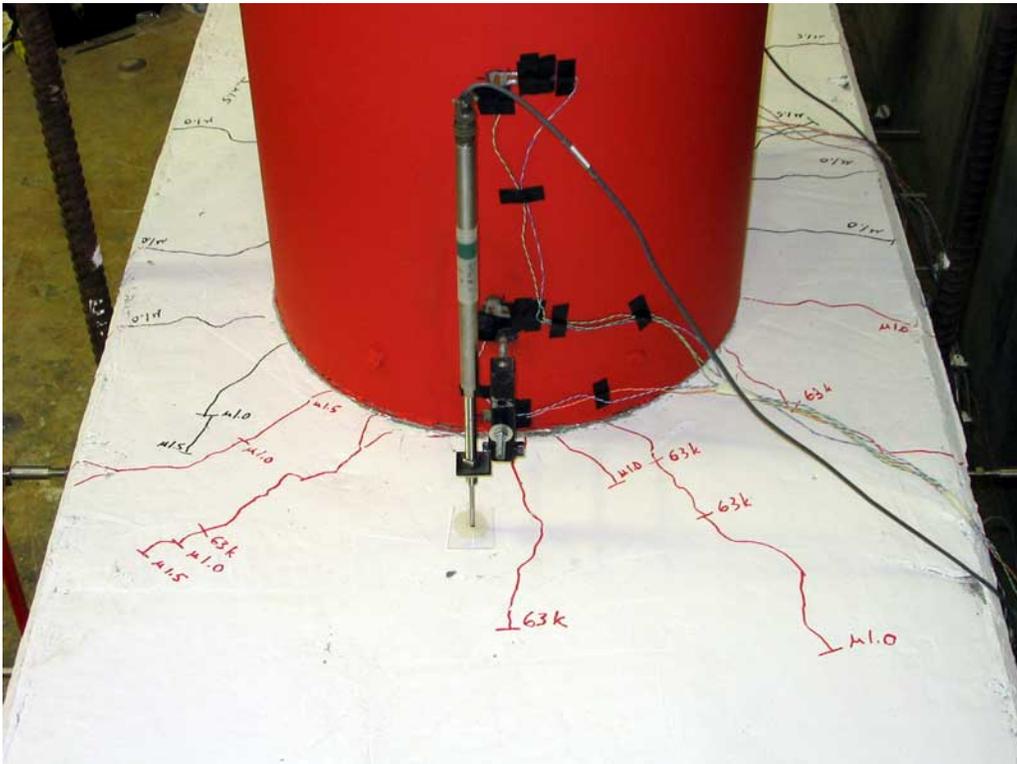
Figure 0-5. Bent Cap Cracking at 1.5 μ_Δ
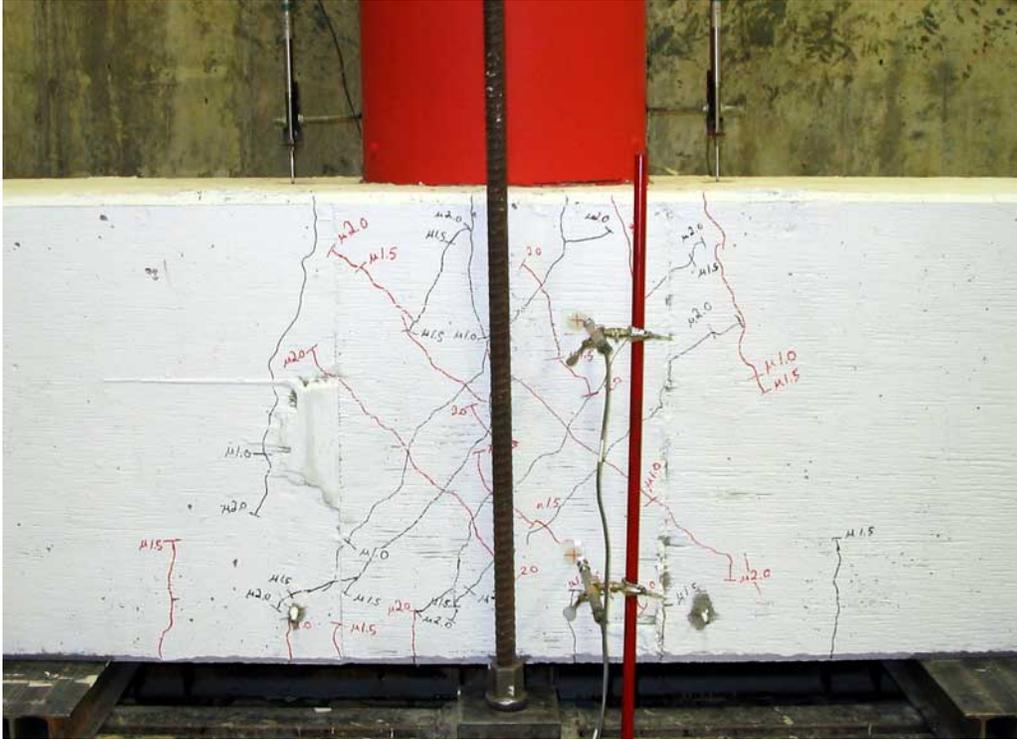
Figure 0-6. Joint Cracking at 2.0 μ_Δ
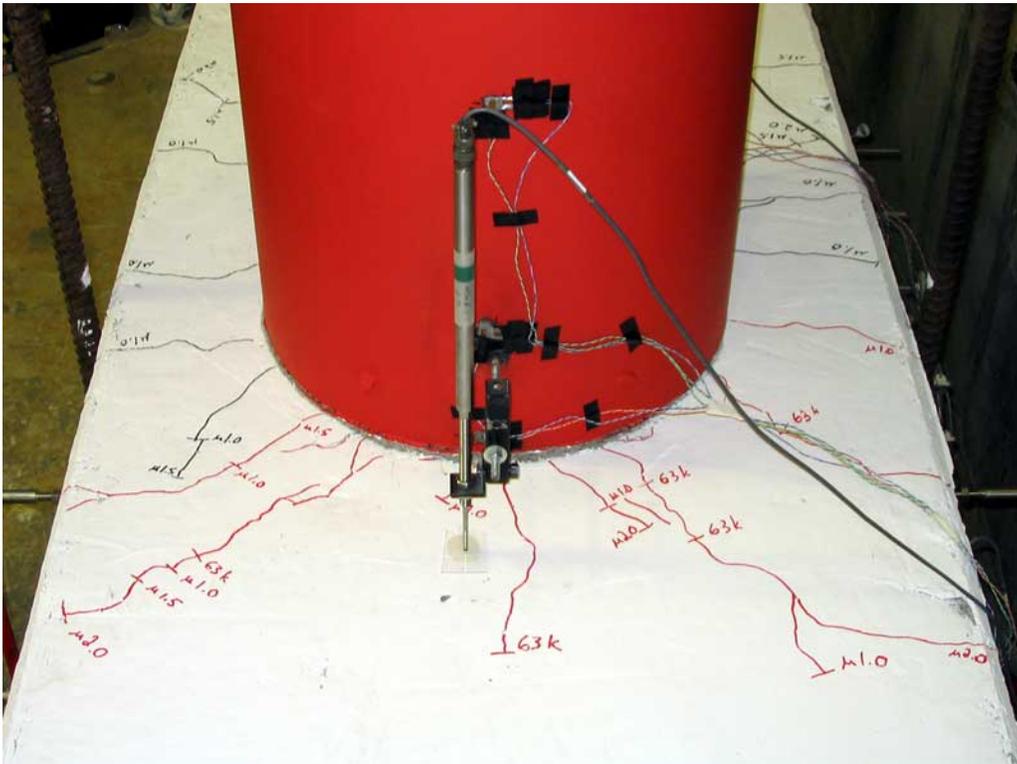
Figure 0-7. Bent Cap Cracking at 2.0 μ_Δ

Figure 0-8. Joint Cracking 4.0 μ_Δ

Figure 0-9. Bent Cap Cracking at 4.0 μ_Δ

Figure 0-10. Joint Cracking at 6.0 μ_Δ
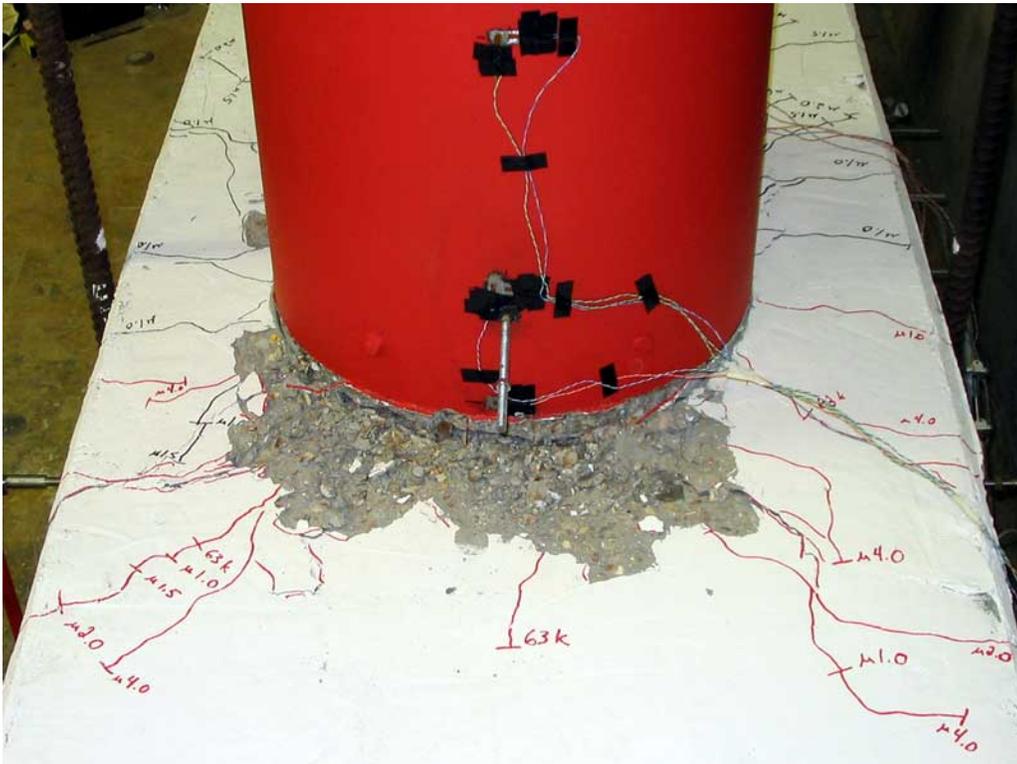
Figure 0-11. Bent Cap Cracking at 6.0 μ_Δ

Figure 0-12. Joint Cracking at 8.0 μ_Δ

Figure 0-13. Bent Cap Cracking – Side "A" at 8.0 μ_Δ

Figure 0-14. Bent Cap Cracking – Side "B" at 8.0 μ_Δ

Figure 0-15. Bent Cap Underside Cracking at 8.0 μ_Δ

Figure 0-16. Bent Cap Cracking Ultimate Damage

Figure 0-17. Column Crushing Ultimate Damage
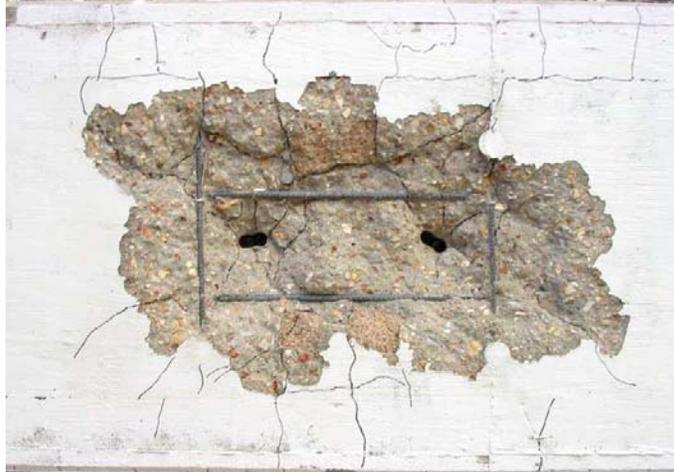
Figure 0-18. Underside of Bent Cap Ultimate Damage

1.41. LOAD DEFORMATION RESPONSE

The load vs. deformation response of Unit 3 is shown in Figure 0-19. After the displacement of 228.6 mm the unit experienced significant loss in the lateral load capacity. There was significant strain penetration around the column, especially after the displacement of 228.6 mm. The reduction of the gap to 13mm prevented excessive crushing of the column concrete and prevented buckling of the column longitudinal bars as previously described in Unit 1 and 2. This further accentuates the conclusion that the reduction in the lateral load in the two previous units was likely from joint shear failure and not due to buckling of the column longitudinal reinforcement. Cracking on the sides of the bent cap resulting from joint shear was minimal and all cracks stayed small as shown in Figure 0-20. The crack pattern was more distributed than in Units 1 and 2. Cracking and spalling of large pieces of concrete occurred on the underside of the bent cap indicating once again anchorage failure as shown in Figure 0-18.

In Unit 3 the maximum registered lateral load was also recorded during the first cycle to the displacement of 152.4 mm. In the push and pull directions the registered lateral loads were +555 and -570 kN, respectively, which are nearly 20% higher than those registered for the previous units. Between the first and second cycles the drop in the lateral load was the same as in Unit 1 or approximately 14%, and between the second and third cycles the drop in the lateral load was 5%, indicating once again stability in the response of Unit 3. Comparisons of load degradation at higher ductility levels are also described in further detail in Section 1.47. The first significant drop in the lateral load capacity of Unit 3 below the theoretical yield load level was observed during the third cycle at the displacement corresponding to the peak load level or 152.4 mm. This indicates a higher load degradation at lower ductility levels, which indicates that reducing the steel shell gap did not translate into an improvement of the seismic response of the test unit. For unit 3 and based on a direct investigation of the test results the new displacement at ductility

level one was set at 42.1 mm, translating in the displacement ductility levels shown in the figure below.

Figure 0-19. Unit 3 - Load Displacement Response

Figure 0-20. Unit 3 Joint Shear Cracks

1.42. LOAD VS. CURVATURE RESPONSE

As before Figure 0-21 shows the measured lateral load versus the computed curvatures at the column to the bent cap interface for Unit 3. As in the previous Units 1 and 2, the diagram depicted in this figure also indicates a good correlation between the pre-test analysis and the experimental test results during the initial stages of testing. However, after peak load there is a considerable deviation between these two curves. As in Units 1 and 2, this can be attributed to large rotations originating solely from within the joint region, which indicates that the response of the three units was very similar.
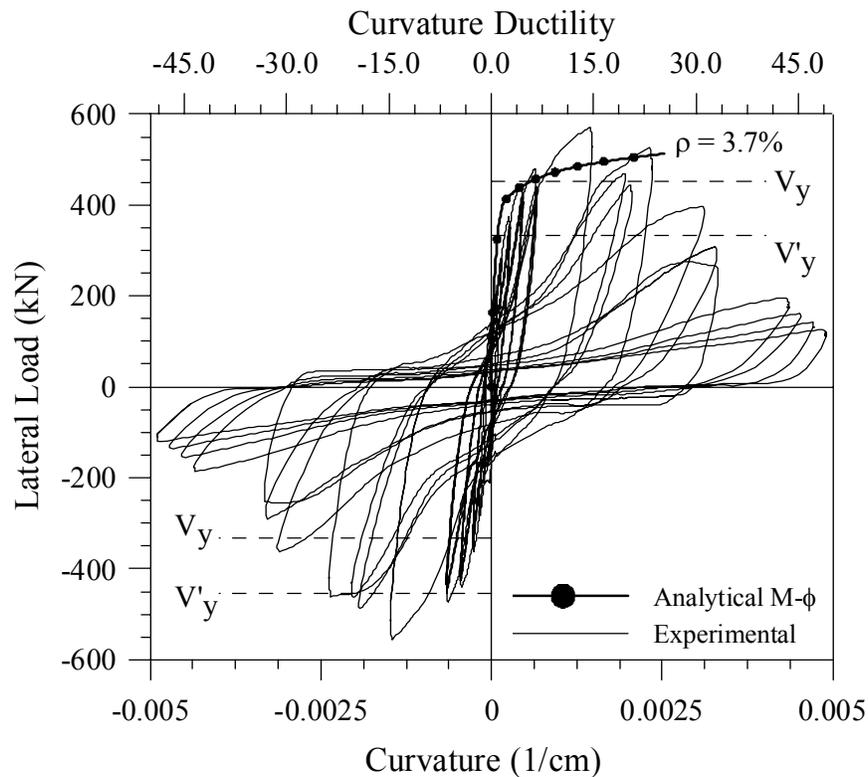
Figure 0-21. Unit 3 – Load versus Curvature Response

1.43. COLUMN LONGITUDINAL REINFORCEMENT STRAINS

The strain histories of the column longitudinal reinforcement gauges at the interface of the column and bent cap for side "A" and side "B" are shown in Figure 0-22 and Figure 0-31, respectively.

The yield strain of the column longitudinal reinforcement occurred at $\pm 2,376\mu\varepsilon$ as determined from tensile testing. The strain profiles for each side of the column are shown in Figure 0-24 and

Figure 0-25. The onset of yielding of the main column longitudinal bars occurred at μ1.0 for each side of the column.
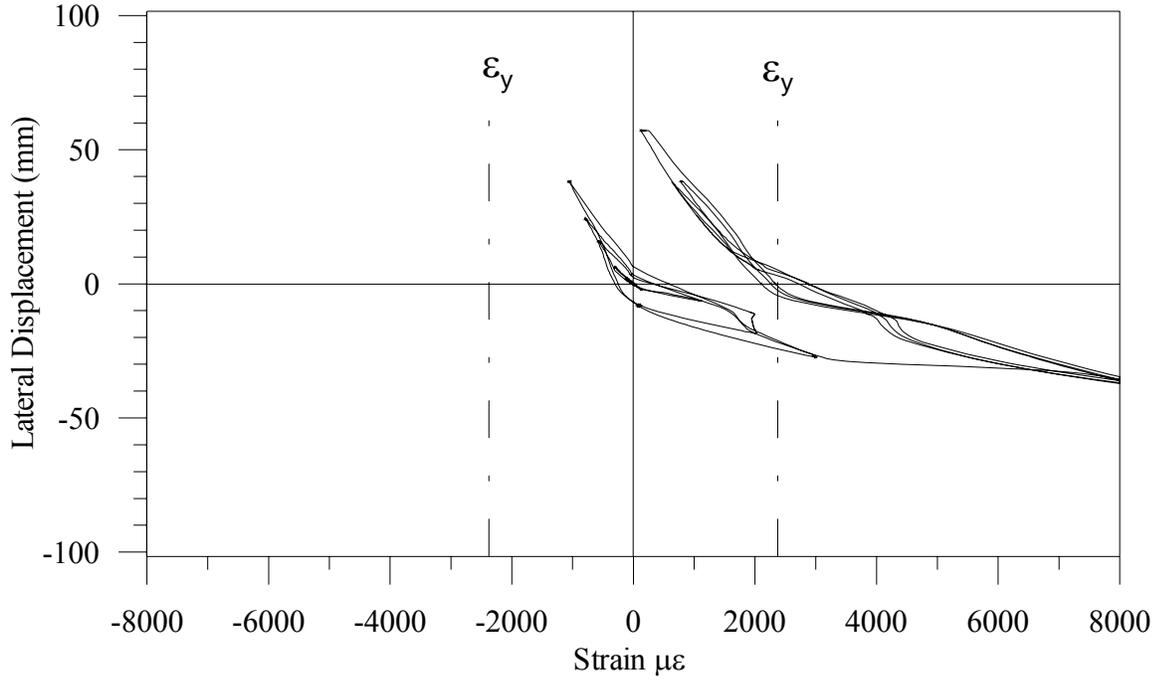
Figure 0-22. Strain Gauge History – C4a
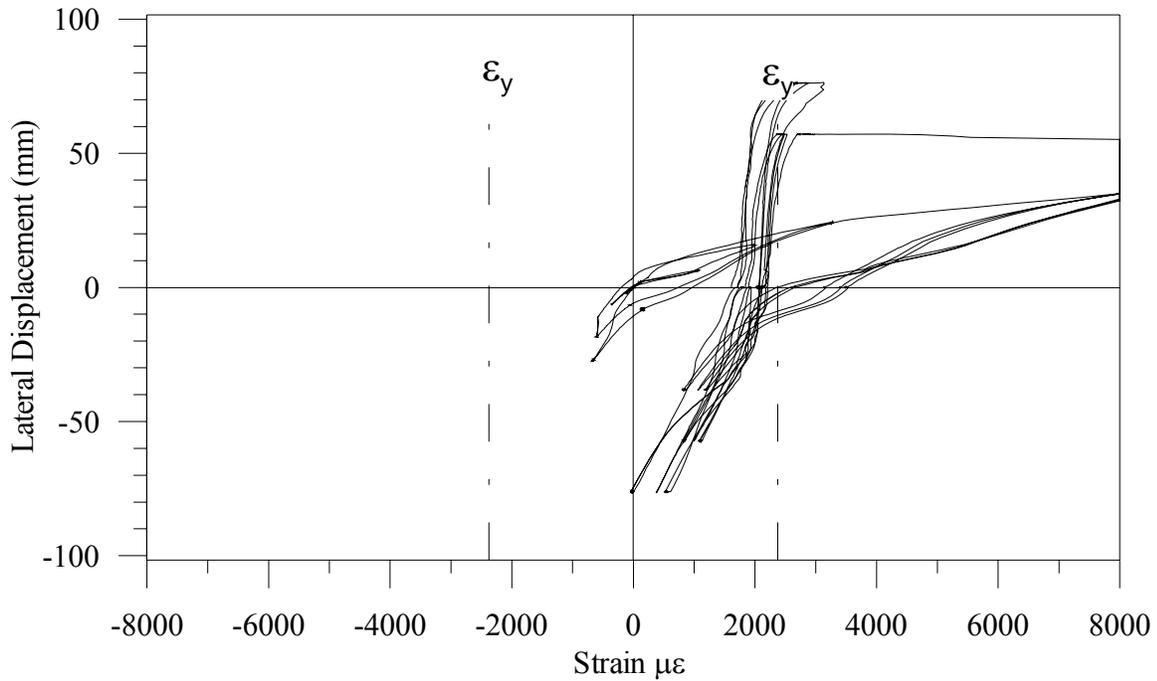
Figure 0-23. Strain Gauge History – C4b
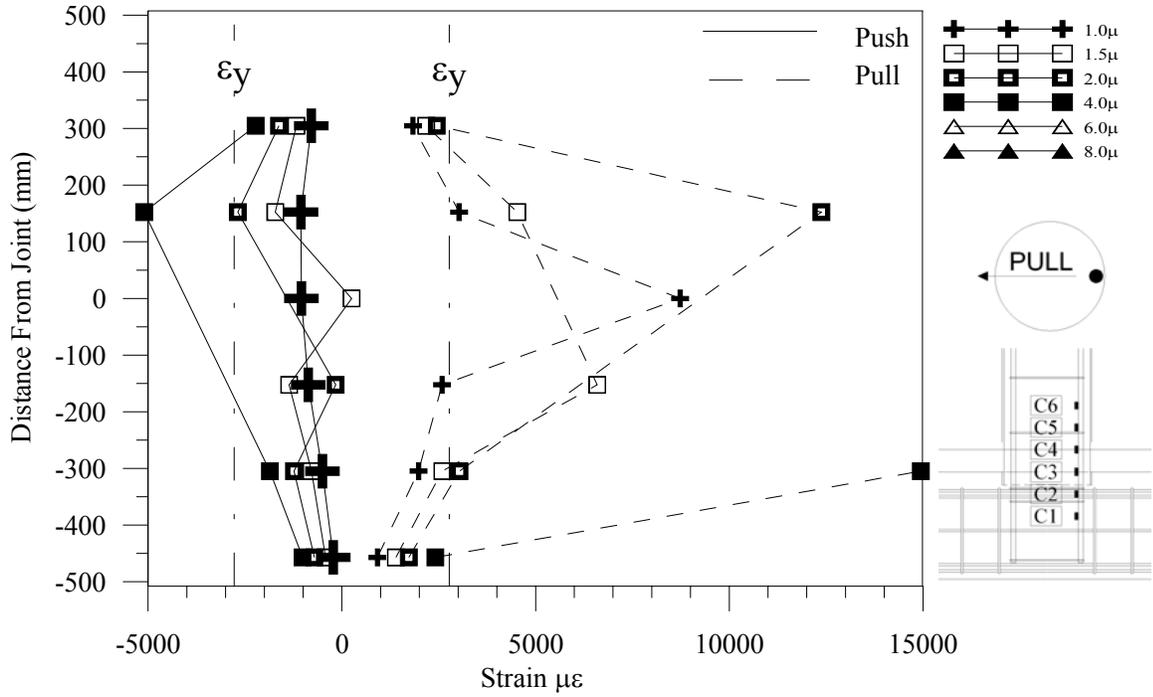
Figure 0-24. Strain Gauge Profile – Side "A"
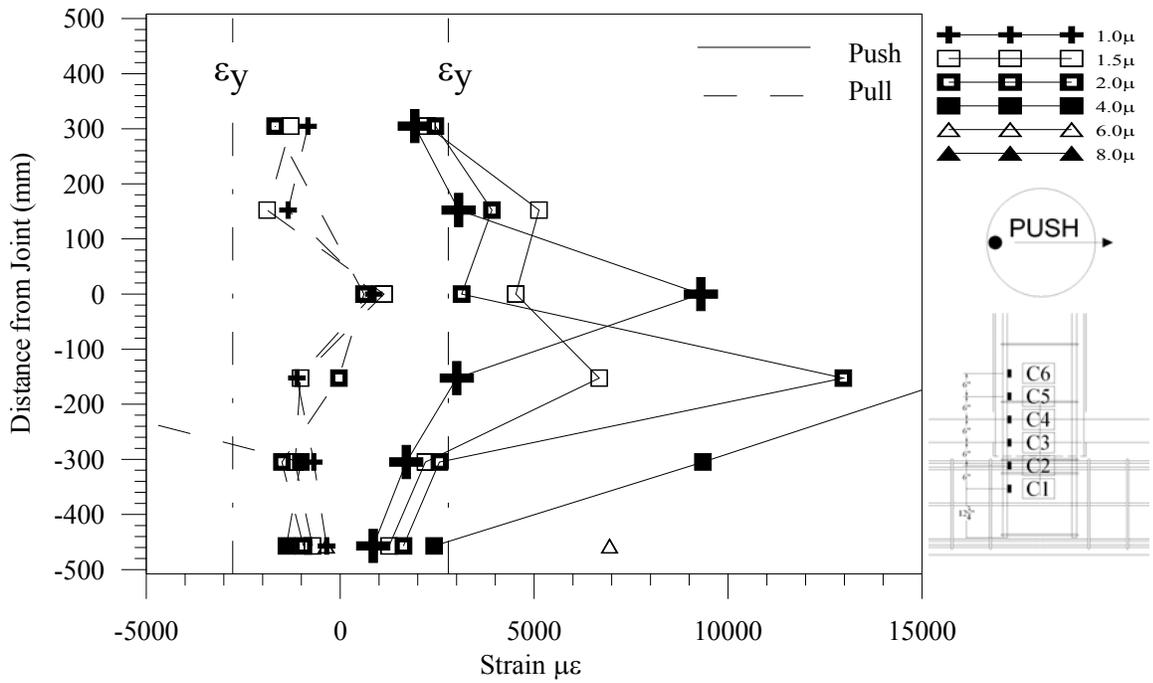
Figure 0-25. Strain Gauge Profile – Side "B"

1.44. JOINT SHEAR REINFORCEMENT STRAINS

The strain gauges from the shear reinforcement are presented in this section. The yield strain of the as-built and retrofit shear reinforcement occurred at ±2626 as determined from tensile testing. Figure 0-26 and Figure 0-27 are the strain profiles for the stirrups in the as-built concrete and the stirrups in the retrofit concrete, respectively. The stirrups stayed below the yield point indicating that joint shear did not occur in the longitudinal plane of the bent cap.
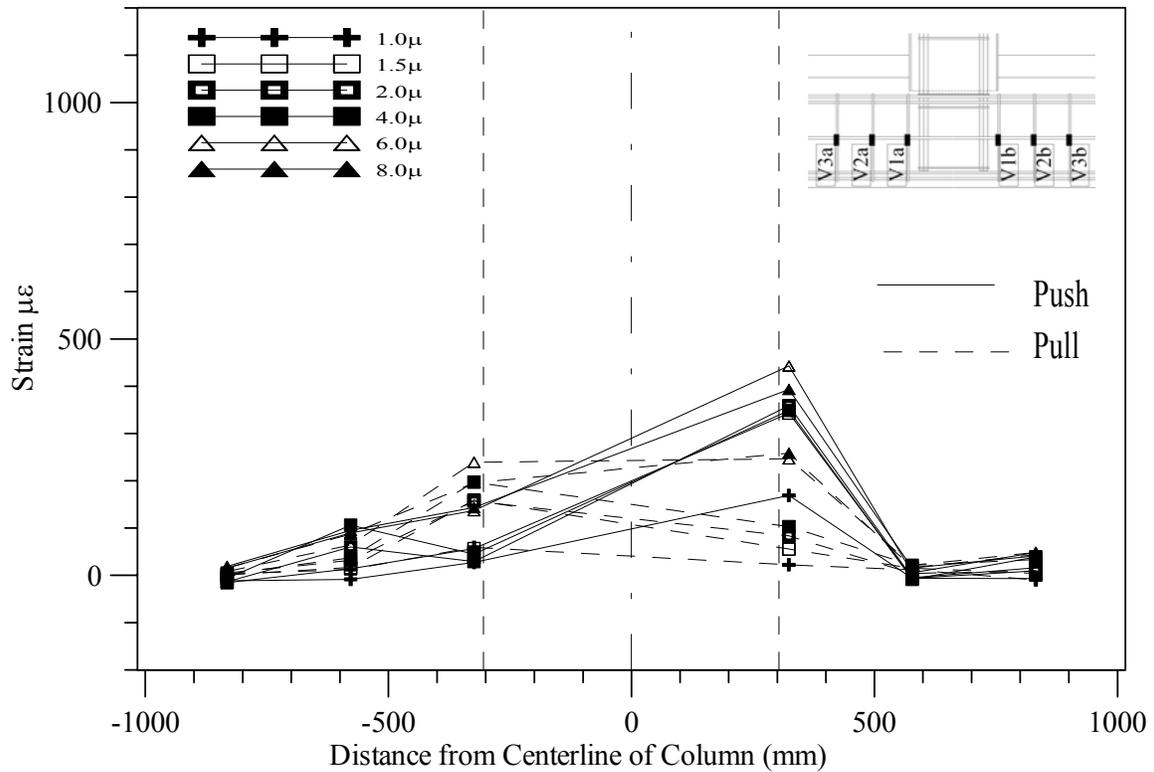
Figure 0-26. Strain Gauge Profile
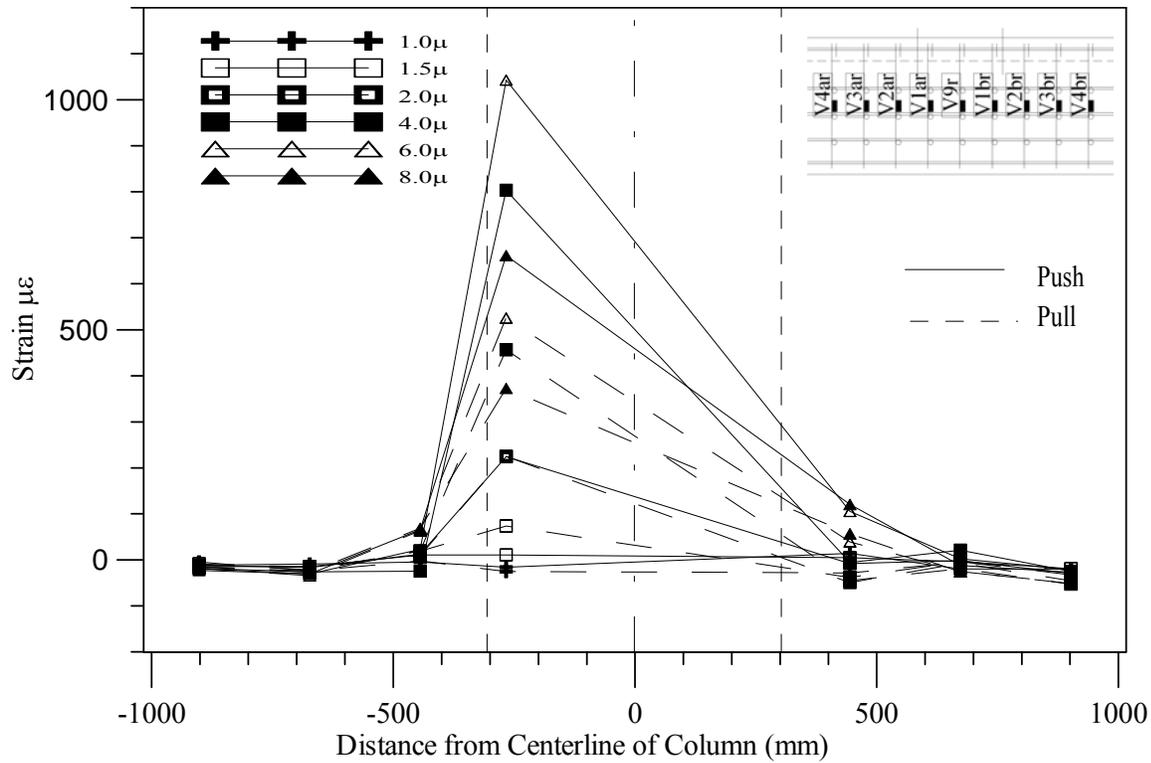
Figure 0-27. Strain Gauge Profile

1.45. BENT CAP LONGITUDINAL REINFORCEMENT STRAINS

The following section presents the strain in the cap beam longitudinal steel. The yield strain for the original longitudinal steel is 2,438 με. The yield strain for the retrofit longitudinal steel is 2,604 με. For both the original and retrofit steel, the steel did not yield, indicating that the cap beam stayed elastic. For similar locations, the strain in both the retrofit steel and the original steel had strain levels that were very close indicating that the entire beam acted as one unit. The strain profiles for the bent cap bottom longitudinal reinforcement for the as-built and retrofit sections are shown in Figure 0-28 and Figure 0-29, respectively.
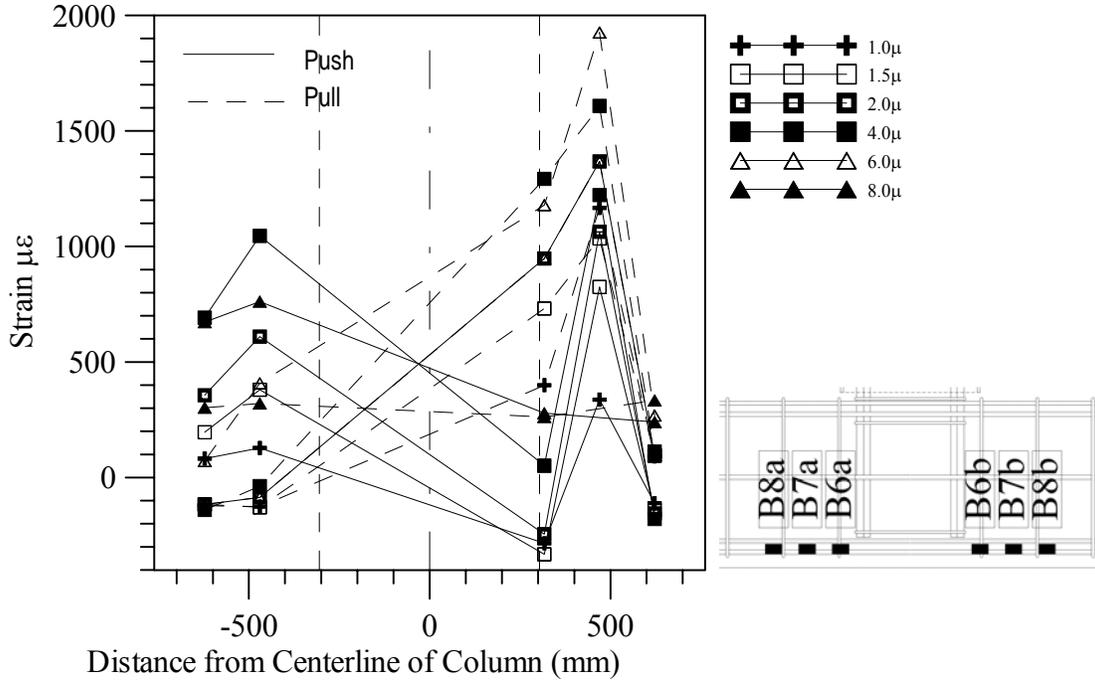
Figure 0-28. Strain Gauge Profile
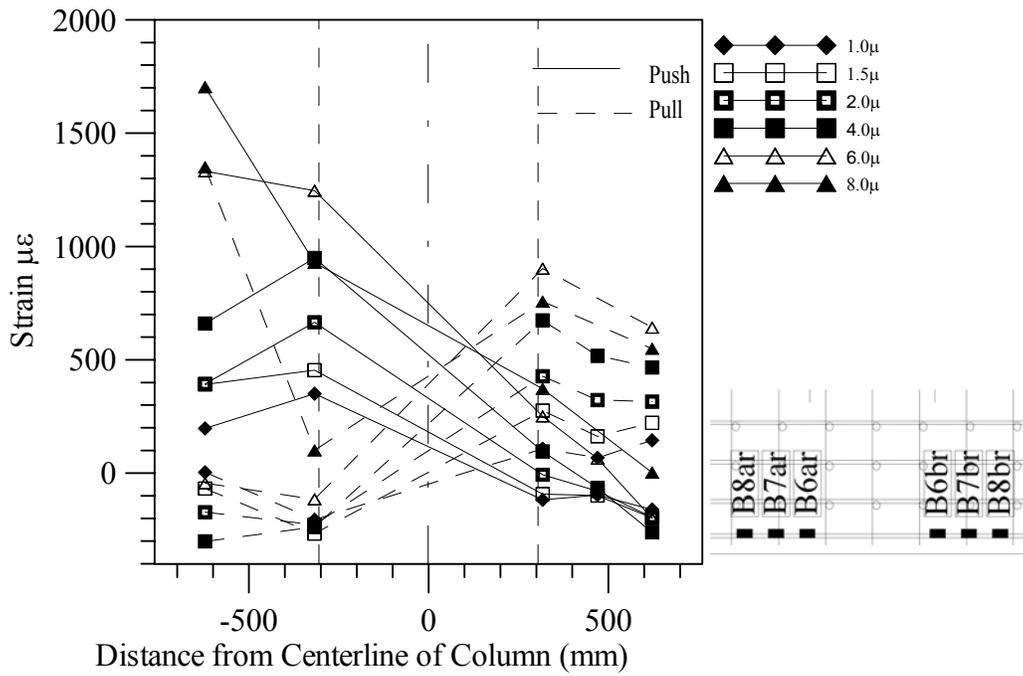
Figure 0-29. Strain Gauge Profile

1.46. JOINT SHEAR ANALYSIS

Joint shear failure did occur as indicated by the degradation of the load and loss of capacity shown by the load vs. deformation curve in Figure 0-19.

The joint shear deformation is larger than the previous Units as shown in Figure 0-30. The post tensioning mechanism prevented excessive dilation of the bent cap preventing large strains in the top transverse reinforcement as shown in Figure 0-32.

The bent cap flexural and shear reinforcement stayed below yield and had similar levels of strain for the as-built and retrofit reinforcement as shown in Figure 0-28 and Figure 0-29, respectively. As with the previous Units, this indicates composite action between the as-built and retrofit cross-sections and that the bent cap stayed elastic forcing the plastic hinge to form in the column.
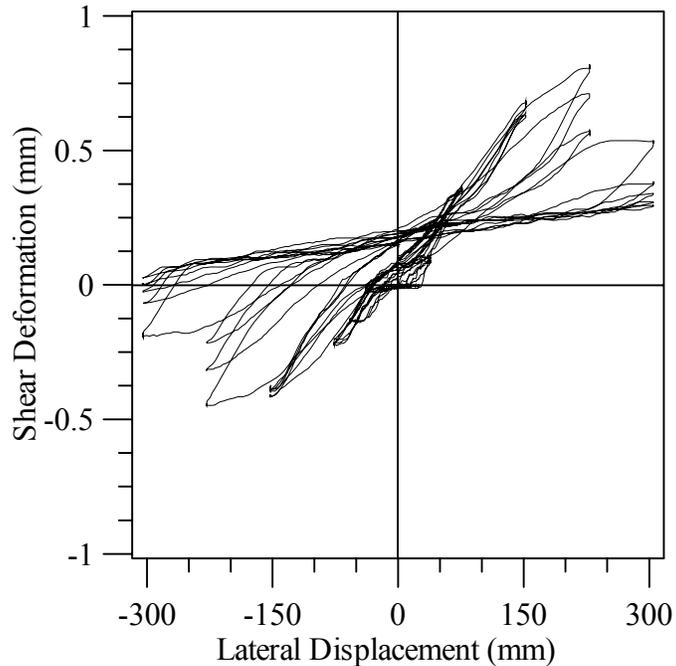
Figure 0-30. Unit 3 Joint Shear Deformation
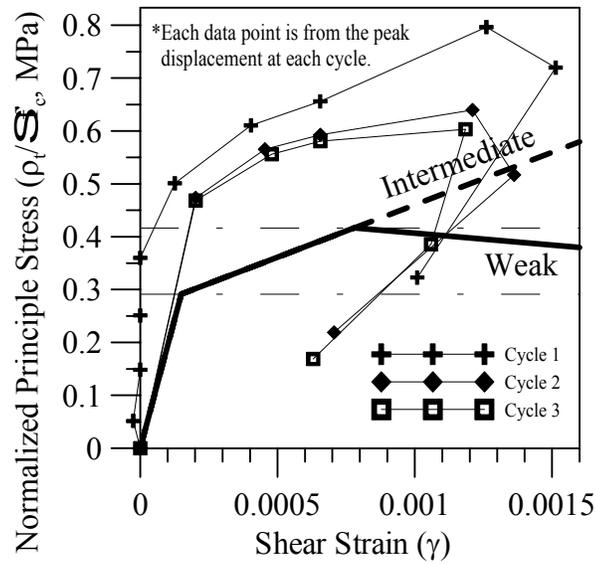
Figure 0-31. Unit 3 Principle Tensile Stress vs. Joint Shear Strain
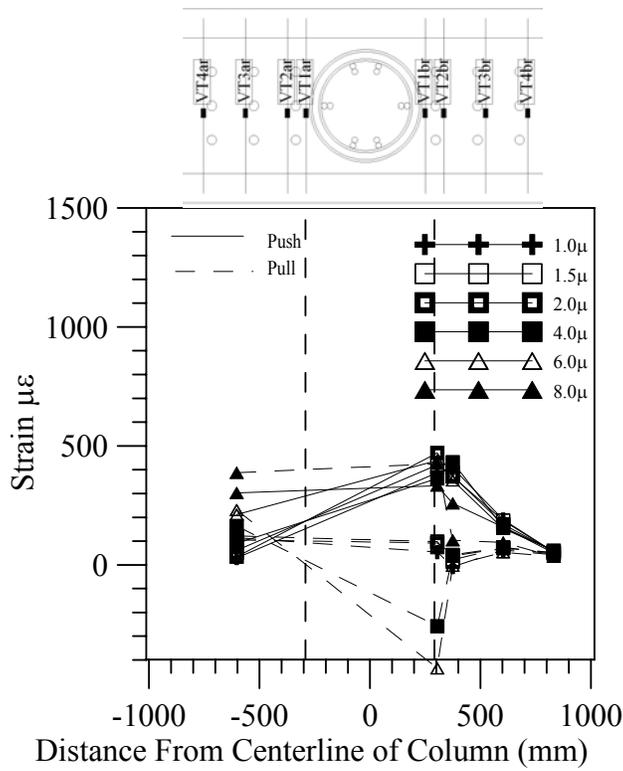
Figure 0-32. Unit 3 Top Transverse Reinforcement Strain Profile

1.47. GENERAL

As previously shown in Sections 1.27, 1.34, 1.41, the load deformation response for the three units are very similar; however, slight deviations in the response of each of these three test units can be outlined either in terms of energy absorption capabilities, maximum achieved lateral load capacity, strength degradation under increased reversed cyclic loads, and damage levels. A brief summary of some of the results derived from the experimental program are shown in Table 0-1. Peak lateral loads and peak principle tensile stresses for the three test units are shown in this table for a direct comparison of the test results. A reasonable comparison among the three test units was performed in terms of energy dissipated through the system, and strength degradation under reversed cyclic loading. These parameters are discussed in the next two sections.

Table 0-1. Peak Values

Unit	Peak Values			Energy	
	Load (kN)	Stress (kN)	Rate*	Dissipated (kN-m)	Rate*
1	+421 -442	0.39 -0.41	-	986	-
2	+440 -460	0.41 -0.43	1.05 1.04	1,154	1.17
3	+555 -570	0.53 -0.55	1.32 1.29	1,007	1.02

* Normalized values in terms of Unit 1 results

1.48. COMPARISON OF DISSIPATED ENERGY FOR THE THREE TEST UNITS

In this section a comparison of energy dissipated through the three test units is used in the context of assessing joint performance. The energy dissipated through the structural system was calculated from the area of the hysteretic loops at each displacement level and results of these analyses are shown in Figure 0-1. The total cumulative energy dissipated for Units 1, 2, and 3 was 986 kN-m, 1,154 kN-m, and 1,007 kN-m, respectively, which shows that Unit 2 had a slightly higher capacity to dissipate the hysteretic energy by nearly 15%. As shown in Figure 0-1, Unit 2 was capable of dissipating higher levels of energy beyond 228.6 mm, which can also be set as the limit for onset of joint shear degradation for Units 1 and 3. Also the higher energy dissipation capacity associated with Unit 2 is evident by the reduced pinching of the hysteresis loops for this unit in comparison to those of Units 1 and 3. This suggests an improved performance for the joint of Unit 2 and hence a greater capacity to dissipate energy.

Referring to Table 0-1 it is important to note that although Unit 3 was not able to dissipate the same level of energy as Unit 2, the principle tensile stresses for this unit exceeded those of Unit 2. Reducing the steel shell gap from 51 mm to 13 mm for Unit 3 provided better confinement of the cover concrete preventing buckling and low cyclic fatigue of the column longitudinal bars. However, the significant increase in the moment capacity of unit 3 led to an increased demand in the joint region. This observation suggests that in design practice combining details of Units 2 and 3 are likely to lead to an improved joint performance. Using these results design
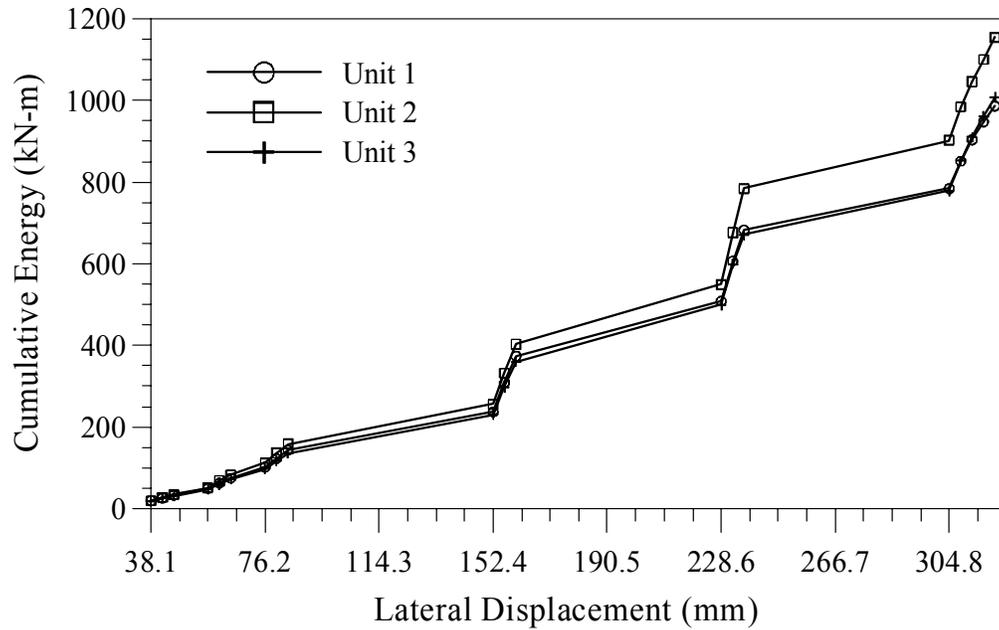
Figure 0-1. Cumulative Dissipated Energy

1.49.   STRENGTH DEGRADATION UNDER REVERSED CYCLIC LOADING

Referring to Figure 0-2(a) it is clear that the three test units reached their peak capacity at the displacement level of 152.4 mm. Also, the peak load achieved in Units 1 and 2 was nearly 1.5 times the section yield capacity. In Unit 3 the maximum achieved lateral load was nearly twice as the yield capacity. This increase in the ultimate capacity of Unit 3 was a direct result of reducing the steel shell gap from 51 mm to 13 mm, which increased the confinement action on the core concrete. As such, one of the immediate conclusions derived from this research project is to stipulate a limit for the steel shell gap length as a means to control the capacity of the column, which is discussed in further detail in Section 1.54.3.

As in the previous section, in this section a comparison of strength degradation under reversed cyclic loading is used in the context of assessing joint performance. In comparison to the analytical models it is expected that under reversed cyclic loading reinforced concrete sections will experience degradation in the lateral strength due to buckling of the longitudinal

reinforcement and joint degradation. However for the three test units, buckling of the longitudinal reinforcement was more prevalent in the Units 1 and 3. In addition, Unit 1 experienced the first drop in the lateral load capacity below the theoretical yield load level during the second cycle to the displacement level of 228.60 mm. Similarly, Units 2 and 3 experienced the first drop in the lateral load capacity below the theoretical yield load level during the first cycle to the displacement level 304.8 mm. These results were used in Section 1.54.3 to establish displacement ductility levels for the design and upgrade of existing bridge bents.
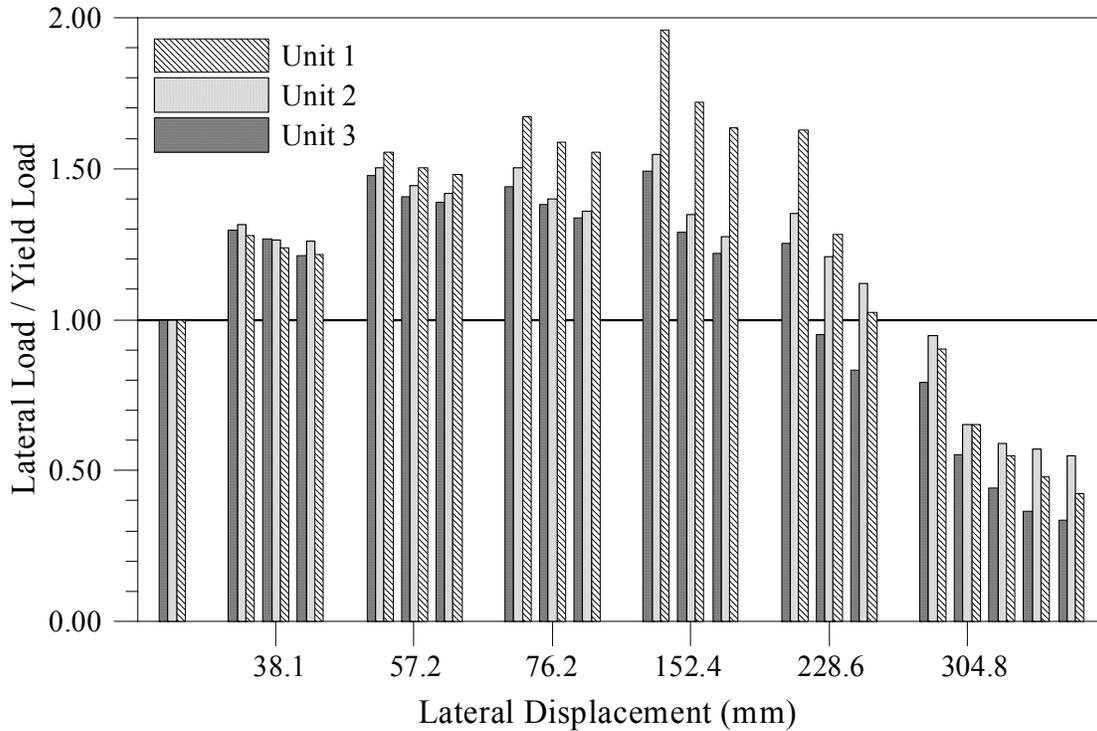
Figure 0-2. Strength Degradation under Reversed cyclic loading

1.50. JOINT PERFORMANCE

Priestley (1993) developed a three point joint stress-strain response model for poorly confined joints using the two principle tensile stress limits stipulated in Eqs. (0-6) and (0-7) as starting points for joint design and assessment. These two points were empirically derived from testing of 26 outrigger-bent knee joints. However, it is important to note that there is no single joint stress-strain model that can represent the complex behavior of all possible joints (Mazzoni and Moehle, 2001). However, the model developed by Priestley has been used by Caltrans (SDC, 2004) as a starting point for seismic design and assessment of bridge joints.

In the evaluation of the three test units three different joint models were developed to evaluate the lateral response of the test units. These proposed models are shown in Figure 0-3 along with the experimentally derived normalized principle tensile stresses versus joint rotation. The

proposed models for each of the joints of Units 1, 2, and 3 are shown in Figure 0-4(a) for a direct comparison, which shows that the joint in Unit 3 achieved higher principle tensile stresses, but the joint in Unit 2 shows lower levels of strength degradation under increased joint rotations.

In Figure 0-3 are also shown the models originally developed by Priestley (1993) and Mazzoni and Moehle (2001). These two models have been proposed in the literature, and as previously stated that have been used to evaluate joint performance under reversed cyclic loads. Joint model *I* is used in the evaluation of unconfined joints and was proposed by Priestley (1993), and Joint model *II* is used in the evaluation of confined joints and was proposed by Mazzoni and Moehle (2001). Both of these joint models are tri-linear models, in which the first two branches are the same for both models with expressions given by:

$$\rho_t = \begin{cases} 1944.444 \times \theta_j \,; & \theta_j \leq 0.00015\,(rad) \Rightarrow \textit{Joint Model I \& II} \\ 0.2576 + 227.273 \times \theta_j \,; & \theta_j \leq 0.0007\,(rad) \Rightarrow \textit{Joint Model I \& II} \\ 0.4480 - 44.804 \times \theta_j \,; \; 0.0007 < \theta_j \leq 0.01\,(rad) \Rightarrow \textit{Joint Model I} \\ 0.625 \,; & \theta_j > 0.00162\,(rad) \Rightarrow \textit{Joint Model II} \end{cases} \tag{0-1}$$

Where θ_j is the joint shear/rotation measured in radians and ρ_t is the normalized principle tensile stresses. The principle tensile stresses were then converted to a moment relation based on the Mohr circle of analysis and on the relation:

$$M_t = w_b \left(0.8 \times h_b\right)^2 \sqrt{\left(\rho_t \chi_i^{N} \times \sqrt{f_c^{'}} + \frac{f_a}{2} \right)^2 - \frac{f_a^{\,2}}{4}} \tag{0-2}$$

Where w_b and h_b are the bent cap width and depth, respectively, $f_c^{'}$ is the concrete compression strength, and f_a is the axial stress on the joint derived from the axial load, P, and is given by $P/w_b h_b$, χ is a damage parameter and is a piecewise linear function that was empirically derived from the test results for each test unit that was developed to simulate the damage that develops within the joint region, and the power N in χ is the cycle number under consideration. The damage parameter χ was then given for each test unit by:

$$\chi = \begin{cases} 1.00 \,; & \theta_j \leq 0.00015\,(rad) \Rightarrow \textit{Joint Model Units 1 and 2} \\ 1.00 - 15.0 \times \theta_j; & \theta_j \leq 0.0007\,(rad) \Rightarrow \textit{Joint Model Unit 1} \\ 1.00 \text{-} 5.0 \times \theta_j; & \theta_j \leq 0.0007\,(rad) \Rightarrow \textit{Joint Model Unit 2} \end{cases} \tag{0-3}$$

Next, substituting the piecewise Eqs. (0-3) and (0-1) into Eq. (0-2) the moment-rotation envelope for each of the test units is obtained and the relations for the three test units are shown in Figure 0-4(b). Results from this section were then used to develop the post-test analysis outlined in the next section.
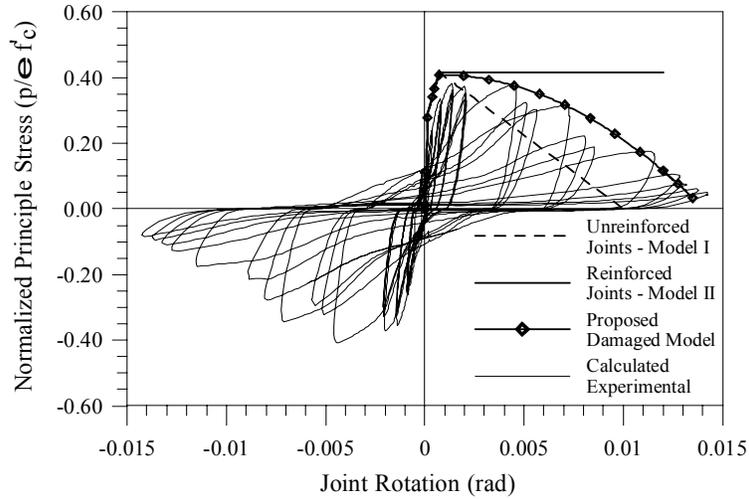
(a) Unit 1
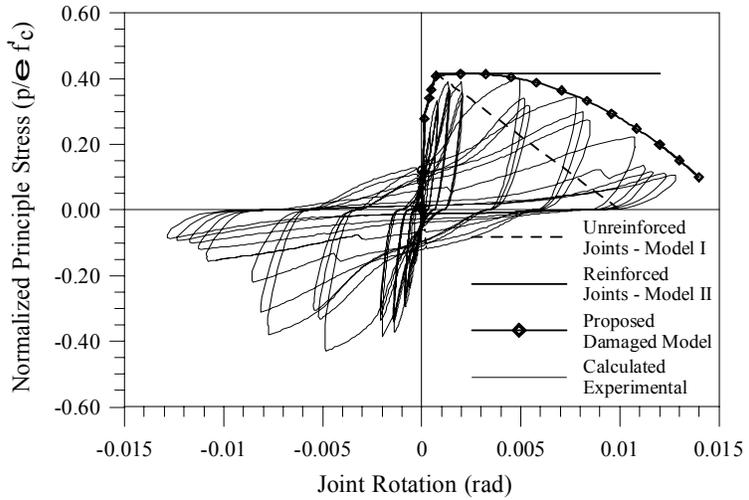
(b) Unit 2
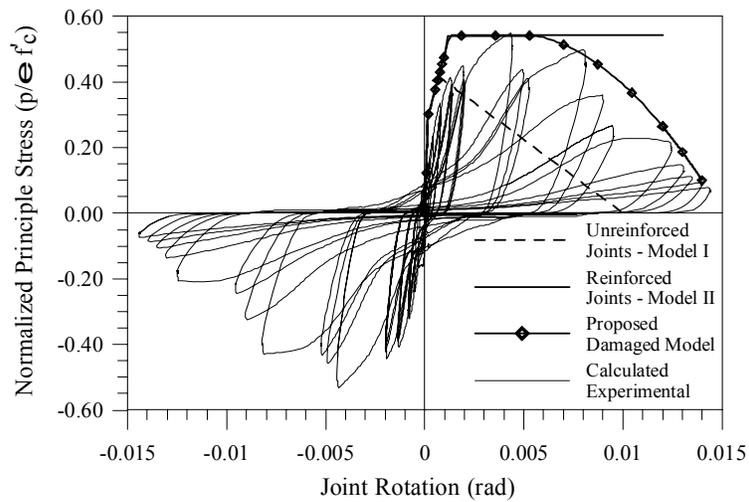
(c) Unit 3

Figure 0-3. Normalized Principle Stresses vs. Computed Joint Rotation

(a) Normalized Stresses   (b) Moment Rotation Envelope
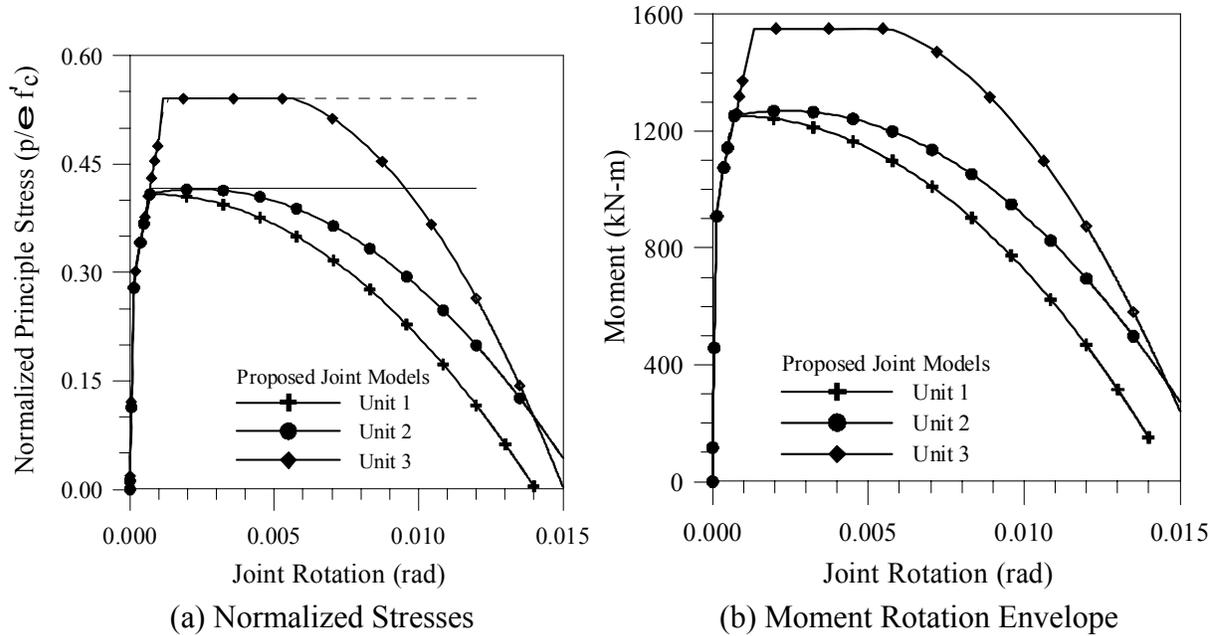
Figure 0-4. Joint models

1.51. POST-TEST ANALYSIS

The pre-test analyses for Units 1, 2 and 3, as described in Section 1.24, were developed without considering any increases in deflections or loss in load capacity deriving from flexibility or damage in the joint. This approach leads to satisfactory results in developing the envelope response of members built with joint shear reinforcement designed according to current seismic design provisions, in which joint flexibility is negligible. However, prior to the 1970's joints were built with insufficient joint shear reinforcement and for these structures other mechanisms of deformation must also be considered in the analysis.

These mechanisms should consider rigid body rotations at the ends of members due to joint flexibility and elongation combined with slip of the longitudinal reinforcement from the joint core. Mazzoni and Moehle (2001) have successfully used these mechanisms combined in a rigid body moment rotation relation. As such, in this research program these additional modes of joint deformation were considered in the analysis in terms of the relation:

$$\Delta V_i = \left(\frac{1}{K_{C,i}} + \frac{(L_C + H_b / 2)^2}{K_{B,i}} + \frac{(L_C + H_b / 2)^2}{K_{J,i}} \right)^{-1} \times \Delta D_i \qquad (0\text{-}4)$$

Where as before, ΔV_i and ΔD_i are the incremental column lateral load and top deflection, respectively, and $K_{C,i}$ and $K_{B,i}$ are the instantaneous tangential bending stiffness for the column and bent cap, respectively, and were obtained in terms of Eq. (0-2). In this form the first two

terms consider only the column and bent cap flexibility, and the last term considers the rigid body rotation at the base of the column due to joint flexibility combined with bar elongation and slip. As such, $K_{J,i}$ is the rotational stiffness of the joint considering joint flexibility plus bar elongation and slip. The joint rotational stiffness was empirically derived for each of the test units by employing a rotational spring element with zero length and moment rotation relation developed based on the joint stress-strain/rotation diagrams presented earlier for joint models *I* and *II*.

Based on the three moment-rotation models shown in Figure 0-4(b) and the analytical model expressed by Eq. (0-4) the curve envelopes for each of the test units was developed and results from this analysis are shown in Figure 0-5. These three curves were then superimposed with the load deformation response curves for each of the three test units shown in Sections 1.27, 1.34, and 1.41. Referring to these experimental results sections there is a good correlation between the proposed joint model results and the experimental curves.
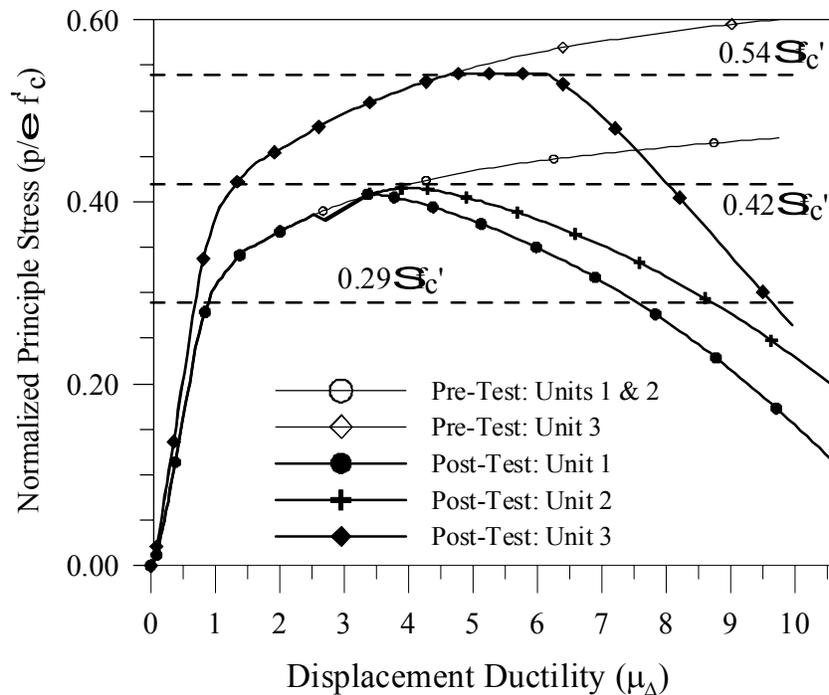

Figure 0-5. Post-Test Analysis

1.52. GENERAL OVERVIEW

This report discusses in detail experimental and analytical findings from a research program conducted for the State of Alaska Department of Transportation and Public Facilities. Part of this research program a total of three 4/5 scale units were cast, retrofitted, and tested under simulated fully-reversed cyclic lateral loading. These three units consisted of a cast in place steel shell (CISS) column foundation shaft and a bent cap configured to form a tee connection. In addition, these units were built to model a bridge bent and tested under simulated seismic loads at the University of Missouri Rolla experimental facilities. Based on these research program, an upgrade method was investigated that can be implemented in field conditions for improving the seismic performance of bridges built in the state of Alaska. Based on the research findings overall design recommendations are discussed in this Section 1.54.

A prototype as-built unit consisting of an interior column and corresponding bent cap was designed and constructed in a T-configuration by including the following design deficiencies: (1) the CISS column foundation shafts have excessive longitudinal reinforcement ratios, (2) the yield moment capacity of the bent cap is below the maximum feasible moment that develops at the column faces, (3) the steel shells are partially embedded in the joint region, which under low levels of rotation impose extensive damage on the bent cap, and (4) the joints have inadequate amounts of joint shear reinforcement to sustain the levels of principal tensile stresses that develop within the joint region, which leads to anchorage failure of the column longitudinal reinforcement and significant strength degradation at low ductility levels.

After construction of the as-built units, the units were modified in order to investigate seismic improvements and propose procedures for field implementation, according to the following seismic improvements: (1) the moment capacity of the column was reduced by cutting a portion of the column longitudinal reinforcement at the connection to the bent cap to levels that can ensure a proper ductile seismic response, (2) a section of the steel shell was cut and removed leaving a gap between the steel shell and the bent cap, and (3) the bent cap dimensions were increased to i) install the additional flexure and joint shear reinforcement thereby increasing the moment capacity of the bent cap, ii) provide adequate reinforcement spacing, iii) reduce the principle tensile stresses, iv) provide for a better transfer of stresses within the joint region, v) increase the development length of the column longitudinal reinforcement, and v) reduce reinforcement congestion in the joint region.

1.53. GENERAL CONCLUSIONS

Overall, experimental results from the three test units cyclic tests showed that the three test units displayed a ductile response up to the displacement ductility of 5 without significant decreases in the strength of the test units, inelastic actions due to flexural yielding of the bent cap, shear failure of the bent cap or joint shear failure. Realizing that for a column with an aspect ratio of 4.5, Priestley *et. al* (1995) recommends that the displacement ductility capacity of multiple column bridge bents should not be any less than 4, experimental results indicate that the displacement ductility levels achieved are within the recommended values.

Beyond the ductility level of 5, the main failure mode of Unit 1 was attributed to joint shear failure due to excessive transverse dilations within the joint region. This was attributed to the transverse horizontal headed reinforcement not been made continuous though the joint region. As such it is recommended that this detail practice not be used in regions prone to seismic events with a combined ductility demand near 4 and under multiple reversed cycles.

An improved joint detail was implemented for Units 2 and 3, in which this transverse reinforcement was made continuous through the joint region. In Unit 2, the main failure mode was attributed to low cyclic fatigue of the column longitudinal reinforcement. Extensive joint degradation was recorded beyond the displacement ductility of 7. In Unit 3 the joint was post-tensioned in the transverse direction while also decreasing the gap length between the steel shell and the bent cap. Beyond ductility level 7 degradation of the lateral load capacity of the column occurred due to joint shear failure. Detailed description for the design of these units and experimental results are discussed within this report.

Based on the experimental results the research team proposes that a displacement ductility of 4 be implemented in the retrofit design for the maximum credible earthquake using the details proposed for Units 2 and 3. At this level it is expected that some level of strength degradation will be observed in the column, but this will not either cause significant decrease in the column axial capacity nor significant wide open cracks in the joint region. Furthermore, any cracks at this level will close under the gravity loads. In addition, for columns with lower reinforcement ratios or deeper bent cap the full dependable moment capacity and displacement ductility of the column can be expected to develop. As such, for these columns higher displacement ductilities levels may be accepted for assessment investigation. This is further addressed in the next section.

1.54. SEISMIC DESIGN RECOMMENDATIONS

Following on the discussion of the experimental results presented in Section 0, this section outlines design recommendations to establish an improved seismic performance of bridge bents built in the state of Alaska using CISS columns. Based on the design and performance of the three test units, the following design recommendations are made for seismic retrofit/upgrade design of multi-column bridge bents with circular CISS-columns. It is assumed that multi-column bents are designed using the capacity design philosophy with hinges forming at the column end.

1.54.1. Column Design

The following seismic upgrade design procedures are proposed for the seismic rehabilitation of circular CISS-columns built with reinforcement ratios greater 4% and/or the steel shell embedded into the bent cap:

i) A section of the steel shell must be cut and removed in order to leave a gap between the steel shell and the new bent cap section, as previously discussed in Sections 0, 0, and 0 during construction of the test units, see Figure 0-2. All the concrete surrounding the column longitudinal reinforcement and located below the line of the new bent cap section should be removed as shown in Figure 0-3.

ii) Following up on the previous recommendation, at least two D-13 field welded hoops must be provided below the steel shell gap region and placed immediately in contact with the column longitudinal reinforcement, as shown in Figure 0-4. Higher number of welded hoops may be required to satisfy the following anti-buckling spacing, *s*, requirements (Caltrans, 2004):

$$s \leq 6d_{bl} \qquad (0\text{-}1)$$

Where d_{bl} is the bar diameter of the column longitudinal reinforcement. This detail is necessary to prevent buckling of the column longitudinal reinforcement within the gap region beyond the damage level corresponding to crushing of the cover concrete.

iii) The steel shell gap should be limited between 35 and 50 mm. The lower gap value will limit increases in the flexural capacity of the column due to excessive confinement of the inner core. The upper bound will be within values that can ensure sufficient displacement ductility capacity, minimum confinement of the plastic hinge region and prevent shear failure of the column.

iv) The column longitudinal reinforcement ratio should be reduced to limits below 4% but not lower than 1% using the procedures outlined in Section 1.14 and 1.15. The upper limit avoids significant amounts of joint shear reinforcement and practical difficulties involving construction of the upgrade bent cap section in columns with large reinforcement ratios.

v) In the evaluation of the flexural capacity of circular CISS columns with a gap region the concrete core should be assumed confined by an equivalent spiral confined section with a spiral area corresponding to the square of the steel shell thickness and a pitch equivalent to the gap length.

1.54.2. Bent Cap Design

The following seismic upgrade design procedures are proposed for the seismic rehabilitation of reinforced concrete bridge bent caps built with insufficient longitudinal, shear and joint shear reinforcement capable of ensuring plastic hinges to form at the column ends:

i) The minimum width of the upgrade bent cap section must be within 1.5 times the outside diameter of the steel shell. This limit will ensure a uniform flow of forces through the joint region. However, as previously discussed in Section 1.11.2, the minimum width of the bent cap, W_b, must satisfy current ACI (ACI 2002) bar spacing and cover concrete specifications for the installation of the new bent cap flexural and joint shear reinforcement.

ii) Redesign of the bent cap height shall be dimensioned according to limits stipulated by Eq. (0-4) (Priestley, 1996), which was established based on the required development length for the column longitudinal reinforcement. A higher bent cap height may be necessary in order to reduce the principle tensile stresses within the joint region as stipulated in Section 1.54.3.

iii) As previously discussed in Section 1.11.1 and Eq. (0-1), the maximum moment demand placed on the bent cap can be established at the column face and may included the effects of the axial load on the columns.

iv) Based on the maximum moment demand computed from Eq. (0-1) increase in the yield moment capacity of the bent cap must be achieved in terms of Eq. (0-2).

v) Referring to a section in its upright position, when an increased in the bent cap bottom longitudinal reinforcement is required (that is top in the test units) at least 4 of these bars should be placed within the width of the exiting bent cap section, as shown in Figure 0-22. Furthermore, at least two of these bars must be placed through the existing concrete core as shown in Figure 0-23.

1.54.3. Reinforced Concrete Joint Design

Design of the reinforcement within the joint region should follow the procedure outlined in Section 1.12.1, which establish design of the joints in terms of the principle compressive and tensile stress limits. Furthermore, design of the joint shear reinforcement within shall be performed in terms of the strut and tie model presented in Section 1.12.2.

i) In addition to the longitudinal reinforcement required to increase the yield moment capacity of the bent cap given by Eq. (0-2), additional longitudinal reinforcement shall be

required to resist the joint shear forces and must be placed in the bent cap according to the design strategy discussed in Section 1.12.3.

ii) Additional internal and external vertical joint shear reinforcement required within the joint region shall be provided according to the limits defined in Section 1.12.4.

iii) An area of horizontal joint shear reinforcement is required within the joint region according to the design philosophy presented in Section 1.12.5.

Based on the experimental results and observed damage levels the following methodology is recommended in addition to the design parameters set by Section 1.12.5.

iii.a) For an upgrade bent cap section when the principle tensile stress are less than $\phi_f \times 0.42 \sqrt{f_c'} (Mpa)$, installation of the transverse reinforcement may be provided in terms of any of the details used in the construction of Unit 1 (two pieces, see detail in Figure 0-1), Unit 2 (single piece, see detail in Figure 0-1), and/or Unit 3 (single piece post-tensioned, see detail in Figure 0-1). At this principle tensile stress limit no reduction in the available displacement ductility capacity of the system is imposed.

iii.b) For bent cap sections with the height, H_b, initially computed based on Eq. (0-4) and that do not meet the limits set above, the bent cap height may be adjusted based on the following expression:

$$ H_b = \frac{1}{\phi_f 0.8} \sqrt{\frac{M_U}{w_b \sqrt{\left(\rho_{all} \times \sqrt{f_c'} + \frac{f_a}{2}\right)^2 - \frac{f_a^2}{4}}}} \tag{0-2}$$

Where M_U is the ultimate moment capacity of the column, ϕ_f is the flexural strength reduction factor equal to 0.9, f_a is the axial stress in the joint and is computed based on Eq. (0-9), f_c' is the nominal design concrete compressive strength, and ρ_{all} is the allowable principle tensile stress limit in the joint in terms of the values shown in Table 0-1.

iii.b) For bent cap sections sized according to Eq. (0-2) the maximum available displacement ductility capacity must be set in terms of the values shown in Table 0-1.

Table 0-1. Allowable

Transverse Reinforcement Details	Allowable ρ_{all}	Allowable μ_Δ
Two Pieces per Figure 0-1	0.42	4
Single Piece per Figure 0-1	0.42	8
Post-Tensioned per Figure 0-1	0.54	8

iii.c) For an upgrade bent cap section when the principle tensile stresses are greater than $\phi_f \times 0.42\sqrt{f_c'}\,(Mpa)$, any of the details previously outlined may be used but the following reductions in the displacement ductility capacity of the system must be implemented:

Table 0-2. Modified Displacement Ductility Capacity

Transverse Reinforcement Details	Number of Peak Cycles, N_f		
	$N_f \leq 2$	$2 \leq N_f \leq 4$	$N_f > 4$
Two Pieces per Figure 0-1	6	4	2
Single Piece per Figure 0-1	6	6	2
Post-Tensioned per Figure 0-1	6	4	2

*Maximum number of peak cycles, N_f, is computed based on Eq.(0-3).

In Table 0-2 the number of cycles of loading, N_f, expected at the maximum displacement amplitude may be estimated from (NCHRP, 2003):

$$N_f = 2 \leq 3.5 \times T_N^{-\frac{1}{3}} \leq 10 \qquad (0\text{-}3)$$

Where T_N is the natural period of vibration of the structure.

When a multiple column bridge bent is designed based on the above recommendations, a ductile seismic response can be expected up to the design drift limit state.

REFERENCES

AASHTO, "Standard Specification for Highway Bridges, Sixteenth Edition," American Association of State Highway and Transportation Officials, 1996.

ATC-32, (1996), "Improved Seismic Design Criteria for California Bridges: Provisional Recommendations," Applied Technology Council, Redwood City, California.

Buckle, I. (2000), "Passive Control of Structures for Seismic Loads." *Proceedings of the 12th World Conference on Earthquake Engineering*, Auckland, New Zealand, 2000, Paper No. 2825

California Department of Transportation (Caltrans), (2001), "Bridge Design Specifications," Sacramento, CA, 2001.

California Department of Transportation (Caltrans), (2004), "Seismic Design Criteria," Version 1.3, Sacramento, CA, USA, February 2004.

Chai, H. Y., Priestley, M. J. N., Seible, F., (1991), "Seismic Retrofit of Circular Bridge Columns for Enhanced Flexural Performance," *ACI Structural Journal*, Vol. 88, No. 5, September – October 1991, pp. 572-584

DesRoches, R., and Fenves, G.L., (2001), Simplified Restrainer Design Procedure for Multiple-Frame Bridges, *EERI Earthquake Spectra*, Vol. 17, No. 4, Nov. 2001, pp. 551-567.

Ereckson, N.J., Silva, P.F., Chen, G., (2002), "Seismic Evaluation of Bent Cap/Column Joints in Missouri," Preliminary Report for Task 6, Earthquake Hazards Mitigation Research Program for Highway Systems.

Ingham, J. M., (1995), "Seismic Performance of bridge Knee Joints." Doctoral Dissertation, University of California, San Diego, 1995.

Krawinkler, H. (1995), "New Trends in Seismic Design Methodology," *Proceeding of the l0th European Earthquake Engineering*, Rotterdam, Netherlands, Aug. 28 – Sep. 2, 1995, Vol. 2, pp. 821-830.

Krawinkler, H. (1999), "Challenges and Progress in Performance-Based Earthquake Engineering." *Proceedings of International Seminar on Seismic Engineering for Tomorrow – in Honor of Professor Hiroshi Akiyama*, Tokyo, Japan, 1999, pp. 1-10.

Lowes, Laura N., Moehle, Jack P., (1999), "Evaluation and Retrofit of Beam-Column T-Joints in Older Reinforced Concrete Bridge Structures," ACI Structural Journal, V. 96, No. 4, July-August 1999.

Mazzoni, S., Moehle, J.P., (2001). "Seismic Response of Beam-Column Joints in Double-Deck Reinforced Concrete Bridge Frames," *ACI Structural Journal*, Vol. 98, No. 3, May-June 2001, pp. 259–269.

Mazzoni, S., Fenves, G. L., Smith, J. B. (2004) Effects of Local Deformations On Lateral Response of Bridge Frames," Report to California Department of Transportation, Contract No. 59A201, EEC-9701568.

Priestley, M.J.N., (1993), "Assessment and Design of Joints for Single-Level Bridges with Circular Columns," University of California, San Diego, Structural Systems Research Project, Report No. SSRP-93/02.

Priestley, M.J.N., Seible, F., Calvi, G.M. (1995) "Seismic Design and Retrofit of Bridges," John Wiley & Sons, Inc.

Sanders, D., Laplace, P., Saiidi, M. & El-Azazy, S. (2002) "Seismic performance of reinforced concrete bridge columns," Third National Seismic Conference and Workshop on Bridges and Highways: Advances in Engineering and Technology for the Seismic Safety of Bridges in the New Millennium, Portland, Oregon, April 2002: pp. 345–356.

Silva, P.F., Seible, F., Priestley, M.J.N., (1997), "Response of Standard Caltrans Pile-to-Pile Cap Connections Under Simulated Seismic Loads," Department of AMES, University of California San Diego, La Jolla, California, November 1997, Report SSRP-97/09.

Silva, P.F., Sritharan, S., Seible, F., Priestley, M.J.N. (1999), "Full-Scale Test of the Alaska Cast-in-Place Steel Shell three Column Bridge Bent," University of California, San Diego, Report to Alaska Department of Transportation and Public Facilities, Juneau, Alaska, Report No. SSRP 98/13.

Sritharan, S. (1998), "*Analysis of Concrete Bridge Joints Subjected to Seismic Action*", Doctoral Dissertation, Department of AMES - Division of Structural Engineering, University of California San Diego, La Jolla, California.

Sritharan, S. Sri, Priestley, M.J.N., Seible, F., (1999), "Enhancing Seismic Performance of Bridge Bent cap-to-Column Joints Using Prestressing," *PCI Journal*, V. 44, No. 4, July-August 1999.

Sritharan, S., Ingham, Jason M., (2003), "Application of Strut-and-Tie Concepts to Concrete Bridge Joints in Seismic Regions," *PCI Journal*, Vol. 48, No. 4, July-August 2003, pp.66-90.